Republic of Iraq

Ministry of Higher Education and Scientific Research

University of Babylon Research College of Engineering

Department of Mechanical Engineering

Experimental Study of the Turbulent Flame Characteristics for Ammonia Blended LPG

A Thesis Submitted to the

College of the Engineering / University of Babylon in Partial Fulfillment of the Requirements for the Degree of Master of Science in Engineering /Mechanical Engineering /power

By

Jaafar Sami Shaban B.Sc. (Mech.Eng. 2008)

Supervised By

Assist Prof. Dr. Samer Mohammed Abdulhaleem

2023 A.D. *1445A.*

وَوَصَّيْنَا الإِنسَانَ بِوَالِدَيْهِ إِحْسَانًا حَمَلَتْهُ أُمُّهُ كُرْهًا وَوَضَعَتْهُ كُرْهًا وَحَمْلُهُ وَفِصَالُهُ ثَلاثُونَ شَهْرًا حَتَّى إِذَا بَلَغَ أَشُدَّهُ وَبَلَغَ أَرْبَعِينَ سَنَةً قَالَ رَبِّ أَوْزِعْنِي أَنْ أَشْكُرَ نِعْمَتَكَ الَّتِي أَنْعَمْتَ عَلَيَّ وَعَلَى وَالِدَيَّ وَأَنْ أَعْمَلَ صَالِحًا تَرْضَاهُ وَأَصْلِحْ لِي فِي ذُرِّيَّتِي إِنِّي تُبْتُ إِلَيْكَ وَإِنِّي مِنَ الْمُسْلِمِين

صدق الله العظيم

سورة الاحقاف اية ﴿15﴾

Certification

I certify that the thesis entitled **“Experimental Study of the Turbulent Flame Characteristics for Ammonia Blended LPG"** Was prepared by **Jaafar Sami Shaban** under my supervision at the University of Babylon in partial fulfillment of the requirements for the degree of Master of Science in Mechanical Engineering (Power Engineering).

I recommend that this thesis be forwarded for examination in accordance with the regulation of the University of Babylon.

Signature

Assist Prof.Dr. Samer Mohammed Abdulhaleem

Department of Mechanical Engineering College of Engineering/University of Babylon

Dedication

I dedicate this work to My great family who offered me immense support and encouragement throughout my work:

My dear Wife Ruwaida

My children Rami Elia

My beautiful daughter Naya

I dedicate this work also to the soul of my dear father how left a long time ago and My mother

Jaafar

Acknowledgments

This thesis would not have been possible without ALLAH (be glorious) for all the blessings upon me.

I would like to express my heartfelt thanks and gratitude to my supervisor, ***Assist prof. Dr. Samer Mohammed Abdulhaleem*** *for his guidance, invaluable instruction, help, and unwavering encouragement throughout the preparation of my study. I'd like to express my gratitude to the head of the mechanical engineering department* ***Assist prof. Dr. Samer Mohammed Abdulhaleem*** *for constructive contribution to this Work.*

My thanks are also extended to the staff of mechanical engineering Department, at Babylon College of Engineering.

Jaafar

ABSTRACT

Experimental studies of premixed, turbulent, gaseous explosion flames in a fan-stirred bomb are reported. The turbulence was uniform and isotropic, while changes in the rms turbulent velocity were achieved by changes in the speed of the fans. Central spark ignitions created mean spherical flame propagation.

The spatial distributions of burned and unburned gases during the propagation were measured High-speed schlieren images also were captured simultaneously the experiment was conducted with different initial pressures (100, 200, and 300 kPa) and equivalence ratios (0.8, 1, and 1.3). The MATLAB program code was used to process and analyze the images that obtained by the Schlieren system.

The distributions of the proportions of burned and unburned gases around circumferences were found for all radii at all stages of the explosion, and mean values of these proportions were derived as a function of the mean flame radius. The flame brush thickness increased with flame radius.

The way the turbulent burning velocity is defined depends on the chosen associated flame radius. Various definitions are scrutinized and different flame radii presented, along with the associated turbulent burning velocities. Engulfment and mass turbulent burning velocities are compared.

It is shown how the latter might conveniently be obtained from schlieren cine images. In a given explosion, the burning velocity increased with time and radius, as a consequence of the continual broadening of the effective spectrum of turbulence to which the flame was subjected.

The key focus was on calculating the speed of turbulent combustion based on the average diameter of the combustion flame, which is affected by the irregular diameter caused by turbulence.

Under certain conditions, it was obtained that the laminar combustion speed is 28.64 cm/sec.

Additionally, when the conditions were changed to have the same equivalence ratio and different initial pressures or the same initial pressure and different equivalence ratios, the calculated turbulent combustion speed was higher at 49.11 cm/sec. This increase in combustion speed under turbulent conditions can be attributed to the beneficial effect of turbulence on combustion efficiency.

According to the results, it is indicated that the turbulence improving the combustion speed and enhancing the efficiency of the fuel mixture burning.

The findings from this study give further understanding on combustion processes by improving combustion efficiency for various applications, such as engines and furnaces.

Table of contents

Nomenclature

Symbol	Definition	Unite
A	Flame Surface Area	m^2
d	Diameter	mm
e	Number of Mole of Component,	mol
J	Ammonia Volume Fraction	
L_b	Markstine Length	
Le	Lewis Number	
M	Mol Mass	kg/mol
P	Pressure	kPa
R	Specific Gas Constant	J/kg.K
r	Flame Radius	mm
Rv	Average radius	mm
$R_\circ$	Universal Molar Gas Constant	J/ mol.K
S_g	Gas Velocity Ahead of the Flame Front	m/sec
S_b	Stretched Laminar of the Flame Speed	m/sec
T	Temperature	K
Ta	Adiabatic Temperature	K
t	Time	sec
Sl	Laminar Burning Velocity	m/sec
St	Turbulent Burning Velocity	m/sec
V	Volume	liter
x	Mol fraction	
Re	Reynolds Number	
Sn	Turbulent flame speed	m/sec

Greek Symbols

Symbol	Definition	
Ø	Equivalence Ratio	
α_T	Temperature Stretch Rate	
β_P	Pressure Dependent Parameter	
ε	Flame Stretch Rate	1/s
ρ	Density	kg/m^3

Abbreviation

Symbol	Definition
CPM	Constant Pressure Method
CVC	Constant Volume Method
DIB	Di isobutylene
dil	Diluent
ext	Extensional
LBV	Laminar Burning Velocity
LPG	Liquefied Petroleum Gas
Mix	Mixture
Ref	Reference
Sch	Schlieren image

CHAPTER ONE

INTRODUCTION

CHAPTER ONE

1.1 Background

Global warming results from increased greenhouse gas concentration (GHG_S), in particular, carbon dioxide (CO_2) in the atmosphere. This atmospheric accumulation of greenhouse gases is largely the result of fossil fuel combustion and other human activities.

Many possible solutions were suggested, and the search for fossil-fuel replacements is a significant challenge for society. Various researches were conducted to evaluate alternative fuel's energy efficiency and environmental impact. The use of ammonia gas represents a possible solution for the storage of intermittent renewable energy.

Ammonia is considered more suitable for storage and transportation compared to Hydrogen gas because the tanks in which ammonia is stored is light, not expensive and its storage is also safer due to the low pressure.

The ammonia energy storage system has great advantages over a wide range and less restriction of geographical conditions compared to many other conventional energy storage method **[1]**.

1.2 Ammonia Fuel

The ammonia NH3 product might be made from biomass, fossil fuels, renewable sources like photovoltaic cells and wind, Ammonia is carbon-free, has no direct effect on GHG, and might be produced utilizing a carbon-free process employing renewable energy sources. Approximately 180 million tons of NH3 are generated as well as transported each year, The Ammonia and LPG properties, are

Listed in Table (1.1) The production of ammonia from natural gas is conducted by reacting methane (natural gas) with steam and air, coupled with the subsequent removal of water and CO_2. The products of this process are hydrogen and nitrogen, which are the feedstock for the main ammonia synthesis.

1.3 LPG Fuel

Iraqi Liquefied petroleum gas (LPG), which consist primarily of propane (C_3H_8) and butane (C_4H_{10}), with minor unit's other materials acquired a byproduct petroleum refining. (C_2H_6) and (C_5H_{12}) the vapor pressure at 37.8 ˚C ranging from (8.4-8.6 kg/cm^2), and the density at 15.6 ˚C ranges from (0.537- 0.541) throughout the month. Specifications for LPG have been obtained from Hilla Gas Depot and the laboratory and it's cooled to a low temperature or high pressure.

When being liquefied LPG, the mixture size is 260 times comparison with the gaseous phase. LPG is a fuel similar to petroleum. It has a Heating value of 45MJ.kg^{-1}**,** Due to LPG efficient combustion characteristics and low emissions it is widely used as an alternative fuel in automobiles **[2].**

LPG is heavier compared with air in gaseous form and contains less water as a liquid. The mixture of butane and propane is colorless, and the smell of LPG can be detected by sniffing it. In terms of using LPG as a fuel, the value regarding its octane number is highly essential; this number (106 - 110) it is higher compared to the octane number for C_6H_6 but lower than the octane number for ammonia, as a result, greater resistance to explosions is provided **[2].**

Table (1.1) characteristics of Ammonia and LPG

Specifications / unit	LPG [2],[10]	NH_3 [11]
LHV MJ/Kg	45.5	18.8
HHV MJ/Kg	49.3	22.5
Density Kg/m^3	0.536	0.37
Octane number	106 -110	130
Minimum ignition temperature K MIT	683-853	930
Boiling point ˚C	-18	-33.34
Flashpoint ˚C	-40	132

1.4 The Importance of Ammonia in Industrial Application: -

Ammonia can be defined as a colorless gas that has a distinctively unpleasant odor. Power engineering, industrial, and agriculture processes use it. A hydrogen energy carrier and a carbon-free fuel, ammonia has a low cost and high efficiency.

The burning of ammonia is presented is a production of carbon monoxide (CO_2) and hydrocarbon in comparison of hydrogen.

This is due to the attractive properties of ammonia such as viable substitute for fossil fuels, because ammonia has a low flame temperature and a high-octane rating

of 130, it may be used at high compression ratios without producing a lot of NOx because it doesn't contain carbon. It can't result from burning carbon monoxide hydrocarbon compared to hydrogen because fuel ammonia is more energy-efficient and the production and storage of hydrogen as ammonia will be cheaper than compressed and cold hydrogen [3].

Since just nitrogen and water are produced from total combustion, ammonia is considered one of the sustainable –carbon-neutral electricity fuels like hydrogen (H_2). When compared to hydrocarbons or hydrogen, ammonia has a lower flame temperature, a narrower burning range, and lower flammability.

Due to such factors, ammonia was not thoroughly investigated. In comparison with hydrogen, ammonia offers a few advantages. Ammonia, for instance, might be stored at room temperature under moderate pressure (0.8 MPa), resulting a low storage cost. In spite of the advantages of ammonia as a fuel, numerous drawbacks such as toxicity and low heating value have previously been identified.

In the 1960s, the studies of New shall, and Stark Mann and Pratt have shown that because of the slower interactions of ammonia, the friction system designed for fuel must be twice as big as possible [4].

1.5 Ammonia and energy

Ammonia can be produced from Renewable source and is one of the most productive chemicals worldwide with a huge production history [5]. Ammonia may be quickly liquefied and stored at 8.5 bar at room temperature, cooled to -33˚ Celsius, and stored at ambient pressure. Ammonia storage is far less expensive compared to hydrogen storage, which needs around 350-700 bar and - 252 Celsius for storage as a liquid at ambient pressure [6].

Ammonia is considered a power carrier that can also be utilized to store renewable energy and for a variety of other applications. Ammonia, for instance, could be utilized as a precursor to other chemicals, such as cleaning products, in the production of explosives and fertilizers **[7].**

As a result, agriculture has the best possibility of producing sustainable ammonia. In agriculture, ammonia derived from renewable energy can reduce emissions from this industry. Actually, fertilizer production emits 1.2% of world greenhouse gas emissions **[8].**

1.6 Flame propagation speeds

Flame propagation speeds under laminar conditions have been measured with great success. The system pressure, system temperature, and equivalency ratio are the only factors that influence the laminar flame speed of an explosive mixture. After accounting for geometry and flame stretch, the observed laminar flame speed may be used to verify chemical kinetics. Another application of laminar flame speeds is to predict the propagation rates of turbulent flames using correlations that are generally appropriate for a particular experimental database. This makes such propagation rates puzzling, in contrast to the laminar case **[9]**. Self-similar scaling of spherically spreading flames was recently found using data from various fan-stirred explosives, including data from the rig constructed **[10]**. These results are exciting because they show that it is possible to create a comprehensive database of turbulent propagation rates for established and emerging fuels relevant to gas turbines and IC engines. Inside such flame bombs, mixing fans are attached to provide the necessary turbulence. This goal was attained by employing a systematic strategy. The following are explanations of the four most important ones **[11].**

1. The primary objective was to modernize the current facility cost-efficiently while minimizing the need for adjustments to the original equipment. Post-combustion pressures and temperatures did not compromise the vessel's structural integrity.

2. Refine the shape of the fans such that the turbulence inside the flame bomb is consistent. After that, the fan-generated flow fields were meticulously measured. The major objective of this dissertation was to enhance the scalability monitoring capabilities of an existing high-pressure laminar flame bomb in the author's lab **[12]**.

3. Improve the control of turbulence parameters in such flame bombs, turbulence conditions are defined by the intensity level and the integral length scale. Therefore, the correlations between the fan-stirred data and the flame speed are affected by geometric factors. Adjustable intensity levels and a sliding scale for the duration of turbulence were included to address this concern.

4. The literature showed various diagnostic techniques relating to fan-stirred bombs, and a process for monitoring turbulent flame speeds was established. Currently, schlieren is important and beneficial for the study due to save the time and accurate flame speed rates. Automated image analysis and post-processing procedures were developed specifically for turbulent combustion. The capabilities of the rig were successfully shown in the Experiment **[13].**

1.7 Turbulent Flame Speed

Turbulent flame speed refers to the rate at which a flame propagates through a turbulent flow. It measures how quickly the flame front advances through a mixture of fuel and oxidizer in the presence of turbulence in which preliminary measurements of LPG-Ammonia-Air mixtures were obtained in various conditions.

In a turbulent combustion process, the reactants (fuel and oxidizer) are mixed by the turbulent flow, creating a highly complex and dynamic environment. The flame speed in such conditions is influenced by several factors, including turbulence intensity, flame stretch, and the interaction between turbulence and chemistry.

The turbulent flame speed is typically higher than the laminar flame speed, which refers to the flame speed in the absence of turbulence. This is because turbulence enhances mixing, allowing for a faster reaction between the fuel and oxidizer. **[14]**

It is important to note that the turbulent flame speed is not a constant value but rather varies depending on the specific conditions. Different experimental and computational techniques are used to measure and model turbulent flame speeds under various operating conditions, such as different fuels, pressures, and temperatures.

Understanding the behavior of turbulent flames is necessary in various fields, including energy conversion, combustion engines, and fire safety, because it's effect as it effects on the combustion processes, stability, and emitted emissions.

Studying the turbulent flame speed combustion process is important in several fields, including combustion science, energy production, environmental engineering, and safety.

1.8 Combustion Efficiency:

Combustion processes are vital in various energy conversion systems, such as internal combustion engines, gas turbines, and industrial furnaces. Understanding and optimizing the turbulent flame speed is crucial for improving the overall

combustion efficiency, reducing fuel consumption, and minimizing harmful emissions [15] .

1.9 laminar and turbulent burning velocity - Definition

Premixed flames are generated by igniting a well-mixed fuel and oxidizer. Practical applications of such combustion are spark-ignition engines, lean-burn gas turbines, and household burners. After the fuel and oxidizer homogeneously mix and a heat source is applied, the flame front starts propagating outwardly through the unburned mixture.

Depending on flow conditions, flame propagation can either be laminar or turbulent. In practical cases, once the spark is initiated, a laminar flame kernel forms at first then rapidly becomes turbulent as it moves towards the unburned mixture. Therefore, understanding of turbulent burning velocity requires a thorough knowledge of laminar combustion as turbulent flame under certain conditions can be treated as an array of laminar flamelets [16].

The one-dimensional laminar burning velocity is a fundamental physio-chemical combustion property of the fuel-air mixture and depends only on the mixture composition, pressure, and temperature. By definition, laminar burning velocity is "the velocity, relative to and normal to the flame front, with which the unburnt gas moves into 5 the front and is transformed into products under laminar flow conditions" [17].

Figure 2.1 (a) shows a schematic representation of laminar expanding flame with burnt and unburnt gases separated by the flame front. Figure 2.1 (b) shows the corresponding grey-scale laminar flame. In most cases, outwardly-propagating laminar flame has a spherical structure with some wrinkling.

This spherical geometry is maintained by a continuous transformation process of the reactants into products with no turbulence affecting the flame propagation. Instead, flame stretch, wall effect, and ignition energy are the only factors that can significantly affect laminar flame propagation and structure.

Moreover, after the formation of the laminar flame kernel at the early stages of the premixed combustion inside the spark-ignition engine, this kernel develops into a turbulent semi-spherical flame.

However, under turbulent flow condition, the flame front wrinkles and develops instabilities due to the turbulent motion and the thermodynamic expansion of gases. Figure 2.2 (a) shows a schematic representation of an expanding turbulent flame with the burnt and unburnt gases separated by the flame front. Figure 2.2 (b) shows the corresponding grey-scale turbulent flame. Similarly, to laminar flame, turbulent flame is defined as, “the average rate of flame propagation through a turbulent premixed gas mixture relative to the flow field through the action of molecular diffusion of heat and mass” **[18].**

Therefore, turbulent flame propagation is initially laminar but affected by turbulent field and scales. Nonetheless, the substantial wrinkling of turbulent flame surface can significantly increase the flame front area, which hence boosts flame propagation speed. Thus, turbulent burning velocity, depending on turbulence intensity, can exceed laminar burning velocity several times under the same experimental conditions.

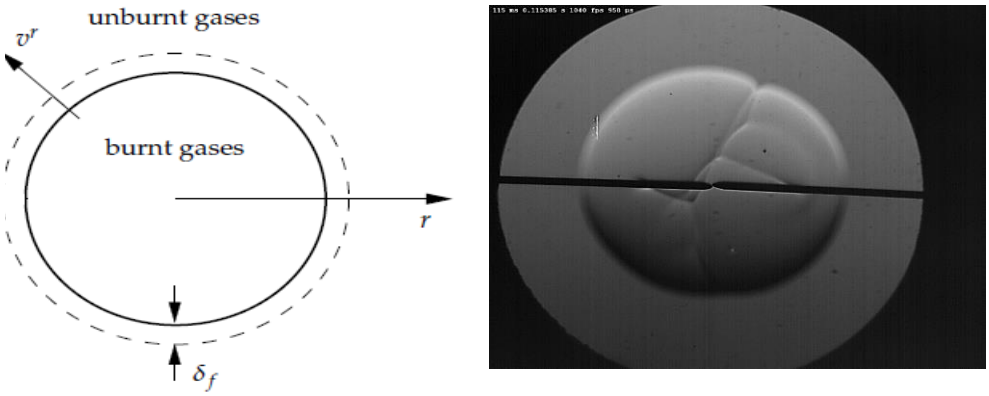

(a) **(b)**

Figure 2.1. Schematic representation of an expanding laminar premixed flame. The solid line represents reaction layer while the continuous line represents the flame front preheat zone ((a) δf and vr are the flame thickness and radial velocity, respectively, b) Grey-scale laminar flame)

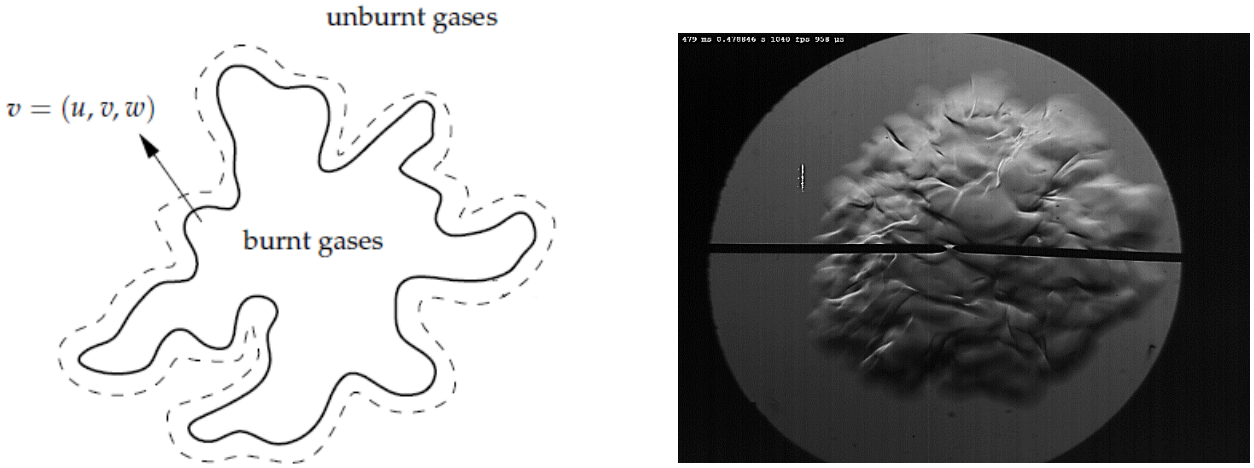

(a) **(b)**

Figure 2.2. a) Schematic representation of an expanding turbulent premixed flame. a) The solid line represents the reaction layer while the continuous line represents the flame front preheat zone [19]. b) Grey-scale turbulent flame

1.10 Safety Considerations

Combustion processes can pose serious safety risks, especially in industrial settings. Turbulent flames can exhibit complex behaviors, such as flame instabilities, flashbacks, and flame quenching, which can lead to hazardous conditions and even explosions. Engineers can design safer combustion systems and develop effective safety measures by understanding the turbulent flame speed and its interaction with various factors, such as fuel properties, flow conditions, and geometry. Alternative .

1.11 Fuels and Energy Sources

As the world seeks to transition to more sustainable energy sources, studying turbulent flame speed becomes crucial for evaluating the combustion characteristics of alternative fuels, such as biofuels, hydrogen, and synthetic fuels. Understanding how these fuels interact with turbulence can help assess their feasibility, performance, and emissions when used in different combustion systems.

Climate Change Mitigation: Combustion processes significantly contribute to greenhouse gas emissions, particularly carbon dioxide (CO2), the primary driver of climate change. By studying the turbulent flame speed and combustion processes, researchers can explore techniques for reducing CO2 emissions, such as low-emission combustion strategies, carbon capture and storage (CCS), and utilization of renewable energy sources.

The study of turbulent combustion is important for practical applications and advancing fundamental scientific knowledge. Turbulence-chemistry interactions in flames are complex and still not fully understood. Studying the turbulent flame speed and its interaction with various turbulent flow phenomena provides insights into

combustion's fundamental physics and chemistry, helping to refine and develop more accurate combustion models and simulations **[20].**

In summary, studying the turbulent flame speed combustion process is crucial for improving combustion efficiency, reducing emissions, ensuring safety, advancing alternative energy sources, mitigating climate change, and advancing fundamental scientific understanding. This research has broad implications across various industries and is essential for sustainable and efficient energy conversion and utilization. **[21].**

Chapter Two

Literature Review

Chapter two

2.1 Introduction

The mechanism of blended turbulent combustion is extremely intricate and poorly understood. The turbulent flame velocity of two fuels in different harsh circumstances is still difficult to compare **(Lipatnikov and Chomiak 2007)[22]**, Although much work remains, our understanding of the broad characteristics of the development of a blended turbulent flame has advanced significantly. Using the most recent experimental datasets on turbulent flame velocities (ST), Lipatnikov and Chomiak **(Lipatnikov and Chomiak 2002)[23]** conducted a thorough assessment Some of the most crucial findings from that meta-analysis and others are presented here.

1. The wrinkle of turbulent eddies increases the surface area of the flame, leading to a higher ST compared to laminar flames. "Turbulent extending" describes this phenomenon. A material's surface area grows exponentially due to the energy cascading between big and minor eddies. **(Lipatnikov 2012)[21]** the surface area created by turbulent stretching is constrained by self-propagation processes, which enable wavy laminar flames to merge.
2. Turbulent flame speeds exhibit nonlinear behavior as a function of turbulent intensity increases ST rises as turbulent intensity levels rise, reach a maximum, and then fall (bending effect), culminating in flame quenching by excessive turbulences The maxima intensity level strongly depends on the fuel and the equipment and cannot be generalized.

3. The main cause of this disparity is the absence of datasets concentrating on the impact of turbulent scales of length on ST, it was shown that a decrease in the

mixture's thermal diffusivity as pressure increased ST decreased the flame's thickness and favored flame instability, Recent studies by Liu et al,**(Kobayashi, Tamura et al. 1996) [24]** found that a rise in turbulent Reynolds number (Re) with pressure is responsible for increased turbulent combustion velocities, They showed that, like laminar flame velocities at a fixed Reynolds number, ST dropped with increasing pressure in a fan-stirred explosive, However, they keep Re constant at high pressures by adjusting the intensity levels and integral length scale.

As a result, the reduction in ST seen with increased pressure may also be explained by a fall in u′ Low Lewis numbers (defined as the ratio of the thermal diffusivity of the mixture to the mass diffusivity of the deficient species in the diluent) are related to higher ST values, whereas higher ST values are connected with mixes with Le > 1.

Mixtures containing Le dramatically boost the local burning rates of extended flamelets (laminar flame segments in a turbulent flow), leading to higher ST values. 4. Because ST is very non-linear, it is difficult to determine the sensitivity of the technique to a single parameter. The primary motivation for this research was to find a method for autonomously adjusting the magnitude and size of turbulence.

The classification of these vocabularies into useful subsets allows for easier exploration. At first, a quick review of laminar flames is provided. The turbulent flame brush is developed to classify the many flame shapes often used in investigations of premixed turbulent combustion.**(Domingo and Vervisch 2022) [25]**

The concept of reaction progress variables is explored in depth, leading to the finding of different flame surfaces using various diagnostics. As a result, the

uncertainty associated with estimating turbulent propagating rates is no longer definition-dependent, Various regimes of turbulent combustion (shown by the Borghi diagram) have been analyzed.

Turbulence can have a significant impact on flame propagation in combustion processes. Turbulence refers to the chaotic and irregular motion of fluid flows, which is characterized by fluctuations in velocity, pressure, and other flow properties. In the context of combustion, turbulence affects flame propagation through a variety of mechanisms:

Enhanced Mixing: Turbulence enhances the mixing of fuel and oxidizer, leading to a more efficient and rapid combustion process. In turbulent flows, small-scale eddies and vortices continually stretch and fold the flame front, exposing fresh reactants to the flame and promoting faster combustion rates.

Increased Surface Area: Turbulence creates a higher surface area for contact between fuel and oxidizer due to the creation of numerous small-scale eddies and mixing zones. This increased surface area accelerates the reaction rates and promotes a faster flame front propagation.

Turbulent Flame Speed: Turbulence can increase the effective flame speed compared to laminar (non-turbulent) flames. The turbulent flame speed is influenced by the interaction between the flame front and the turbulent eddies. This can lead to a higher propagation rate for the flame.

Flame Stretching: Turbulence can stretch and distort the flame front, causing its shape to become more convoluted and complex. Flame stretching is influenced by the local flow velocity gradients, and it can either enhance or suppress flame propagation, depending on the conditions.

Turbulence Intensity: The intensity of turbulence can impact flame propagation. High turbulence intensity might lead to better mixing and faster combustion, while excessive turbulence can also lead to flame extinction due to poor fuel-oxidizer mixing.

Turbulent Combustion Regimes: Turbulent combustion can exhibit different regimes based on the interaction between turbulence and flame dynamics. These regimes include the laminar flamelet regime, distributed reaction regime, and the thin reaction zone regime. Each regime is characterized by different interactions between turbulence and combustion chemistry.

Turbulence Modeling: Predicting turbulent flame propagation accurately requires complex modeling approaches, as turbulence is inherently challenging to simulate and analyze. Researchers often use techniques such as Reynolds-Averaged Navier-Stokes (RANS) simulations, Large Eddy Simulations (LES), and Direct Numerical Simulations (DNS) to study turbulence-flame interactions.

Turbulent Combustion Instabilities: In some cases, turbulence can lead to combustion instabilities, where pressure fluctuations couple with the heat release from the flame. These instabilities can result in undesirable effects like flame blowout, increased emissions, and even damage to combustion systems.

In practical applications, understanding and controlling the interaction between turbulence and flame propagation are crucial for optimizing combustion processes in various industries, such as energy generation, transportation, and manufacturing. Proper design and operation of combustion systems require a balance between enhancing combustion efficiency through turbulence and avoiding detrimental effects like combustion instability

2.2 Turbulent flame speed

The term "turbulent flame speed" describes how a flame spreads within a turbulent flow. It determines how rapidly the flame front travels through the fuel/oxidizer combination in turbulent conditions Because of its relevance to the issue, this discussion will be limited to flames that spread spherically Measurements of the velocities of laminar flames are discussed in detail by De Vries **(De Vries 2009)[26]**. A spreading flame in a sphere is one of the most common geometries for studying laminar propagation velocities The experimental setup is a sealed cylinder or spherical container with a central hole for a spark plug.

A spherical flame starts to spread at virtually constant pressure, and then the pressure rises dramatically (usually by a factor of 10 to 7) Flame propagation rates can be estimated by visually monitoring the flame's expanding radius or applying a thermodynamic model to the dynamic pressure trace of the combustion process. Flame grenades may be observed at two different velocities **(Bradley, Gaskell et al. 1996)[27]**. For starters, the rate at which the flame's front edge spreads into the unburned mélange (or any other surface within the flame, as determined by diagnostics) is a key factor. This measurement is the rate at which unburned gases are consumed at the flame front and is also known as stimulation, engulfment, or displacement speed. Using the pressure tracer from a dynamic pressure sensor located within the flame explosion, one may calculate the rate at which burned gases are produced by multiplying the pressure trace by the density of the burned gases. The term "laminar combustion velocity" describes this phenomenon.

Designers of internal combustion engines (IC engines) are interested in flame speeds (how far a flame goes when ignited). When calculating the pressure rise due

to an explosion, the latter value (burning velocity) is relevant in safety applications. For non-stretching, planar flames, the two speeds are the same.

2.3 Turbulent flame brush

A turbulent flame brush refers to the structure and behavior of a turbulent flame, a combustion process involving a mixture of fuel and oxidizer in the presence of turbulence. In a turbulent love, the flame front is not a simple, smooth surface but a complex, wrinkled structure known as a flame brush.

Various flame fronts with varying curves and intensities characterize the flame brush. It consists of a network of flame surfaces, with areas of high flame intensity known as "flamelets" interspersed with lower-intensity regions The flame brush structure arises due to the interaction between the turbulent flow and the chemical reactions occurring in the flame.

Turbulence plays a crucial role in enhancing combustion by increasing the mixing of fuel and oxidizer, which leads to quicker reaction rates and higher heat release. The turbulent flow causes the flame to fold, stretch, and interact with different regions of the mixture, resulting in a highly complex flame brush structure**(Tamadonfar and Gülder 2015)[28].**

The flame brush concept is essential in understanding the fundamental characteristics of turbulent combustion, such as flame propagation, flame stabilization, and pollutant formation. It is particularly relevant in practical combustion applications, such as internal combustion engines, gas turbines, and industrial furnaces, where understanding and controlling turbulent flames is crucial for efficient and clean combustion.

Contact a turbulent flame A laminar flame front is a high-temperature zone (light wave) that travels into an explosive mixture at laminar flame speed. In contrast, a turbulent flame brush (t) is denser than a laminar flame.(Benim and Syed 2015) **[29]**

Depending on the flow turbulence, the laminar flame structure may be maintained. The combustion zone, bounded by burned and unburned gases, is called the flame brush. Based on the turbulent flame brush, the numerous flame morphologies typically employed in premixed turbulent combustion can be divided into two main categories**(Lipatnikov 2012) [21]**:

(a) developing or growing a flame brush

(b) fully evolved flame brush

Examples of the former include Bunsen burners, v-flames, and fan-stirred explosives. In contrast, the latter consists of twin counter-flows, stagnation flows, and low-swirl flames (see Fig. 2.1).

A fluctuating flame with a spatially airable flame brush is stabilized at the burner periphery for the Bunsen flame. The thickness of the flame brush increases as one moves away from the flame receptacle.

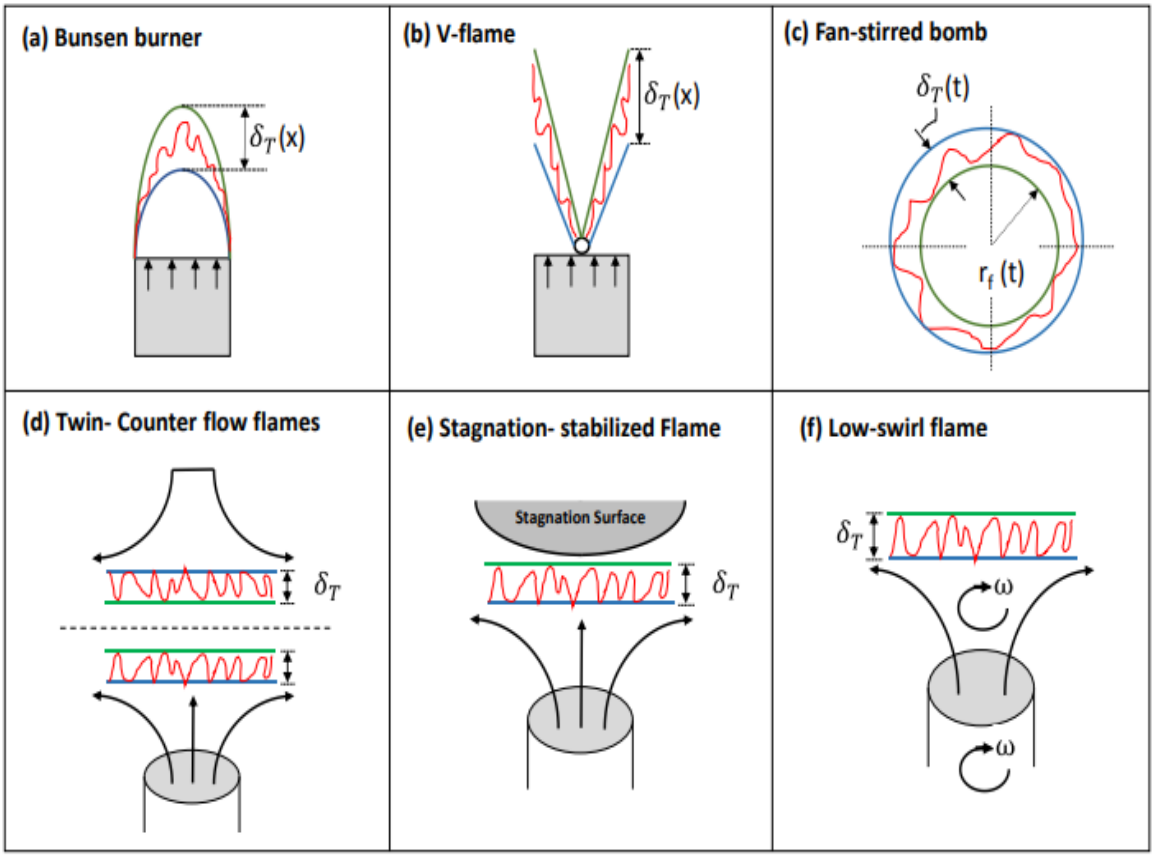

Figure (2.1) Turbulent flame brush thickness. Developing flame brush (brush thickness varies spatially or temporally) - (a) Bunsen burner (b) v-flame (c) fan-stirred bomb. Fully developed flame brush (characterized by constant brush thickness) (d) stagnation flow burner (e) low-swirl burner

The result is the formation of an inverted conical v-flame, which is stabilized by recirculation zones behind the rod Figure (2.1) Turbulent flame brush thickness. Developing flame brush (brush thickness varies spatially or temporally) **(Halouane, 2017) [30]**.

For the Bunsen flame, a fluctuating flame with a spatially variable flame brush is stabilized at the burner's periphery. As one proceeds away from the flame receptacle, the flame brush increases in thickness. Putting a rod in the center of the burner's

outlet produces a V-shaped flame. As a result, recirculation zones behind the rod stabilize the formation of an inverted conical V-flame.

Extends in a spherical manner. The turbulent flame brush is created by turbulent eddies' random advection of the flame's surface **(Lipatnikov 2012)[21]**. In such a framework, Taylor's law of turbulent diffusion governs the development of the mixture layer, comparable to the flame brush's expansion. Consequently, the increase in bristle thickness can be represented by**(Renou, Mura et al. 2002) [31]**.

$$\delta_t = \sqrt{2\pi}\, L' \left\{ 2t' \left[1 - \frac{1}{t'} \left(1 - e^{-t'} \right) \right] \right\}^{0.5} \qquad (2.1)$$

$$\mathrm{L}'_0 = L_T \Big/ \left(1 + {}^{s_L^0}\!/_{2u'} \right) \qquad (2.2)$$

$$\tau'_T = \mathrm{L}'_0 / u' \quad and \; t' = t/\tau'_T \qquad (2.3)$$

Statistically, stationary flame brushes can also be attained in premixed turbulent combustion. The mean brush thickness is constant after the initial ignition transient for twin-counter flow, stagnation, and low-swirl flames. Nevertheless, the principle regulating these flames' vegetation growth differs from the developing flames discussed earlier. Here, the mean flow is decelerating away from the burner for the completely developed brush case.

For example, the velocity fields of a stagnation flame can be characterized as $ux = U - atx$ and $ur = atr/2$ for the axial and radial velocities respectively (x is the distance from the burner output) **(Lipatnikov 2012) [21]**.

As we move away from the stagnation surface, the random advection of the flame by turbulent eddies is countered by the strong mean flow gradient (at the mean strain rate).

The mean strain rate then limits the flame brush's fluctuations The same principle can be applied to twin-counterflow and low-swirl stabilized flames with divergent mean flows (from the burner output). While this class of flames is useful for determining the properties of fully developed turbulent flames, practical flames (IC engines and gas turbines) are developing in nature and take considerably longer ($\sim \tau t SL2$) to reach full development. **(Lipatnikov 2012) [21]**

2.4 Reaction progress variable

In the context of chemical reactions, the reaction progress variable (also known as reaction extent or reaction coordinate) is a measure that describes the progression of a chemical reaction from the starting materials to the products. It quantifies the time to which a reaction has occurred and provides a way to track the transformation of reactants into products.

The reaction progress variable is typically represented by a parameter, denoted as "x" or "ξ" (xi), which ranges from 0 to 1. At the beginning of the reaction, when no products have formed, the value of the reaction progress variable is 0. As the reaction proceeds and products are created, the value of the reaction progress variable increases towards 1.

The reaction progress variable c in a tumultuous flame brush identifies surfaces by determining the degree of combustion completion, typically ranging from 0 (unburned gas) to 1 (burned products) defined as the normalized temperature, density (Eq. 4),

$$\langle c \rangle = \frac{\bar{T} - T_u}{T_b - T_u} = \frac{\bar{\rho} - \rho_u}{\rho_b - \rho_u} \qquad (2.4)$$

The reaction progress variable is often related to the stoichiometry of the reaction. For example, in a simple reaction where reactant A is converted to product B, the reaction progress variable can be defined as the ratio of the amount of A that has reacted to the initial amount of A present.

In fan-stirred explosives, optical techniques such as Schlieren imaging and indirect methods, such as the pressure-trace method, are frequently employed. The c of the average flame surface identified by the two techniques is distinct. Bradley et al. **(De Vries 2009) [26]** discovered that the Schlieren edge coincided statistically with a flame surface with an average c of 0.1. In the same investigation, they also

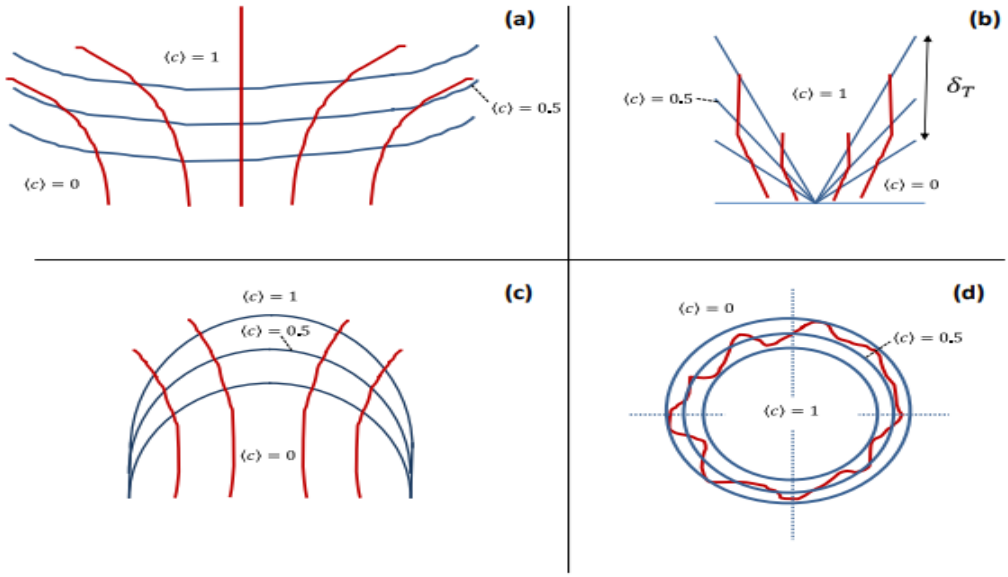

Figure 2.2 $\langle c \rangle$ Isocontours for various flame configurations- (a) stagnation flow-stabilized burner (b) V-Flame (c) Bunsen burner (d) spherically (statistical) expanding flame. The various isocontours in spherical flames are identified by their corresponding radii

determined that the c = 0.6 flame surface correlates directly with the radii deduced from the dynamic pressure trace. Figure (2.2) shows different contours for a few flame configurations. The reaction progress variable is useful for understanding and analyzing reaction kinetics, as it allows scientists to determine the rate at which a reaction occurs and to compare reaction rates under different conditions. It also helps in the development and optimization of chemical processes and the design of reaction mechanisms.

2.5 Turbulent propagation rates

Turbulent propagation rates refer to the speed at which turbulence propagates through a fluid or gas. Turbulence is characterized by irregular and chaotic motion of fluid particles, which can occur at various scales, from large-scale eddies to small-scale fluctuations.

The propagation rate of turbulence depends on several factors, including the nature of the flow, the Reynolds number, and the length and time scales involved. In general, turbulent propagation rates are relatively fast compared to laminar flows.

In a turbulent flow, energy is transferred from large-scale eddies to smaller scales through a process called energy cascade. This transfer of energy leads to the propagation of turbulence throughout the fluid. The speed at which this propagation occurs can vary depending on the specific flow conditions.

It is important to note that turbulent propagation rates are highly complex and can be challenging to predict accurately. Numerical simulations and experimental measurements are often used to study and characterize turbulent flows and their propagation rates in specific situations.

Dependency in the definition Two common measures of turbulent combustion rates are global consumption (UT, c) and displacement speeds (ST, c), both of which appear in the literature**(Renou, Mura et al. 2002) [31]**.

The rate of global consumption is calculated by dividing the mass burned over a mean flame surface by the product of the flame's surface area and the density of any extra gases that aren't being consumed.

The measured wave speed is subtracted from the velocity of the unburned gas in a direction normal to the flame to determine the displacement speed, also known as the entrainment speed or engulfment speed.

ST, c is often calculated at the flame brush's periphery, whereas UT, c is typically measured at the brush's center, where c = 0.5, with a value of c of 0.05 or 0.1 measured at the flame's front.

UT, c might be used if the rate of consumption of reactants was required. ST, c is sufficient for determining the rate at which the flame's leading edge will travel a certain distance (for instance, within an engine). There should be no direct comparison between consumption and displacement speeds It's only possible to compare flame forms by their respective speeds within each category.

An easy way to illustrate the difference between the two definitions is to consider the case of a planar turbulent flame with an evolving flame brush. Inside the brush, you can make out several distinct "c" surfaces, all moving at different velocities but having the same total area (A) For spherical flames, this difference is proportional to dT/dt, whereas for burner flames stabilized at the flame holder, it is proportional to U/dT/dx (where U is the mean flow velocity and x is the axial distance from the flame holder) **(Lipatnikov and Chomiak 2002) [23]**.

Therefore, the rate of displacement is what distinguishes one surface from another. As a result, the displacement velocity inside the flame brush varies with c and cannot be accurately defined for a flat scenario.

The global consumption speed for the planar turbulent flame**(Lipatnikov and Chomiak 2002) [23]** is obtained by dividing the global burning rate over the flame brush, d dt (c A dx), by u A; UT is independent of c and is well-defined (a single value) for the fundamental planar shape. Curved and defined by an evolving flame brush, real flames have not yet been observed in practical applications.

Using the same reasoning, we can show that the curved flames cannot have a fixed ST, c value Since the areas of the different surfaces vary due to flame curvature, the estimation of UT, c, also depends on the titer surface used. The divergence in optimization, dependent on the flame shape, significantly affects the changes in adjustments, speeds, and fuel consumption **(Wabel, Skiba et al. 2017)[32]**.

Displacement speeds exceed consumption speeds in devices with diverging streamlines, such as low-swirl burners and fan-stirred bombs. On the other hand, Bunsen burner flames display an opposite pattern because of the negative-stretch configuration, which is convex toward the unburned gas **(Renou, Mura et al. 2002) [31]**.

The turbulent combustion regime diagram is a graphical representation that illustrates the relationship between turbulence intensity and combustion regime in a combustion system. It helps to understand how the level of turbulence affects the combustion process and the resulting flame behavior.

In the diagram, the x-axis represents the turbulence intensity, which is a measure of the turbulent motion or agitation present in the combustion system. It could be

quantified using parameters such as the turbulence kinetic energy or the turbulence intensity scale. The y-axis represents the combustion regime, which refers to the nature of the flame and its characteristics.

The diagram typically consists of multiple regions or zones that correspond to different combustion regimes. These regions may vary depending on the specific classification scheme used, but some commonly recognized regimes include:

Laminar Flame: This region represents low turbulence conditions where the flame is steady and exhibits laminar characteristics. The flame front is smooth and well-defined, with minimal flame wrinkling.

Turbulent Flame: As the turbulence intensity increases, the flame transitions into the turbulent regime. In this region, the flame becomes highly wrinkled and exhibits increased flame surface area due to the interaction with turbulent eddies. Turbulent mixing enhances fuel-air mixing and combustion rates.

Distributed Combustion At higher turbulence intensities, the flame becomes more distributed and fragmented. The combustion process becomes more chaotic, and the flame no longer maintains a well-defined front. Flame structures become smaller and more dispersed throughout the combustion region.

Turbulent Combustion In this regime, the combustion process is dominated by turbulence. The flame is highly unstable, with intense flame front wrinkling and significant flame interactions with turbulent eddies. Turbulent mixing becomes the primary mechanism for fuel-air mixing and combustion **(Poludnenko and Oran 2011)[33]**.

The specific shape and boundaries of the regions on the diagram can vary depending on the combustion system and the characteristics of the fuel being burned. Experimental data and computational simulations are often used to determine and validate the boundaries of each regime.

The turbulent combustion regime diagram is a useful tool for understanding and optimizing combustion processes in various applications, including internal combustion engines, gas turbines, and industrial furnaces. By analyzing the combustion regime and its relationship with turbulence,

According to Damköhler **(Peters 1999) [34]**, turbulent flame propagation may be broken down into two distinct regimes: large-scale turbulence and small-scale turbulence. The relationship between the furrowed flame front and the turbulent flow field in large-scale turbulence is fundamentally kinematic and scale-free.

A function for a ratio of turbulent to laminar burning velocity in terms of the turbulent magnitude u′ and SL (Eq. 5) **(Pocheau 1992)[35]**- with n, C =1) was obtained by comparing the mass flux of unburned gas of a wrinkled flame surface burning at the laminar flame speed with that of a mean flame front burning with the turbulent burning velocity.

As turbulence altered the reaction zone and the unburned reactants, he demonstrated that this ratio depends on the ratio of turbulent to molecule diffusivities (Eq. 6). It is obvious that the turbulent burning speed is always greater than the laminar flame, and this holds throughout all turbulence regimes.

2.6 Spherically expanding turbulent flames

Measurement of turbulent flame speeds (ST) inside a fan-stirred vessel was first demonstrated by Semenov **(Yakovenko, Kiverin et al. 2022)[36]**. Subsequently, several research groups have developed similar apparatus. The flame kernel is initiated at the center of the vessel and grows radially outwards while subjected to a zero-mean, uniform turbulence. High-speed schlieren imaging, laser tomography, and pressure trace measurements are the commonly employed measurement techniques used to track the flame propagation rate. This configuration offers several advantages over a burner-type setup wherein high mean flow velocities are required to achieve strong intensity levels and to stabilize high SL flames on the burner. Moreover, the uniformity of the flow field is difficult to control in a burner and is affected by the downstream decay of turbulence due to boundary layer interference**(Renou, Mura et al. 2002) [31]**.

Table 1. Experimental conditions

Conditions	Fuel/air mixture	u' (m/s)	u'/U (%)	L_0 (mm)	τ_T (ms)	Φ	S_L^0 (m/s)	u'/S_L^0	Re_T	Le
C1	C_3H_8/air	0.34	9	6.5	19.1	1.00	0.40	0.85	146	1.40
C2	CH_4/air	0.34	9	6.5	19.1	1.00	0.37	0.92	146	1.01
C3	H_2/air	0.18	4	3.0	16.7	0.27	0.18	1.00	36	0.33
C4	C_3H_8/air	0.51	12.5	6.0	11.8	1.00	0.40	1.28	202	1.40
C5	CH_4/air	0.51	12.5	6.0	11.8	1.00	0.37	1.38	202	1.01
C6	H_2/air	0.34	9	6.5	19.1	0.27	0.18	1.89	146	0.33

A fan-stirred vessel eliminates such disadvantages associated with a flowing system and enables flame speed measurements in HIT conditions even at large values of u′. However, turbulent explosion vessels are extremely challenging to design and are highly cost prohibitive to build.

Additionally, the problem of unsteady flame propagation is compounded by the lack of a well-defined surface that can be used to tag the measured 46 burning velocity. Nevertheless, recent studies **((Renou, Mura et al. 2002) [31])** have shown these difficulties can be circumvented through appropriate assumptions. Table 2 surveys some of the existing facilities developed to study spherically expanding, turbulent flames. Some cells in the table are left blank as data were not provided in the literature. The two parameters that are commonly used to describe such flow fields are the turbulence intensity (u′) and the integral length scale (LT). There is sufficient clarity on the effect of u′ on turbulent flame speeds. ST initially increases with u′, reaches a maximum and then decreases until flame quenching is observed.

Table 2. Mean direction cosine

Fuel/air mixture	u'/S_L	$1/\langle\lvert\cos\theta\rvert\rangle$	STD $(\langle C\rangle, t)$	$1/\langle\lvert\sigma_y\rvert\rangle$	STD $(\langle C\rangle, t)$	$\langle 1/\lvert\cos\theta\rvert\rangle$	STD $(\langle C\rangle, t)$	$\langle 1/\lvert\sigma_y\rvert\rangle$	STD $(\langle C\rangle, t)$
Propane/air	0.85	1.60	0.015	1.92	0.017	3.02	0.158	3.16	0.175
Methane/air	0.92	1.58	0.024	1.90	0.019	2.96	0.315	3.10	0.230
Hydrogen/air	1.00	1.50	0.018	1.81	0.018	2.71	0.332	2.91	0.293
Propane/air	1.28	1.52	0.012	1.89	0.013	3.02	0.166	3.19	0.189
Methane/air	1.38	1.57	0.015	1.88	0.016	2.94	0.267	3.09	0.219
Hydrogen/air	1.89	1.54	0.017	1.85	0.014	2.80	0.197	2.96	0.188

At low-intensity turbulence (u′ < SL), flame propagation dominates the flame wrinkling caused by turbulence, and this regime is not of relevance to industrial systems. However, at higher intensity levels (u′ > SL), marked intensification of flame speeds due to the enhanced heat and mass transfer rates is affected by turbulent diffusion.

The turbulence intensity inside a fan-stirred vessel is typically varied by adjusting the rotational speeds of the fans. The mean velocity is negligible at the center of the vessel and gradually increases as the fans are approached.

A majority of the facilities listed in Table 1 report a uniform velocity field in a spherical region at the center of the vessel with the exception of two studies. Leisenheimer and Leuckel **(Zhen and Leuckel 1997)[37]** and Weiß et al. **(Weiß, Zarzalis et al. 2008)[38]** have indicated the existence of a non-linear, radial velocity distribution inside a spherical flame speed vessel

2.7 Turbulent combustion regime diagram

The turbulent combustion regime diagram is a graphical representation that illustrates the different combustion regimes experienced in turbulent flow conditions. It typically plots the turbulence intensity (or turbulence level) against the Damköhler number (Da) or the Karlovitz number (Ka)**(Martínez-Sanchis, Sternin et al. 2022) [39].**

The turbulence intensity characterizes: The level of turbulence in the flow, indicating how turbulent the mixture of fuel and oxidizer is. It is usually measured using parameters such as the turbulent kinetic energy or the root-mean-square velocity fluctuations.

The Damköhler number (Da) and the Karlovitz number (Ka): provided information about the relative timescales of chemical reactions and turbulence in the combustion process. It is defined as the ratio of the characteristic turbulent timescale to the characteristic chemical reaction timescale.

The Damköhler number compares the turbulent mixing timescale with the chemical reaction timescale, while the Karlovitz number compares the turbulent eddy turnover timescale with the chemical reaction timescale.

The turbulent combustion regime diagram typically consists of multiple regions or zones that represent different combustion regimes. These regimes include:

Laminar Flamelet Regime: This regime occurs at low turbulence intensities and low Damköhler or Karlovitz numbers. In this regime, the combustion process is primarily governed by laminar flame propagation, and the flame structure is relatively unaffected by turbulence.

Distributed Reaction Regime: This regime occurs at moderate turbulence intensities and intermediate Damköhler or Karlovitz numbers. In this regime, the combustion process is influenced by both turbulent mixing and chemical reactions. The flame structure becomes more wrinkled and fragmented due to the interaction between turbulence and combustion.

Turbulent Flame Regime: This regime occurs at high turbulence intensities and high Damköhler or Karlovitz numbers. In this regime, the combustion process is dominated by turbulent mixing, and the flame structure becomes highly convoluted and fragmented. Turbulent eddies promote rapid mixing of the reactants, enhancing combustion.

The boundaries between these different regimes on the diagram are not sharply defined but rather represent transitional regions where the influence of turbulence and chemical reactions gradually changes.

In turbulent flame propagation, Damköhler hypothesized that large-scale and small-scale turbulence could be distinguished. In large-scale turbulence, the interaction between the furrowed flame front and the turbulent flow field is inherently kinematic and scale-free.

The ratio of turbulent to laminar burning velocities can be calculated in terms of the turbulent intensity u′ and SL (Equation 2.5) **(Pocheau 1992) [39]**- with n, C =1) by comparing the mass flux of unburned gas from a wrinkled flame surface burning at the laminar flame speed to that of a mean flame front burning at the turbulent burning velocity.

Because turbulence altered both the reaction zone and the unburned reactants, he demonstrated that this ratio is proportional to the ratio of turbulent to molecular diffusivities (Equation 2.6). The turbulent flame travels faster than the laminar flame, regardless of the turbulence regime.

For large-scale turbulence1, $\frac{S_T}{S_L} = (1 + C\,(\frac{u'}{S_L})^n)^{\frac{1}{n}}$ (2.5) For small-scale turbulence, $\frac{S_T}{S_L} = \left(\frac{D_t}{D}\right)^{0.5} = (\frac{u'}{S_L}\frac{L_T}{\delta})^{0.5}$ (2.6)

Where LT represents, respectively, the integral length scale of turbulence and the laminar flame thickness, several regimes of turbulent combustion have been identified and classified in the Borghi diagram (Fig. 2.4) **(Borghi 1985)[40]** since the classical Damköhler formulation. Re, Da, and Ka define the boundaries of the

Borghi diagram, a log-log plot of the normalized intensity (u′/SL) and the normalized turbulence length scale (LT/).

The region below ReT = 1 defines laminar flame propagation. In the region circumscribed by ReT 100, a weak turbulent sub-regime exists in which the turbulent field does not adhere to the classical Kolmogorov scaling. Re > 1 characterizes the numerous tumultuous combustion regimens considered here. When chemical time scales are longer than turbulent ones, the well-stirred reactor regime corresponds to Da 1. When Ka 1 and Da > 1, the flame mode of turbulent flame propagation is present.

In the flamelet mode, the laminar flame structure, which consists of the reaction and preheats zones, is unaffected, and the flame front propagates as laminar flame segments furrowed by the superimposed turbulent field. In the flamelet regime, the smallest eddy present in the turbulent flow is larger than the laminar flame thickness.

The increase in turbulent burning rate is controlled by two competing processes: the creation of the flame surface area via wrinkling by turbulent eddies and the destruction of the flame surface area via self-propagation of the leading edge of the flame brush**(Lipatnikov 2012) [20]**.

The flamelet mode can be subdivided into the wrinkled and corrugated flamelet regimes (mild and moderate turbulence, respectively), and u′/SL= 1 separates the two regimes. Ka = 1 (the Klimov-William's limit) distinguishes the flamelet from the distributed-reaction-zone regime (Ka > 1 and Da > 1) of turbulent combustion.

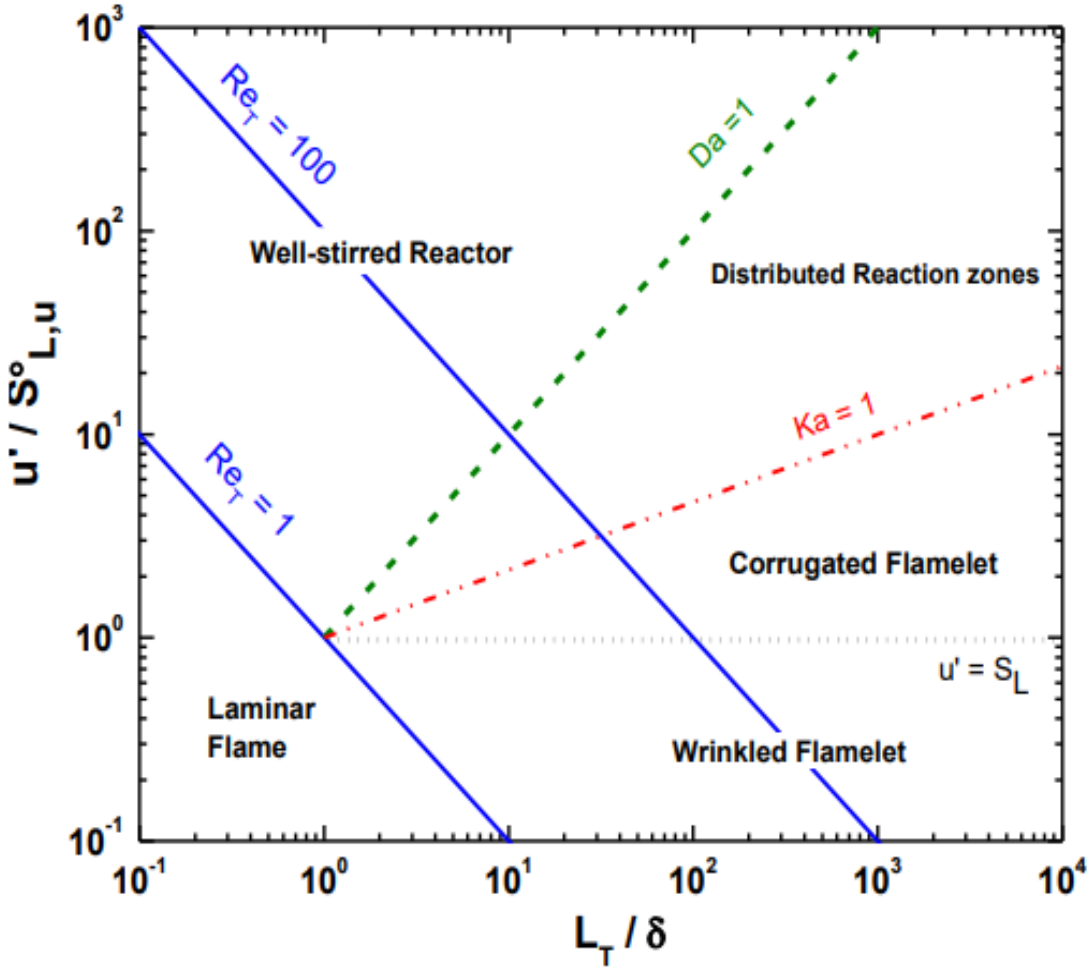

Figure (2.4) Classical turbulent combustion regime diagram (Borghi diagram).

2.8 summery

The terms employed in premixed turbulent combustion pertinent to this study were thoroughly discussed. As a flame is rippled by eddies in a turbulent flow, a dense zone with density fluctuations and heat release proportional to the concentration of unburned gas is produced.

Such dense zones are typical of turbulent premixed combustion and are known as the turbulent flame brush. The numerous geometrical configurations of premixed turbulent combustion were categorized as flame brushes that were either growing or fully developed. The flames of a Bunsen burner, a V flame, and a spherically expanding flame varied. The density of the bristle For the Bunsen burner and V-flames (spatially variable), the brush thickness increased in the axial direction away from the burner outflow.

In contrast, for fan-stirred explosives (temporally variable), the brush thickness decreased as the flame expanded. Flow deceleration away from the burner exit in twin-counterflow, stagnation flow, and low-swirl-stabilized burners enabled the brush to adjust to flow perturbations, resulting in nearly constant thickness or a fully developed flame brush.

Similarly, the growth in flame brush thickness can be predicted using Taylor's law of diffusion, and flames in practical combustion systems such as gas turbines and internal combustion engines are also characterized by expanding flame brushes.

The reaction progress variable, whose values ranged from 0 (for reactants) to (for products), was used to distinguish between different flame surfaces within the flame brush. The propagation rates for all geometries varied based on the response progress variable.

The reaction progress variables (c) were specified at various radii within the flame brush of fan-stirred explosives, and their corresponding flame surfaces expanded at different rates. The c of the two most commonly used diagnostic methods in fan-stirred explosives, Schlieren imaging and the pressure-trace method, was (100, 200 and 300 kPa) respectively

Two definitions of turbulent combustion rates have been clarified in depth Global consumption speeds were the rate at which gases were burned, while global displacement speeds were the rate at which a tumultuous flame front diffused into an unburned mixture. Streamline divergence led to a disparity between the two rates. While consumption speeds can be unambiguously defined for planar and tumultuous flames, propagation rates are not well defined for curved flames.

Moreover, within each group, the rates varied based on the flame surface used (a variable for reaction progress).

Finally, the traditional Borghi diagram for turbulent combustion regimes was discussed. The flamelet mode, which maintains the laminar structure of the flame, and the narrow reaction zone regime, in which turbulent eddies penetrate the preheating zone and modify radical transport, have been identified. Using the non-dimensional parameters Reynolds, Damköhler, and Karlovitz numbers, the boundaries between the creased and corrugated flamelet, restricted reaction zones, and well-stirred reaction regimes were determined.

Laminar-flamelet instability (Darrius-Landau) persisted only at low turbulence levels (u′ SL), and the region affected by the instability was depicted on the 1Borghi diagram.

2.9 Aims of The Study

The main aim of this study is to use ammonia as fuel is a practical approach to have the way towards allowing a carbon economy. Ammonia consists of approximately 18% of hydrogen in mass and is accepted as an enabling factor for the combustion of hydrogen with current transport and storage infrastructure.

Liquefied gas petroleum is a good catalyst for ammonia gas during the combustion process due to the high flame speed of LPG compared to ammonia gas, the Boiling point for ammonia equal (-33.34 ˚ C), and the Boiling point for LPG equal (- 44 ˚C) the fuel (ammonia and LPG) and air with pre-calculated data into the combustion chamber, an ignition system, consisting of a coil, electronic push-button, and two opposite electrodes are used to ignite fuel/air mixtures and used in this optical study technique, Schlieren photography, and high- speed camera. the experiment conducted with different initial pressure (100 – 200 – 300 kPa) and initial temperature of (298K). Besides.

the tested equivalence ratios range (0.8, 1, 1.3). The objectives of this work are to use different percentage ammonia and LPG as fuel

To measure experimentally the turbulent flame speed of premixed LPG/ ammonia /Air mixture.

- To use different percentage ammonia and LPG as fuel
- To measure experimentally the turbulent flame speed of premixed LPG/ ammonia /Air mixture.
- To calculate the turbulent burning velocity

Chapter three

EXPERIMENTAL SETUP AND PROCEDURE

Chapter three

3.1 Introduction

An existing laminar flame speed bomb was upgraded to measure turbulent flame speeds as a part of study, to that effect, mixing impellers were installed inside it to generate HIT conditions. The impeller geometry was optimized model of the vessel, The objective of this chapter is to provide a complete description of the features of the upgraded flame bomb and the associated experimental procedure, and is organized as follows, First, the high-pressure, cylindrical laminar flame bomb is introduced. The features of the fan-stirred vessel are then described. For simplicity, schlieren photography was adopted as the diagnostic technique for both laminar and turbulent combustion studies. The post processing procedure used for laminar flame studies was modified for turbulent flames.

3.2 Experimental setup

A description of the experimental rig the chamber and measuring instruments used to investigate experimentally effect of ammonia blending ratio with LPG on combustion system safe operation and flame stability are presented. All experiments were conducted in the Mechanical Engineering Department Laboratories at the University of Babylon **[41]** The complete setup rig is shown in figure (3.1). It consists of the following units:

1. Combustion chamber unit
2. Ignition system and Control unit
3. Impeller Unit
4. Mixture Preparing Unit
5. capturing unit

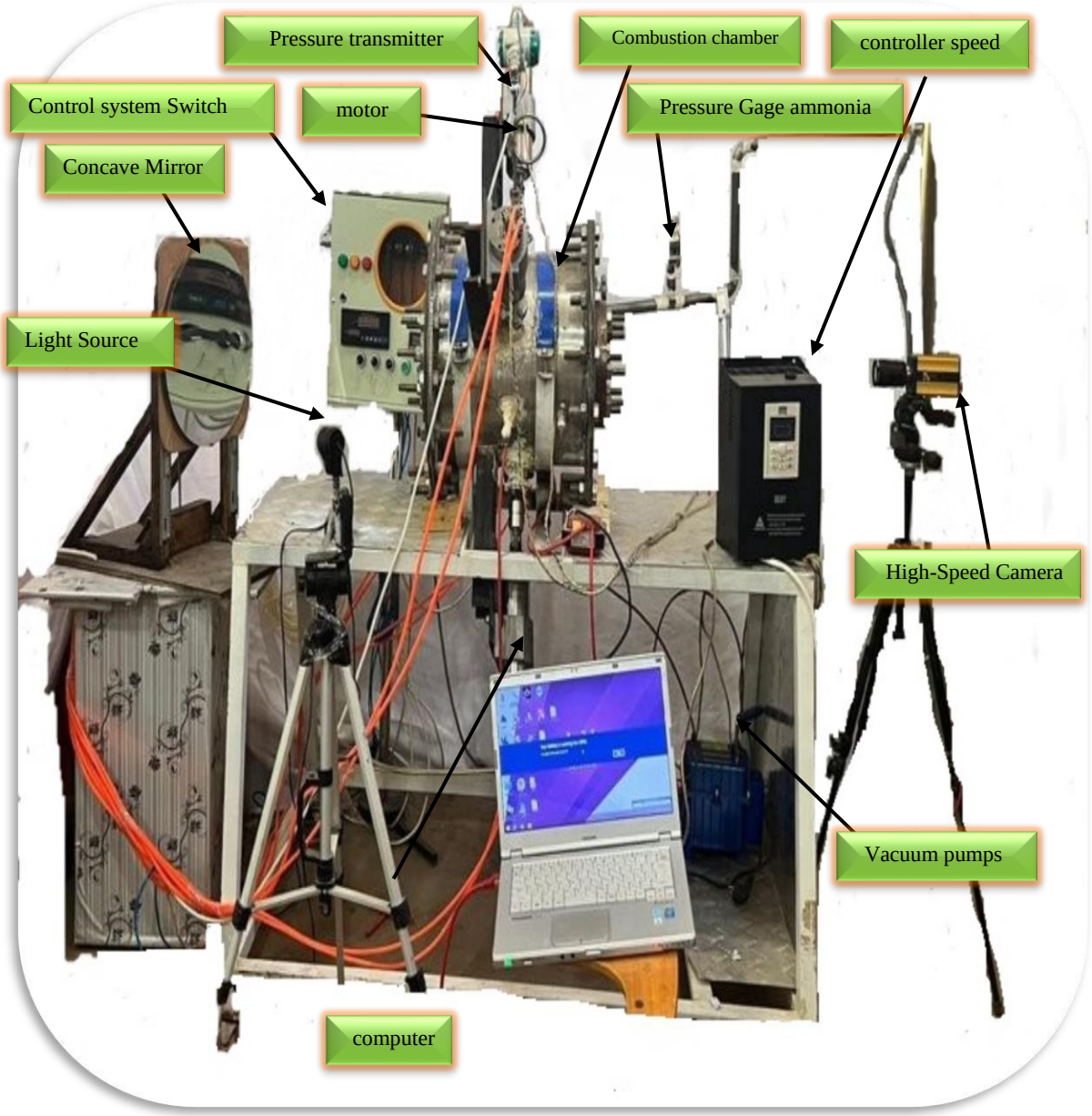

Figure (3.1) photograph of the experimental rig and tools used in the study

3.2.1 Combustion Chamber Unit: -

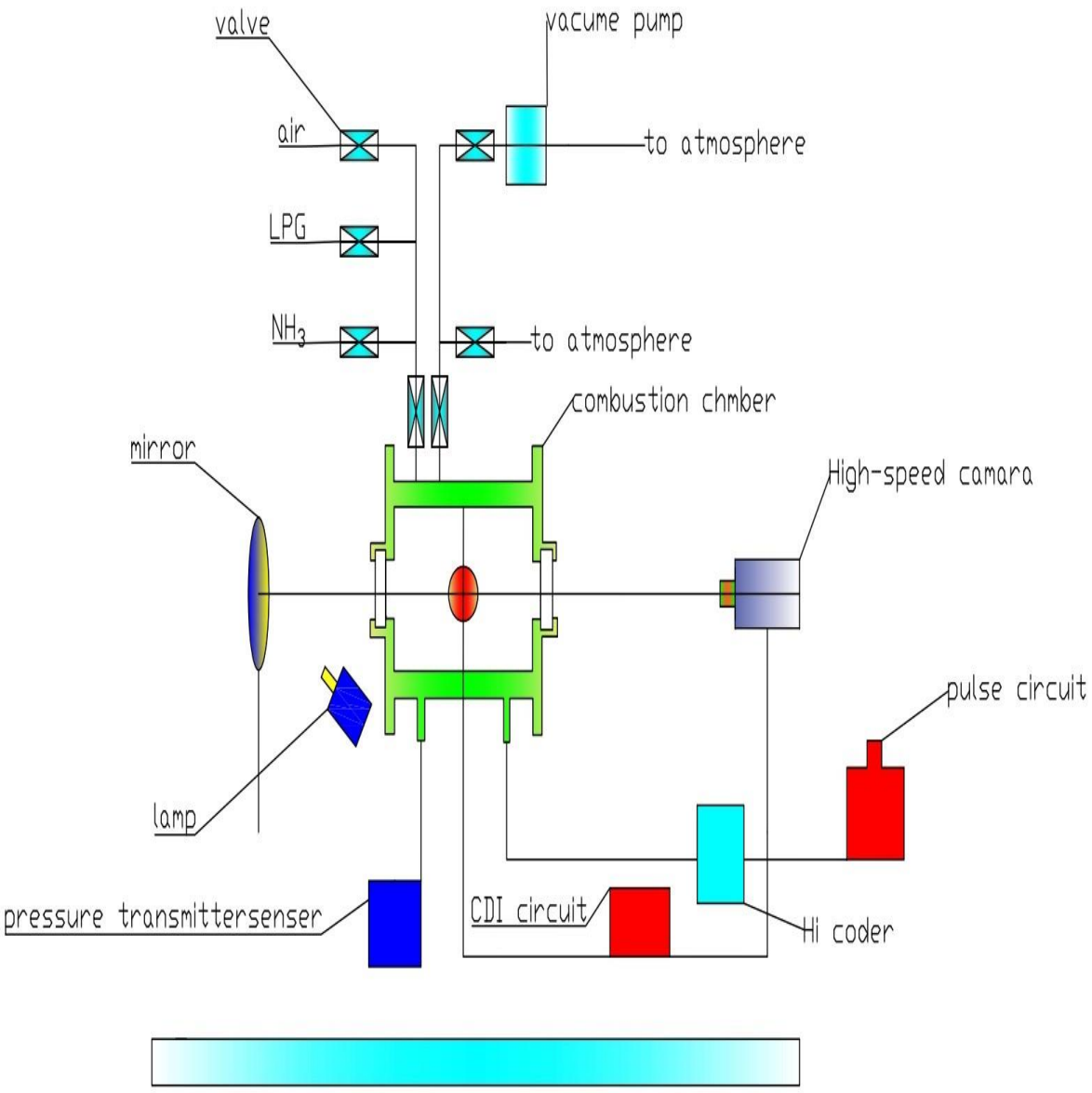

Figure (3.2) schematic diagram for the experimental rig setup

3.2.1.1 Combustion Chamber

A cylinder with a fixed size made of stainless steel that is resistant to experimental conditions, material type Stainless – steel type 304, and its thickness is 12 mm and contains six holes with a diameter of 15 mm .

The volume of the cylindrical chamber is (0. 04899 m^3) with an inner diameter of 395 mm, length 400 mm, two flanges with 12 mm thick lower and upper flanges with diameters of 407mm and 570 mm respectively, which have been made of stainless steel in order to resist the external conditions.

These flanges have been joined with the combustion chamber by sixteen of the hex bolts type 12.1 for every one of the flanges.

The resister–pressure quartile windows of (100 mm, 140 mm) size have been installed on two combustion chamber sides by the flanges for the purpose of allowing the processes of combustion to be accessible optically **[42]**.

The cylinder was provided with two electrodes that was connected centrally to the system of the ignition as shown in figure (3.3). A pressure gauge of type QYBO2 SERIES PRESSURE AND DIGITAL PANAL METER – SERIES.

A fan system was added to obtain turbulence inside the combustion chamber. Four electric motors were installed at an angle of 45 degree using channel iron. And 10 mm thickness plate was welded to it, with four holes perforated for the purpose of installing the electric motor base.

The electric motor was connected to a rotating shaft, and the rotating shaft was connected to a mechanical system containing rollers and a seal. Mechanical, and the group was connected to the fans of the electric motor that needed cooling, so a system of pumps was connected to circulate water inside the

electric motor through a special passage for this purpose. Has been installed in the combustion chamber as shown in figure (3.4).

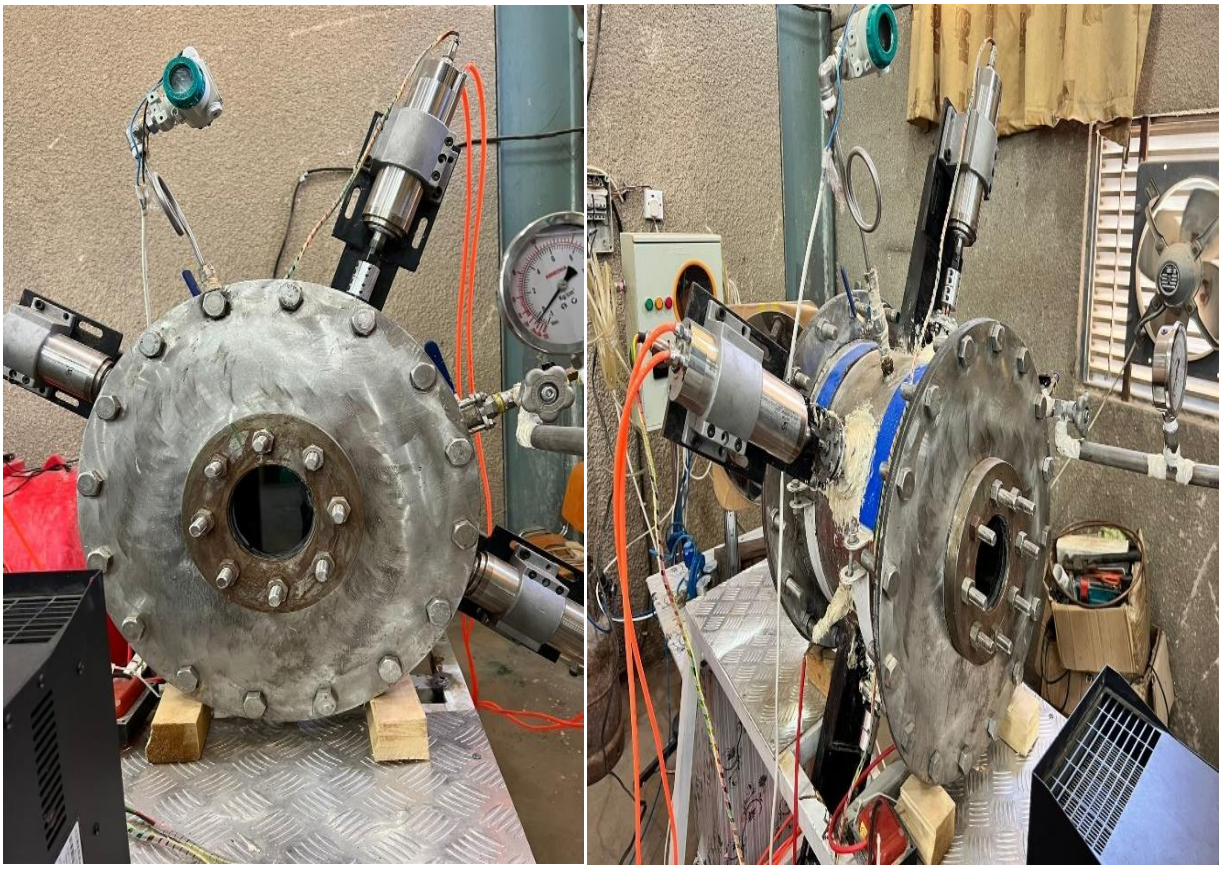

Figure (3.3) Photograph of the Combustion Chamber Unit.

3.2.1.2 Pressure Gauge Transmitter: -

This series of products is suitable for petroleum, chemical, metallurgy, electric power, water conservancy, scientific research, environmental protection, and other various enterprises and institutions, to realize the measurement of fluid pressure and is suitable for various occasions all-weather environment and all kinds of corrosive fluid**.**

- Features Pressure Gauge Transmitter

1. Multi measure range selection
2. Digital LCD display
3. Convenient debugging for zero range
4. Intrinsically safe explosion-proof
5. High performance-price ratio
6. High precision & stability

-Specifications Pressure Gauge Transmitter

Measure range	-0.1 - 100 MPa	Precision	0.2 % - 0.5%
Overload	Output	Output	wi h
Stability	<0.1% /year	Power supply	
Display	5 – digit LCD	Display range	-
Operating temperature	-	Relative humidity	<80%
Thread	M20 * 1.5	Interface material	Stainless steel

Figure (3.4) QYB102 Pressure Transmitter

3.2.1.3 Thermal Gasket: -

To get the required scaling for the combustion chamber and to make sure that no leakage between the flanges. Two thermal gaskets are utilized for every one of the flanges of (1.5). The gasket has made of material thermal asbestos gasket, which is partly yielding such that it can be deformed and fill spaces that they have been designed.

Figure (3.5) Detailed views of the using Thermal Gasket

3.2.1.4 Safety Valve: -

A safety Valve is installed in the lower edge of the combustion chamber for the prevention of any extreme increase of the pressure, which results from the burning procedure within a chamber, and is seized for opening at a high level of the pressure (i.e. 60 bar) for the purpose of avoiding explosions or damage of cylinder.

3.2.1.5 Impeller Unit: -

3.2.1.5.1 Motor

The electric motor was used for the purpose of moving the fan and making turbulence, as a special type was chosen for this purpose. This electric motor has several advantages, including speed control by controlling the frequency, as it can work from 0-400 Hz and a capacity of (2.2) kilowatts.

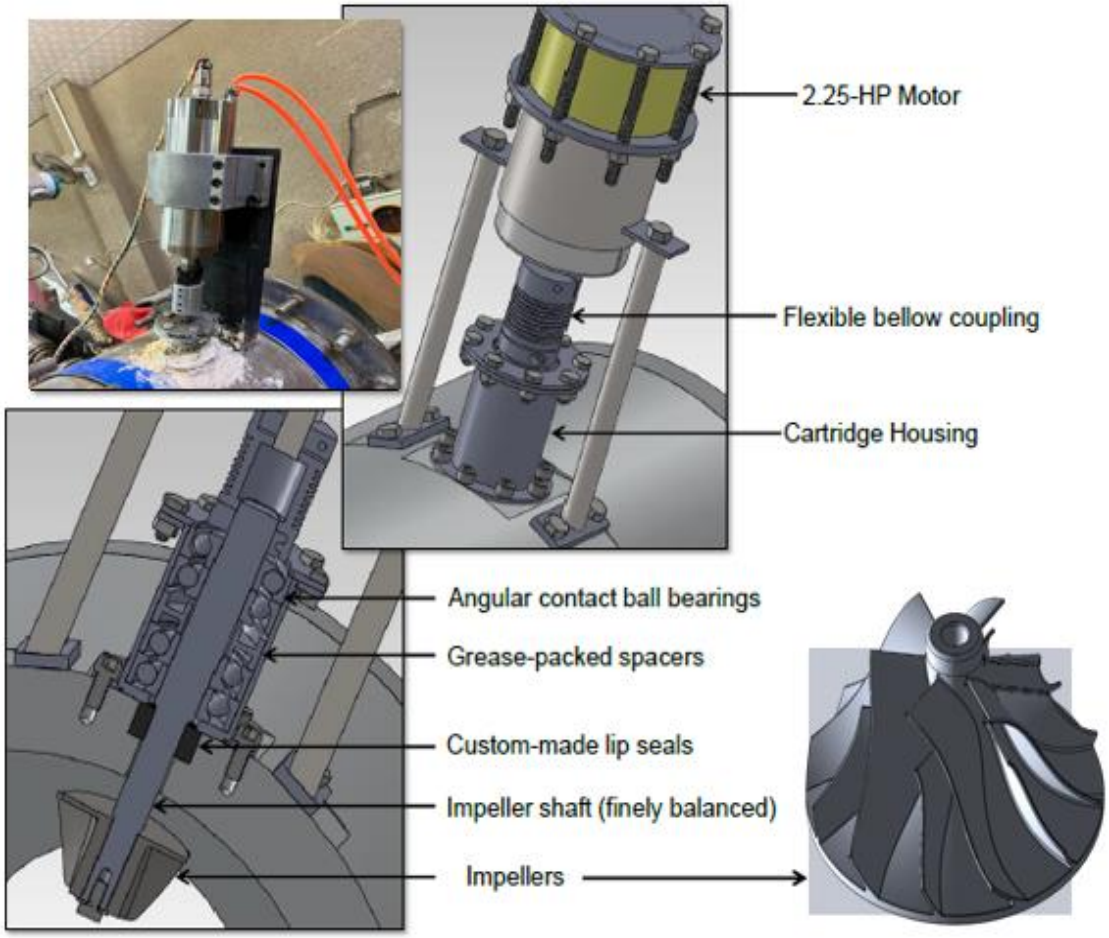

Figure (3.6) Detailed views of the impeller assembly. Various components namely, coupling, cartridge housing, bearings, spacers and seals are shown

Figure (3.7) Detailed views of the spindle motors

Water-cooling is a common method used to cool down spindle motors during operation, especially when they generate significant heat. Water is circulated through the motor to dissipate the heat and maintain the motor's temperature within safe operating limits. This cooling method helps improve the motor's performance, reliability, and longevity 2.2 kW power rating suggests that the motor can deliver 2.2 kilowatts of mechanical power during operation. This power level determines the motor's capability to drive the spindle and perform cutting, milling, or other machining tasks. It is important to consider the power requirements of the specific application to ensure the motor can handle the workload effectively **[43]**.

When using a water-cooling spindle motor, it's necessary to have a water-cooling system in place. This typically involves a pump, hoses, and a radiator or heat exchanger to facilitate the circulation and cooling of water through the motor. The

water-cooling system helps maintain the motor's temperature, preventing overheating and ensuring optimal performance.

Overall, a 2.2 kW water-cooling spindle motor is a powerful component used in various industrial machining applications, providing efficient cooling and reliable operation for demanding tasks [44].

3.2.1.5.2 Controller speed

Frequency control is one of the important parts that have been added, as this device controls the amount of fan speed using frequency, where the speed is controlled by increasing or decreasing the frequency value. This device has the ability to connect four electric motors and they are controlled at the same time, and this gains a lot of time and gives High accuracy of work

Figure (3.8) Details views of the Controller speed

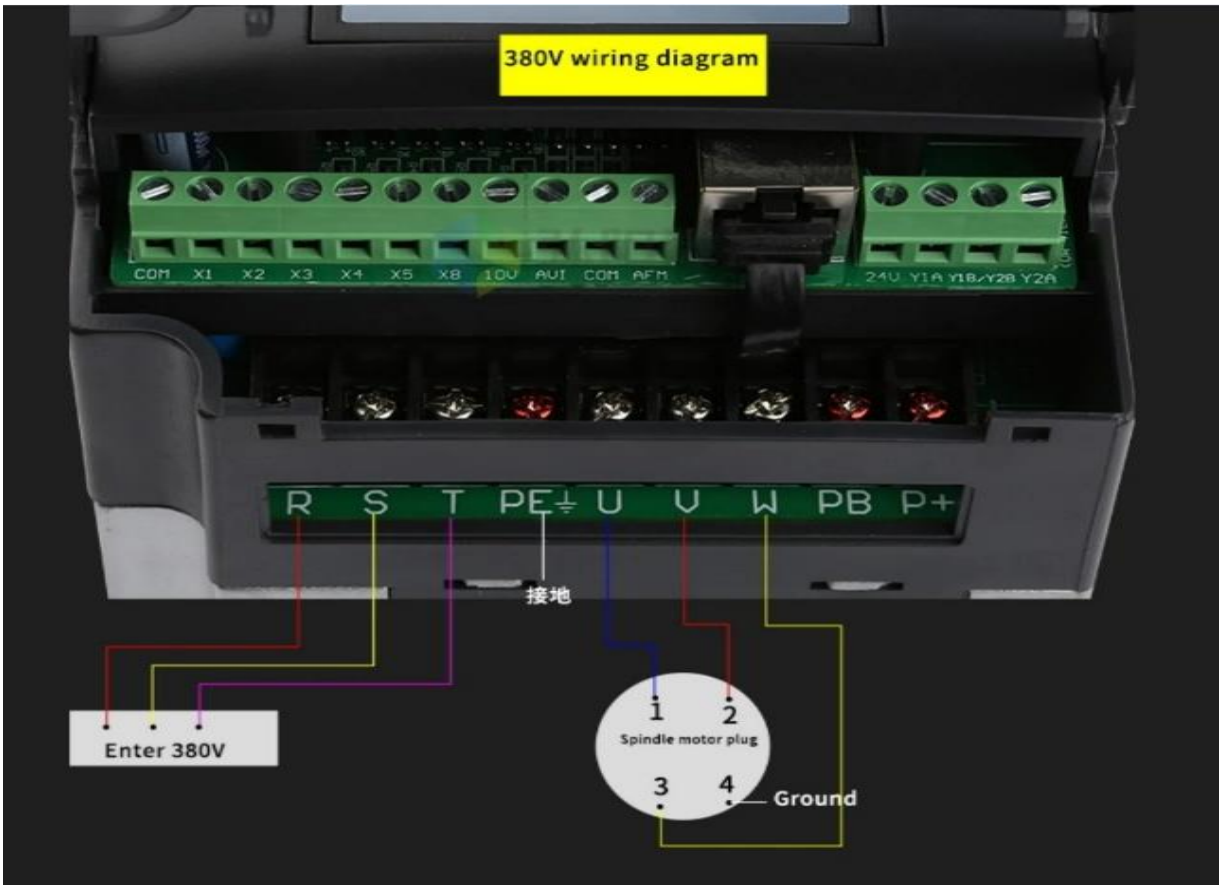

Figure (3.9) Details views of the Controller speed

Inverter advantages

1. The output voltage adjustment method is PWM control and easy to use

2. Protection functions are very strong

3. Built-in fan overheat protection

4. Overload, overcurrent protection

5. Powful function

Inverter characteristics

Restart after instantaneous power failure: after instantaneous power failure, it can be restarted by frequency tracking mode

1. Stall prevention: Stall prevention during acceleration/deceleration operation.
2. Short circuit of output terminal: electronic circuit protection
3. Protection function: return current, overvoltage, under voltage, overload, overheating, voltage anti-stall, current anti-stall, etc.
4. Other functions: reverse rotation limit, direct start and fault reset function after booting, parameter lock, etc.
5. Overload protection: G type machine: 110% rated current for 10 minutes; 150% rated current per minute, 180% rated current per second
   P type machine: 100% rated current for 10 minutes; 150% rated current per second
6. Overvoltage: 220V line: DC voltage>400V; 380V line: DC voltage>800V
   Insufficient voltage: 220V line: DC voltage <200V; 380V line: DC voltage <400V

3.2.1.5.3 Water pump

Water pumps were used for the purpose of cooling the electric motors and were carefully chosen in order to cool them well. A tank of 1000 liters of water was used in order for the pumps to withdraw water from the tank and push it through plastic tubes and into the electric motor, where there is a water inlet that surrounds it,

allowing water to enter around the motor. And his exit from another special hole with another plastic tube to reach the tank

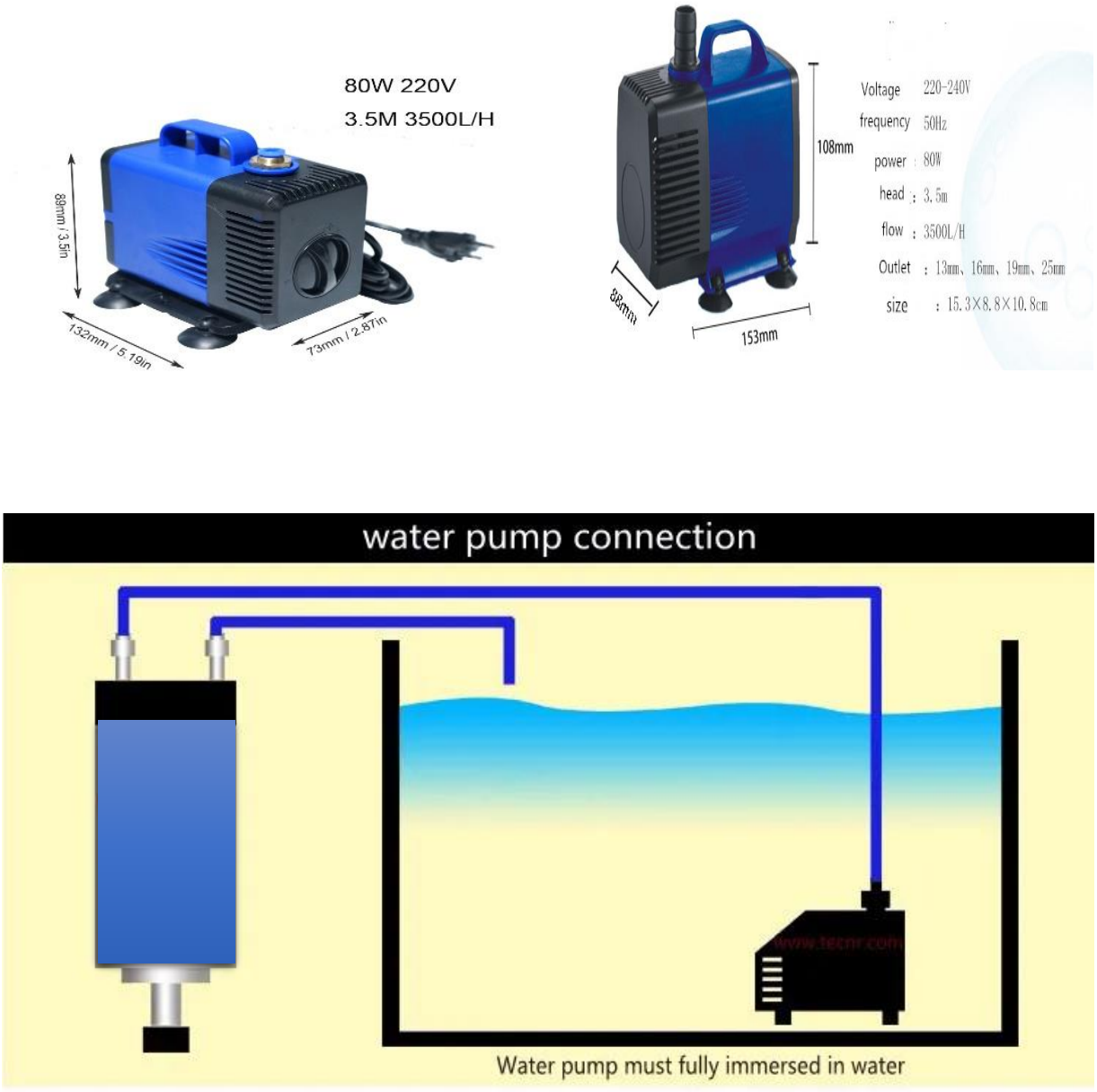

Figure (3.10) Details views of the water pump

3.2.1.5.4 Mechanical rotation and fans

A mechanical rotation part was added to control the rotation of the fan, as well as isolation of the combustion chamber due to the work of holes for the fan and to give friction to the rotor axis with the outer hull of the combustion chamber and to prevent fuel leakage from the combustion chamber, so a part called the mechanical seal was placed A mechanical seal is a device used to seal the gap between two surfaces in mechanical equipment, typically rotating shafts or spindles, to prevent leakage of fluids such as liquids or gases. It is commonly used in various industrial applications, including pumps, compressors, mixers, and other rotating equipment **[45]**.

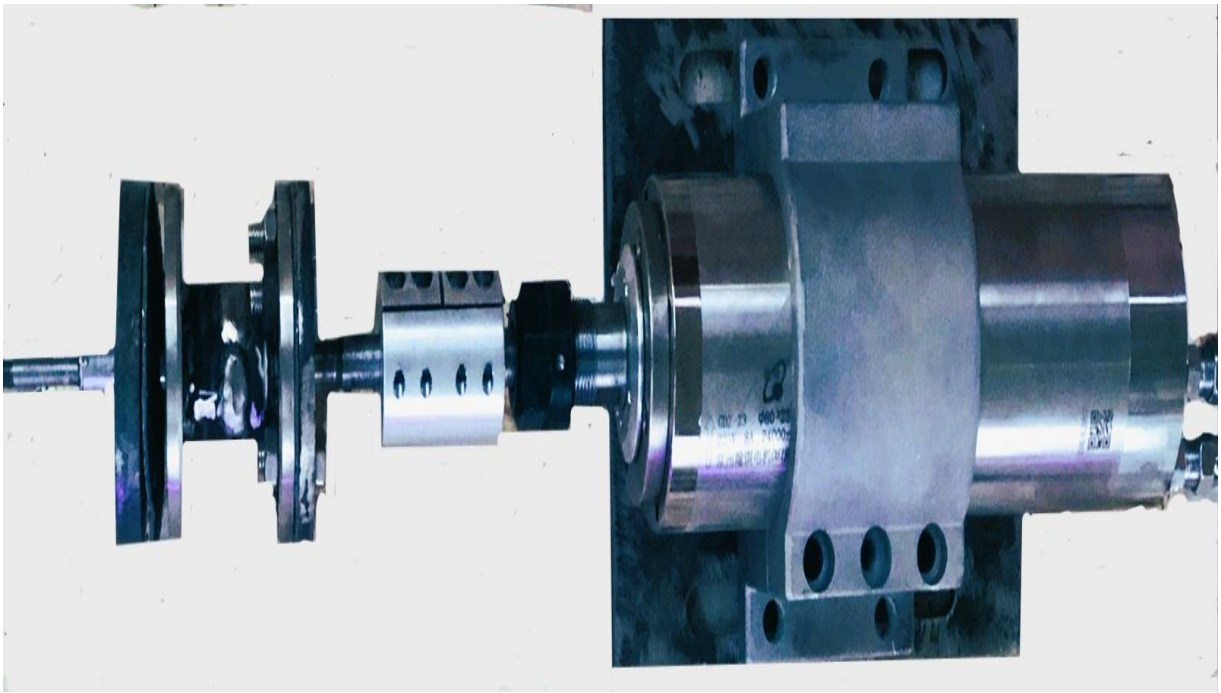

Figure (3.11) Detailed views of the spindle motors and assembly part

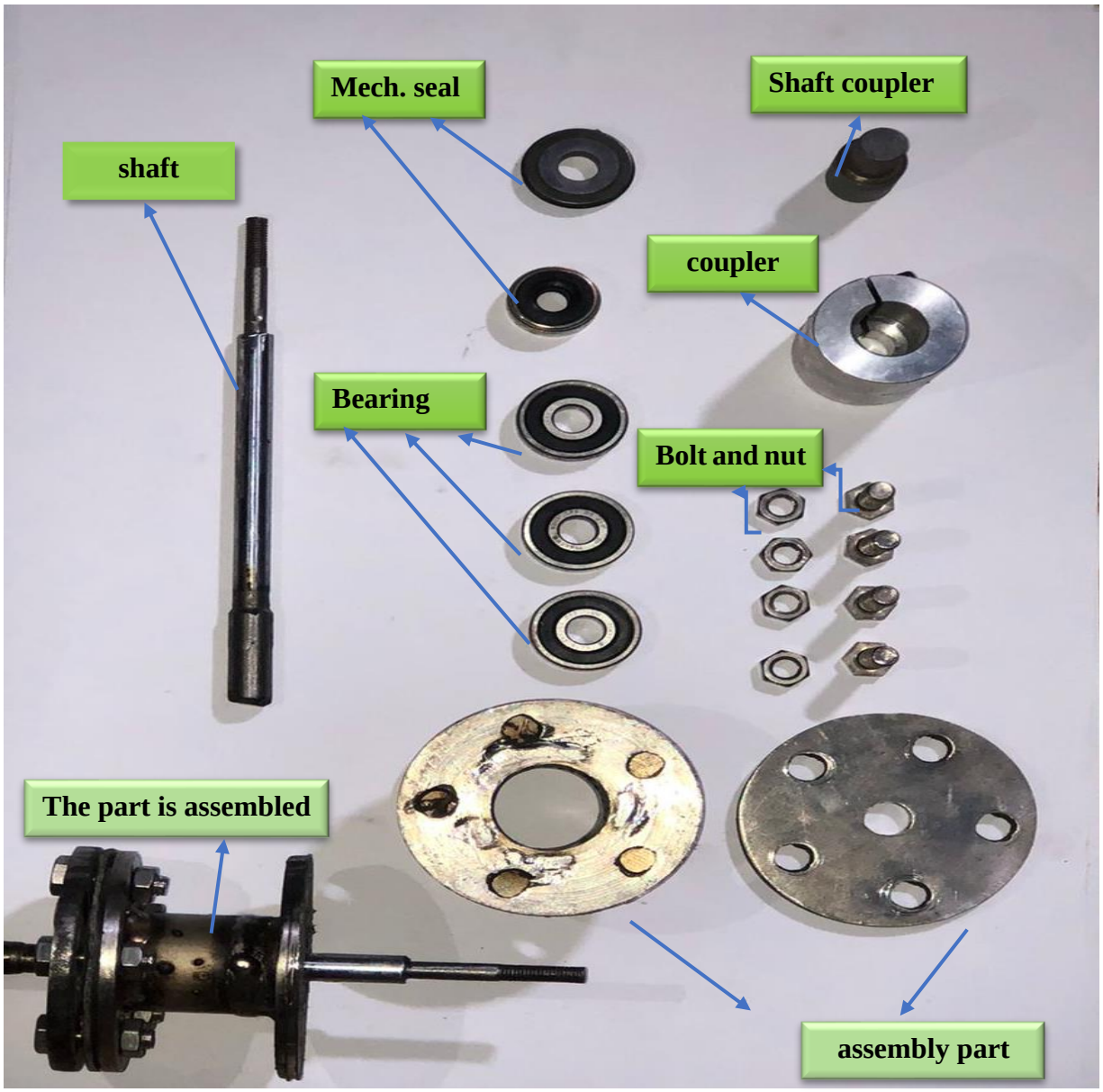

Figure (3.12) Detailed views of the assembly part

The primary purpose of a mechanical seal is to create a barrier between the process fluid inside the equipment and the external environment. This barrier prevents the

fluid from leaking out and contaminants from entering the system. Mechanical seals are designed to withstand high pressures, temperature variations, and the rotational movement of the shafts,[46] Here are some key components and features of a typical mechanical seal:

Seal Faces: Mechanical seals consist of two primary seal faces, known as the stationary seal face and the rotating seal face. These faces come into contact with each other to create the seal. Common materials used for seal faces include carbon, ceramic, tungsten carbide, and silicon carbide [47].

Secondary Sealing Elements: In addition to the primary seal faces, mechanical seals may include secondary sealing elements such as O-rings, gaskets, or elastomeric bellows. These components provide additional sealing and flexibility to accommodate shaft movements.

Seal Housing: The seal housing holds the seal components in place and provides support. It typically includes a gland plate or gland follower that applies the necessary force to maintain proper contact between the seal faces. Springs: Mechanical seals often incorporate springs to apply a consistent force between the seal faces. These springs compensate for wear and thermal expansion, ensuring an effective seal over the life of the equipment.

3.2.1.5.5 Impeller

in the study, radial-type fans used experiments. These fans were designed to direct the flow towards the walls of the vessel rather than towards the center. This particular configuration was chosen because it was found to result in higher turbulence intensities, which are beneficial for mixing applications in chemical reactor designs [48].

The study focused on two important geometric parameters of the fan blade design: the pitch angle (measured in degrees) and the number of blades. These parameters were systematically varied to understand their effects on turbulence intensities and mixing efficiency.

Figure (3.13) Detailed views of the Impeller

Pitch Angle: The pitch angle refers to the angle between the fan blade's chord line and the direction of the fluid flow. By adjusting the pitch angle, control how aggressively the fluid was pushed by the fan. Higher pitch angles might generate more turbulent flow patterns, potentially leading to better mixing.

Number of Blades: The number of blades on the fan is another critical design parameter. A higher number of blades could lead to more frequent interactions with the fluid, enhancing turbulence and mixing. On the other hand, too many blades might also create more resistance, affecting the overall efficiency.

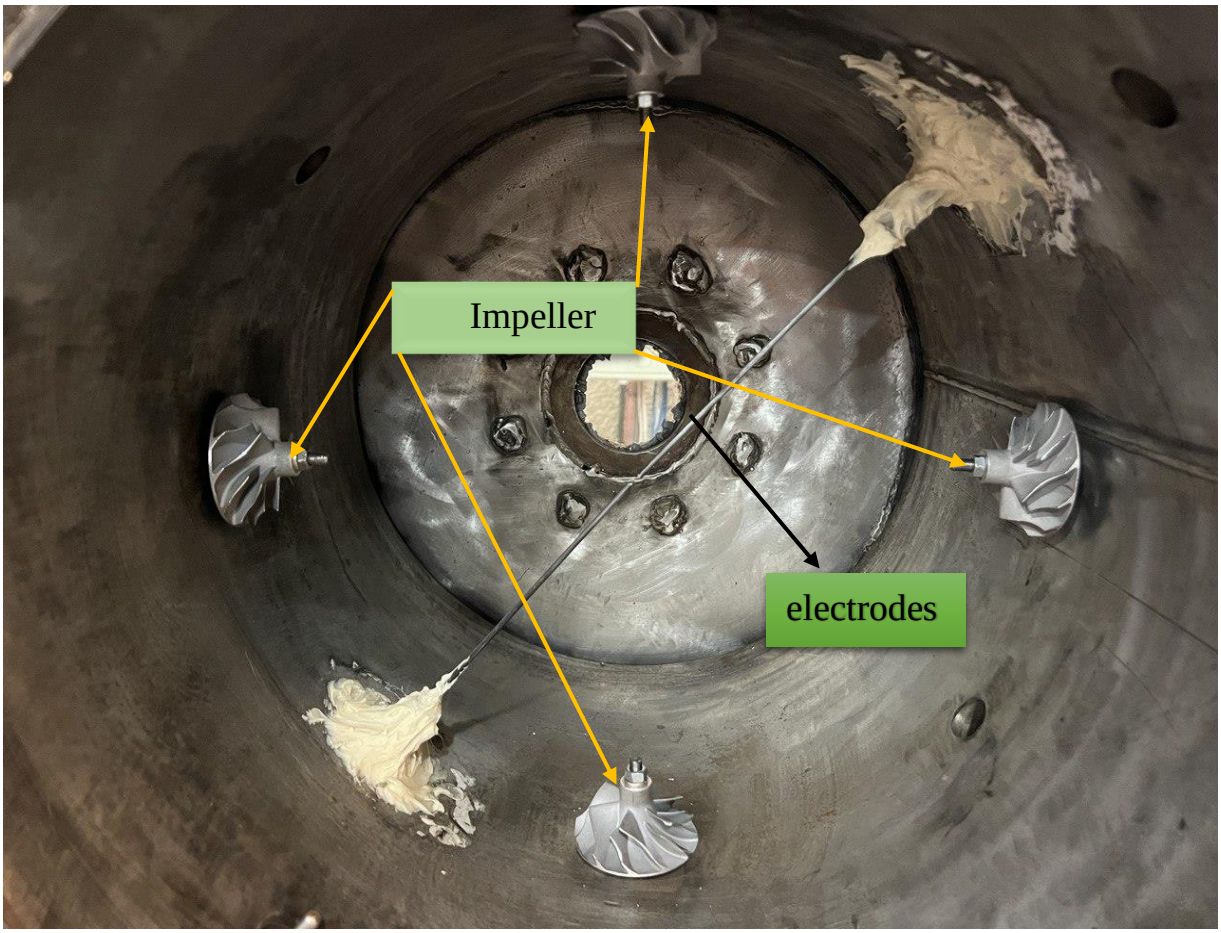

Figure (3.14) Detailed views of the Impeller inside the combustion chamber

Experiments with different combinations of pitch angles and blade numbers to observe how these variations influenced turbulence intensities and mixing efficiency within the chemical reactor.

The results of the study could provide valuable insights into optimizing the design of radial-type fans for high-shear applications in chemical reactors, allowing for more efficient mixing processes and potentially improving the overall reactor performance.

3.2.1.6 Vacuum pump

The chamber of the combustion is emptied from the products of the combustion and then cleaned by the air after every process of combustion utilizing by using vacuum pump type an ¼ HP, 220V-50HZ.

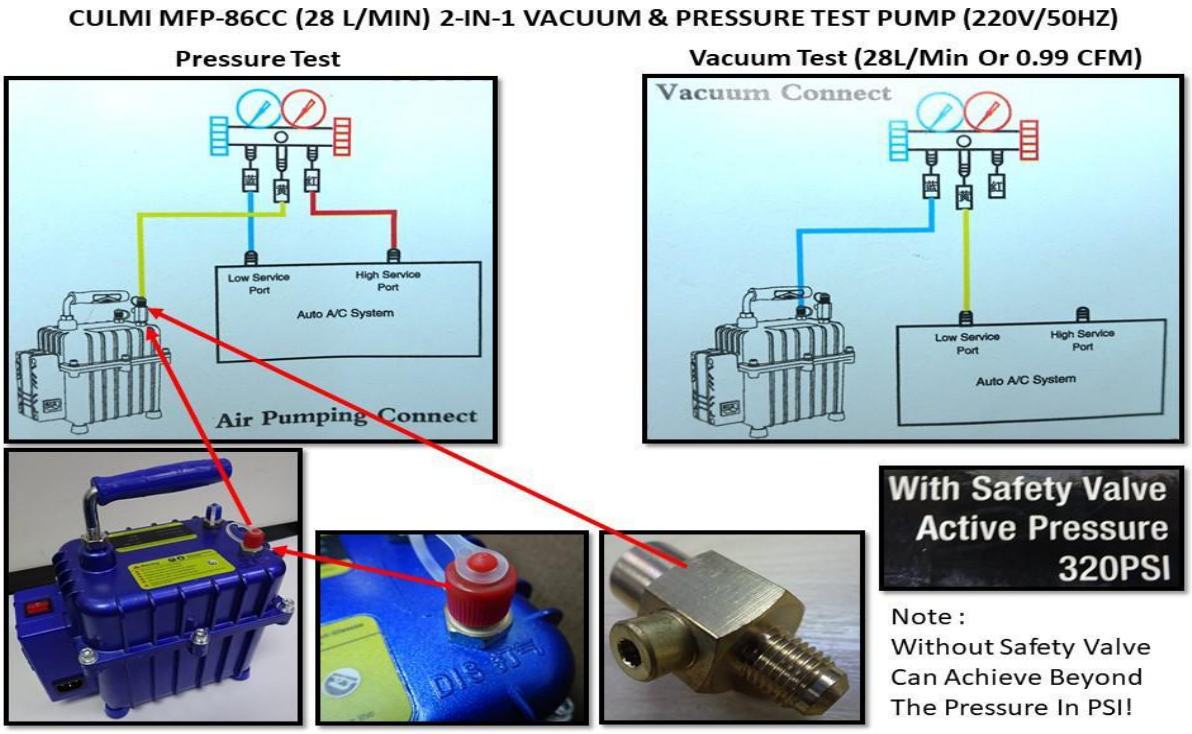

Figure (3.15) Detailed views of the using vacuum pump

3.2.2 Ignition Circuit: -

For the purpose of producing a strong spark, an electronic circuit has been utilized for providing power to the electrodes as shown in Figures (3.5 a and b) A continuous current energy source is produced from a current–line converter (220 VF). The transformer (2*5000 V) HOSEL) is 10 KV at peak. The electronic circuit is utilized

for controlling the spark duration, it is placed in front of the transformer for the production of on/off for the initiation of spark in the chamber of the combustion

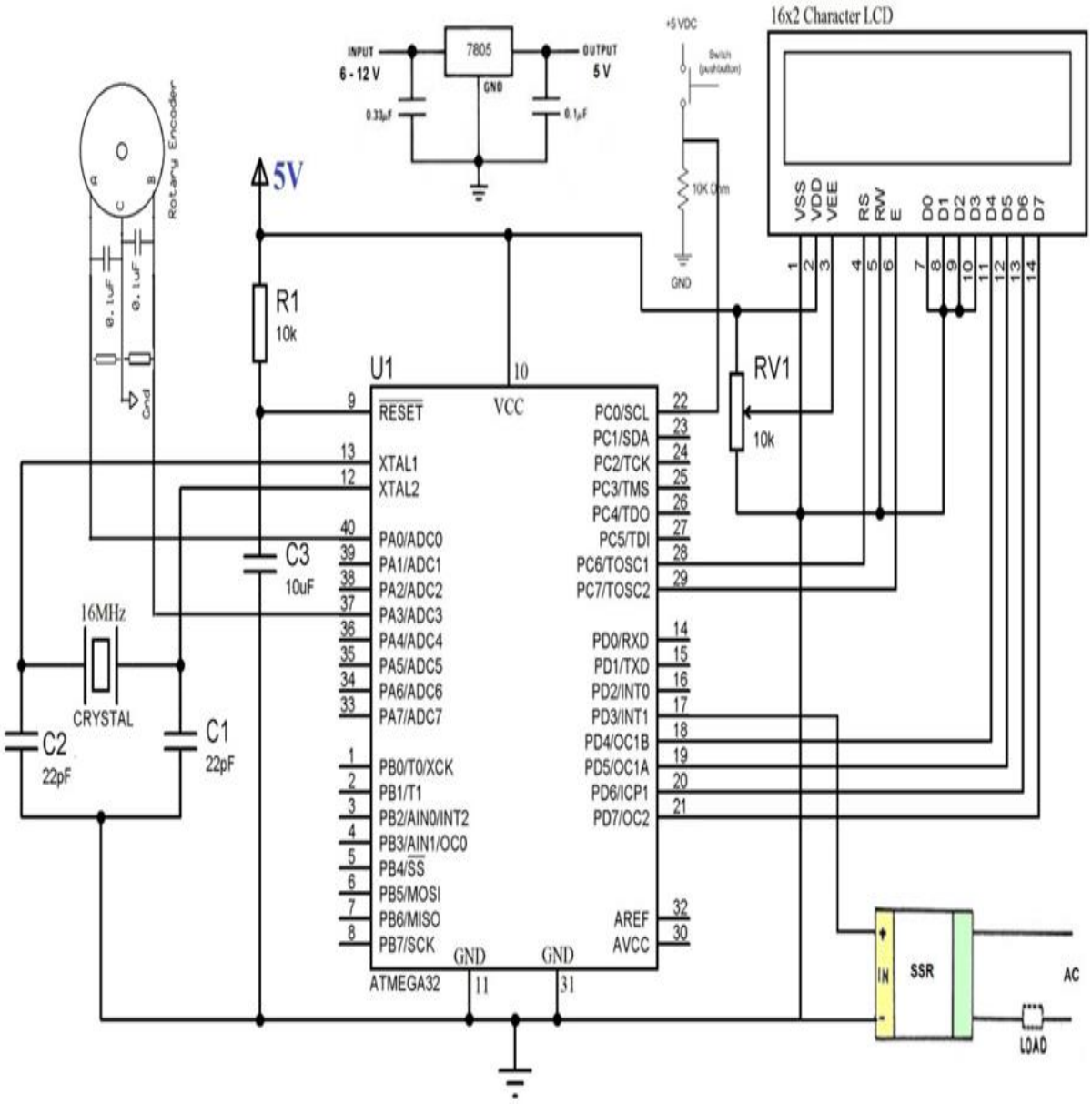

Figure (3.16) Schematic Diagram of Electronic Circuit for the Ignition Unit.

Figure (3.17) Photograph of The Electronic Circuit Controlling the Duration of Ignition. (CDI)

Figure (3.18) Photograph of Transformation Type

Ignite the mixture at appointing along the central axis of cylindrical with the use of intensive discharge flaring (CDI). The spark electrode diameter is 2.0 mm and the

spark gap is fixed at 1.5mm. Electro-static energy that is charged in the CDI circuit capacitor

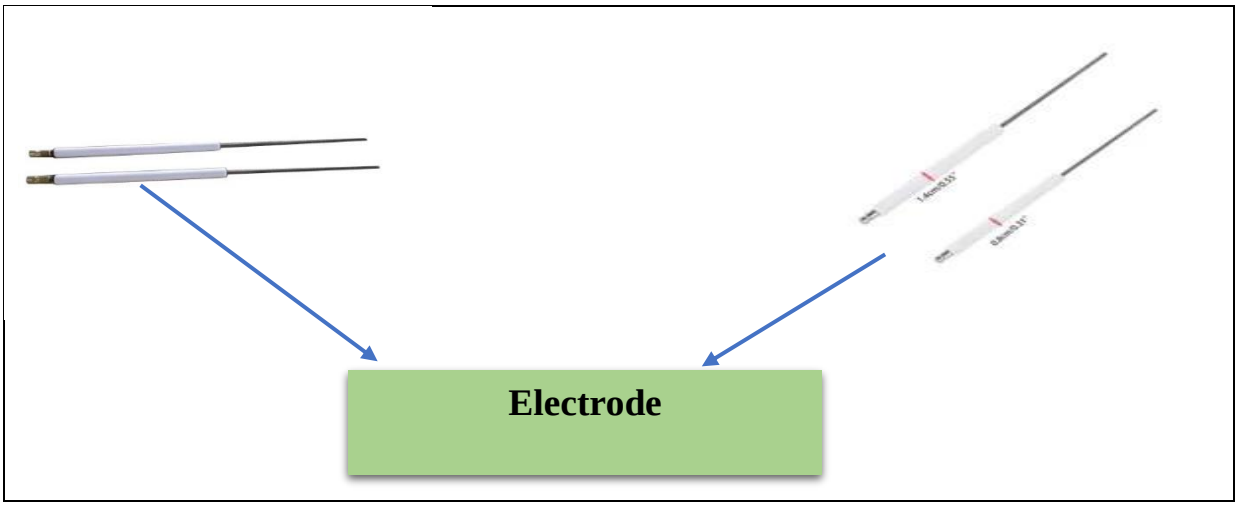

Figure (3.19) Modified Electrode Used in the combustion chamber

3.2.3 Mixture Preparing Unit: -

The mixing process is based on Gibbs – Dalton law of partial pressures for each component depending on the blend, equivalence ratio, and the total mixture pressure. The preparation of the mixture is done inside the combustion chamber in the following steps:

a. The recalculated volume of liquid is injected by syringe to the combustion chamber through the liquid fuel injection valve. the required volume of the fuel is calculated from its vapor partial pressure according to the ideal gas law PV=mRT

b. The required gaseous fuel is admitted from its tank to the combustion chamber according to its partial pressure, while opening the inlet and pressure transmitter valves, and closing the other valves.

c. Evacuated the gaseous injection unit, and the tube which connects it to the combustion chamber, because it contains a gaseous fuel from step (c). This process takes place by turning the switch of vacuum pump on, while closing the inlet valve.

d. Air is admitted to the combustion chamber until reaches the required total pressure, by turning the switch of the air compressor on, while opening the inlet and pressure transmitter valves, and closing the other valves.

e. The mixture is left for 5-6 minutes to ensure perfect mixing before igniting the mixture.

3.2.3.1 Air Compressor: -

One compressor (OD DARI type, DEC 720/520HP4 40068, IT., 2002) has been utilized for providing air at high pressure to the unit of the mix-preparation. The capacity of the compressor is (270 Liter), works at (1160 RPM), and maximal working pressure is (10.50 bar) as shown in Figure (3. 7).

Figure (3.20) Photograph Air Compressor

3.2.3.2 NH_3 Storage Tank: -

The ammonia fuel tank is a cylindrical bottle with a capacity of 40 kg a height of 1.20 m and a diameter of 30 cm, it contains a high-pressure valve with a value of 100 bar and is resistant to acid corrosion, and is connected to 1/2-inch stainless steel tubes, and these tubes are connected to each other by welding and connected to the ammonia gas pressure gauge.

To control more precisely the ammonia gas entering the combustion chamber, the operation is carried out by placing a valve before the combustion chamber before the position of the ammonia pressure gauge, as the ammonia gas needs a pressure gauge of a special type within the required quantity.

3.2.3.3 LPG Storage Tank: -

The LPG Storage Tank is a cylindrical bottle with a capacity of 30 kg and connected with a gas regulator that controls the amount of gas leaving the fuel tank. This regulator is connected with the control unit through high-pressure plastic tube that withstand 6 bar pressures.

Note that the pressure of a fuel tank during the opening of the fuel tank valve and regulating the flow rate using the second regulator, the gas flows to the control unit for the purpose of entering the gas into the combustion chamber,

The switch for the LPG gas is opened from the control unit, which in turn opens the celluloid from closed to open to allow the passage of gas towards the combustion chamber to complete the injection process, the main valve of the combustion chamber is closed.

3.2.3.4 Ammonia Gauge Pressure: -

Ammonia gauge Regulator, Dial size: 4" (100mm), connection: ½ ", range (-1 to 12 bar) the gauge gives the gas pressure before entering the combustion chamber. Also, a pressure gauge was used to control the amount of entering the combustion chamber. As shown in Figure (3.8).

3.2.3.5 LPG Pressure Regulator: -

A pressure gauge was used to control the amount of LPG in the model AW40 and port size ¼, 3/8, ½, set pressure range 0.05 to 0 .85 Mpa, drain capacity (cm^3) 45, and Mass (kg) 0.72 to prevent the occurrence of ignition or Gas leakage because the regulating meter has the property of non-leakage and non-return of gas in the opposite direction as shown (3.22).

Figure (3.21) Photograph of Ammonia Gauge Pressure

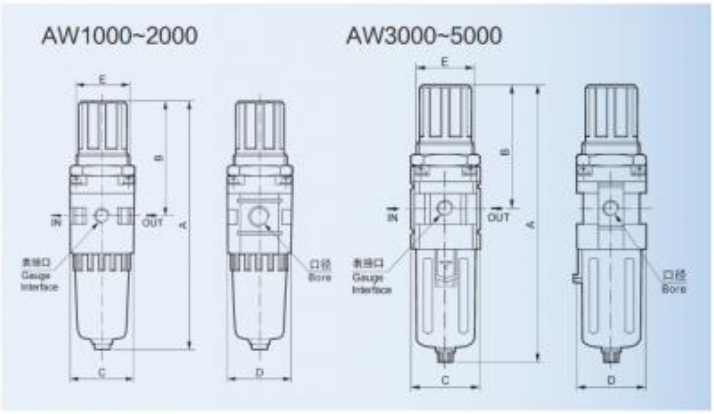

型号 Model	口径 Bore	A	B	C	D	E
AW1000	M5	109.5	50.5	25	28	28
AW2000	G1/8" ~ G1/4"	164.5	78	40	40	34
AW3000	G1/4" ~ G3/8"	211	92.5	53	53	40
AW4000	G3/8" ~ G1/2"	262	112	70	70	54
AW4000-06	G3/4"	267	114	70	70	54
AW5000	G3/4" ~ G1"	338	116	90	90	54

Figure (3.22) Photograph of the LPG Pressure Regulator

3.2.4 Control Unit: -

The control unit is an electric board. It contains a three-way solenoid valve in order to control the type of gases entering the combustion chamber type Festo, so

Figure (3.23) Detailed views of the control unit

It is in a closed state in the normal position and linked to an open and close switch to control the flow of gases entering the combustion chamber. The control unit, as shown in figure (3.10) contains a transformer for the purpose of operating the solenoid valve. It is operated on 24 volts, and the transformer converts the current from 220 volts to 24 volts. The control unit is equipped with two display screens, one of which helps to display pressure readings during the injection process, and the other displays the temperature before conducting the experiment. The main purpose of the control unit is to control the gases entering the combustion chamber during the charging process and to measure the temperature of the laboratory during the experiment.

This unit is equipped with pipes connected with solenoid valves, and these pipes are equipped with two valves on both ends of the control unit. The function of one of these valves is to prevent gas from returning in the opposite direction during the injection process. The second valve and its function are to empty the pipes from the previous gas for the purpose of injecting the next gas.

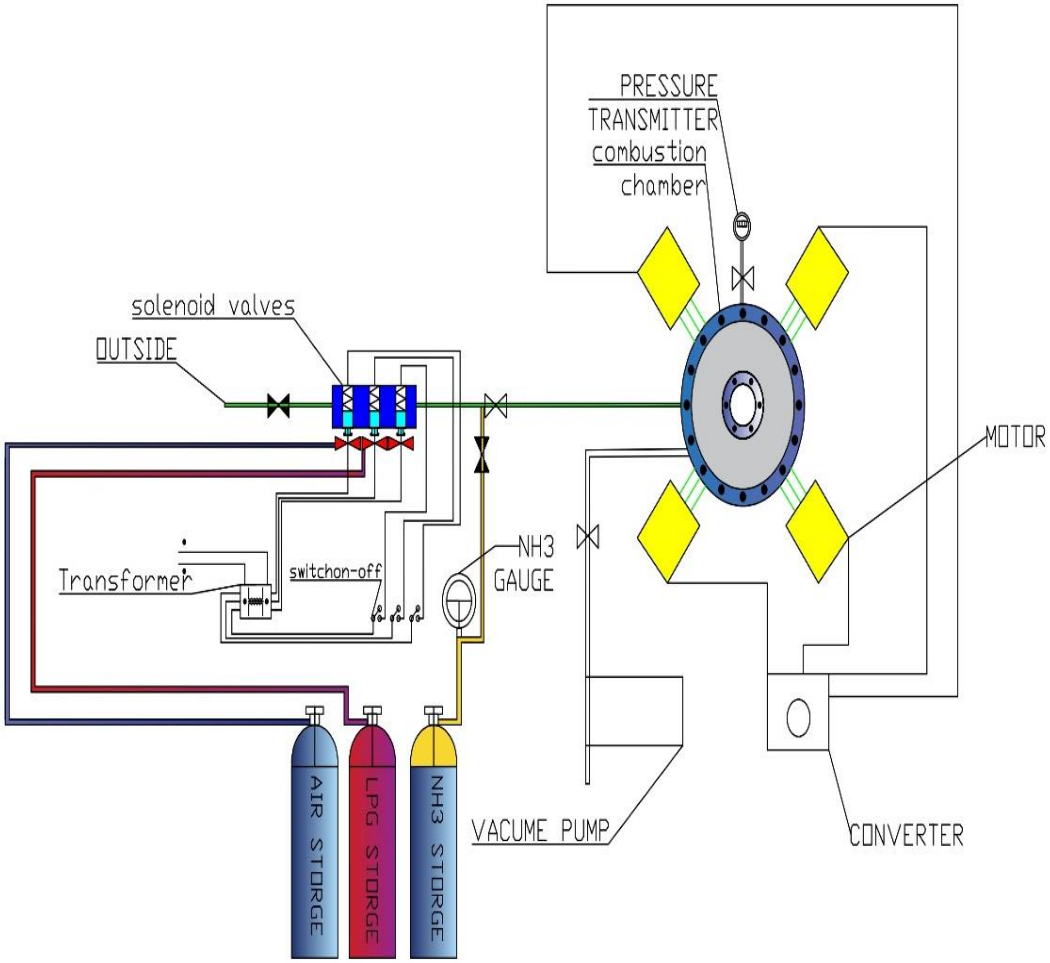

Figure (3.24) Schematic Diagram of the Operation of the Control Unit

The switch for the LPG gas injection is opened, as the gas begins to flow into the combustion chamber at a rate of (0.06 - 0.16 m^2/ sec) as well as for the air. The remaining gas is disposed of in the pipes after closing the combustion chamber valve and opening the gas outlet valve for the purpose of unloading the pipes from the previous gas, where the values and quantities of materials inside.

3.2.5 Capturing Unit: -

An optical system has been utilized for the visualization and recording of flames and flame flashback process with a camera of high-speed. A source of light and a concave mirror is depending on Schlieren photography from **[49].**

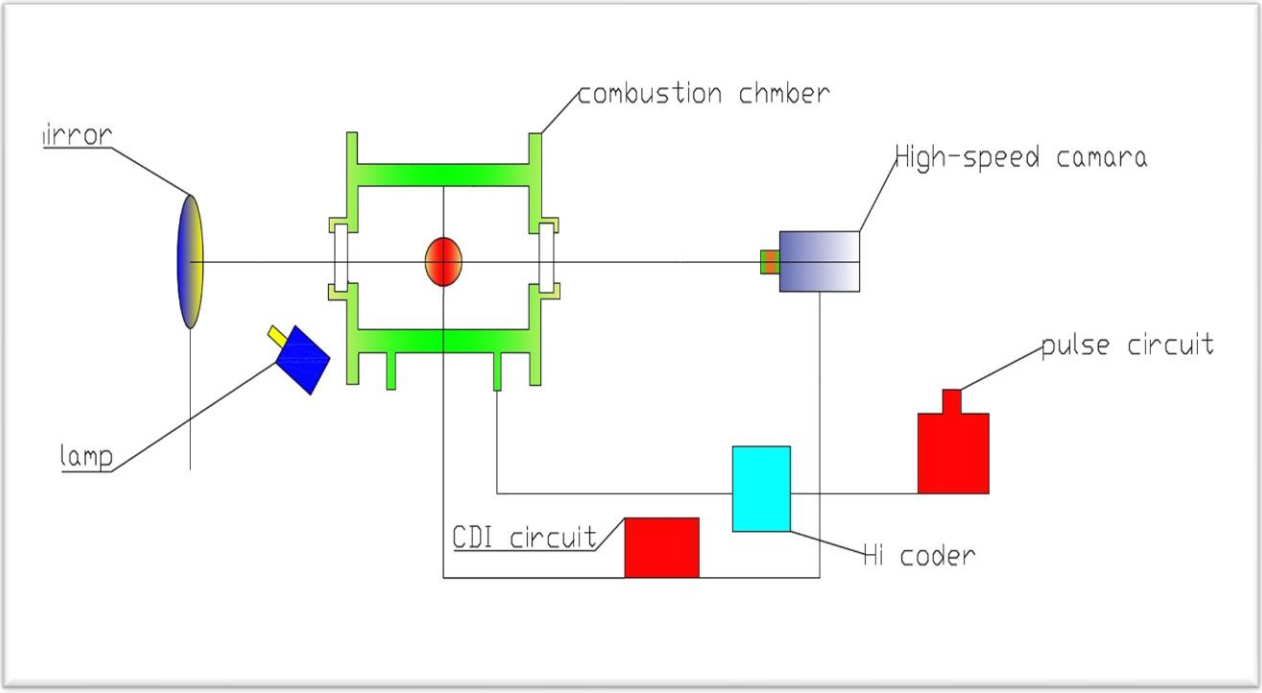

Figure (3.25) Schematic diagram for capturing unit

3.2.6 Concave Mirror

A concave mirror is used for the generation of virtual as well as real object images. Parabolic shape focuses the parallel ray's o one point. The mirrors focal length was 68 cm and its diameter 40.5 cm. This mirror is shown in Plate (3.26a) and (3.26b).

Figure (3.26a) Concave mirror

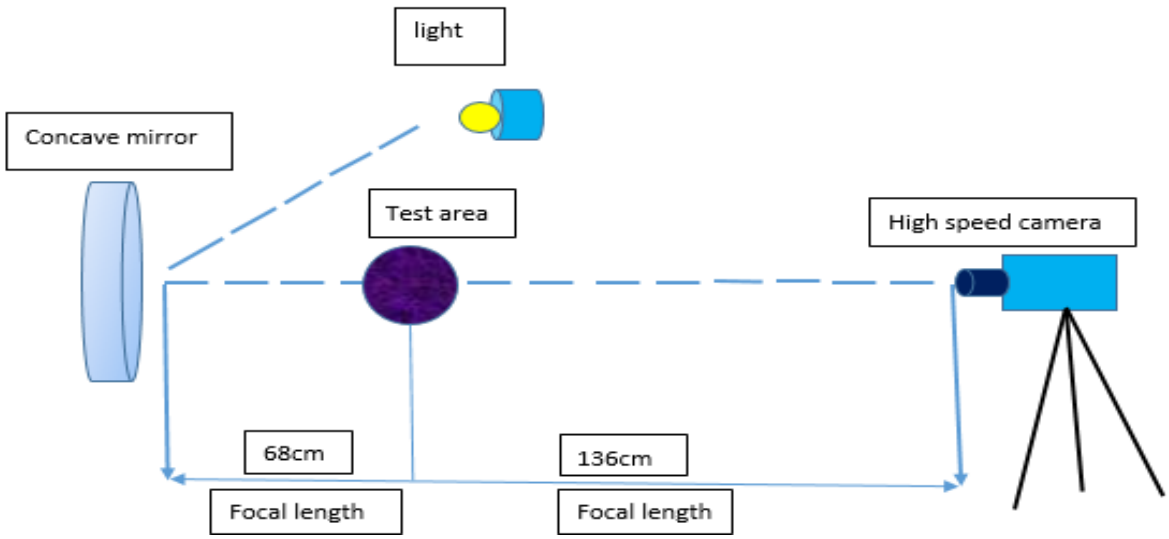

Figure (3.26b) Schematic diagram for capturing unit

3.2.7 Camera and Light Source: -

The high-speed portable camera type (AOS-Q-PRI) with high accuracy of the picture (3 M Pixel) and an inner memory of 1.3 GB and 16000 fps. Is used for the purpose of measuring the spread of the flames as can be

As seen from Figure (3.11) the preparation that used in the experiment was 576x500 lams for 4,000 tyros/sec., the total time for recording was 1.10 seconds, and 10% of the time designated as pre-operating for the purpose of ensuring

The fact that all of the operations were recorded in the case of operating the operators, the ignition unit and the camera. A NE-2 Narrator with a size of 5 mm (continuous current 12-volt energy) was placed in a closed box with one exit; a lens (5 mm) focal length placed before the lamp to assemble and then disperse light, then scatter it out.

Figure (3.27) AOS -Q PRI High-Speed Camera.

3.3 Test Procedure: -

The mixing process relies on the Gibbs - Dalton Law for partial pressure of each component of the mixture to obtain a precise parity ratio. The mixture was prepared within the mixing combustion chamber. The total absolute pressure (5bar) per test by: -

3.3.1 Combustion Chamber Preparation Processes

To make a homogenous mixture for exact equivalence ratio and Ammonia – LPG –air blending, there are steps to prepare the mixing chamber.

3.3.2 Cleaning Process

The outer flanges are opened and then the rig lining is cleaned with a clean cloth to get rid of the soot generated after the explosion process if any, as well as cleaning the windows quartzes.

3.3.3 Vacuum Process

The vacuum process takes place by closing all the valves except the valves of the vacuum pump and the vacuum gauge so that the pump can sufficiently clarify the combustion chamber from any previous air until its pressure reaches approximately (-0.95 bar). After the unloading process, leave the rig for five minutes, noting the pressure transmitter and tracking the pressure to make sure that there is no leakage of the mixture during the injection process inside the combustion chamber.

3.3.4 Mixing Process inside the Combustion Chamber

The gases are admitted into the combustion chamber after it is completely emptied from the air. Ammonia gas is injected, then liquefied petroleum gas, and then air from the special storage tanks for each gas. The mixture enters into the combustion

chamber at required initial pressure, and after that, it closes all the fuses and waits for a period of 10 minutes prior to the ignition for the purpose of stabilizing the mixture, obtaining laminar flame, and sustaining a mixture free of the eddies and turbulence.

3.3.5 Combustion and Recoding Processes: -

The homogeneous mixture was prepared in the preceding steps thereafter.

a) The **i**nitial values of the temperature and pressure shall be adjusted on the initial status of the test**.**

b) The electronic transformer of pressure begins recording the pressure of combustion.

c) Determine the ignition duration (5-second ms).

d) D. High – Speed camera have to size at the time of formation (1.1) seconds with 10% pre – operability and the illuminating system begins to lighten

a) Both the ignition logging operators and the camera are moved.

b) The data is recorded and photos are captured. Step (a) has been repeated with a variety of initial conditions.

e) 3.4 Analysis Assumption

Laminar burning velocity can be calculated through a series of calculations, from the Schlieren photographs taken during each test. To make use of data from the bomb, many assumptions need to be made. These have been developed by many authors**.** **[50]** Which include

1. The non–burned regular gas is in a state of rest in principle .
2. The total mass and volume of the contents of the receptacle are preserved

3. Pressure is supposed to be regular through flame during combustion analysis
4. The mixture is burning in the middle of the pot with a small temperature entrance.
5. The preface of flame extends to the outside spherically and remains the smooth flame speed is fast enough to buoyancy is negligible
6. The flame front itself is an external heat constant system
7. The flame front is infinitely thin
8. No chemical reaction and no dissociation occur in the unburned gas.
9. There is no heat transfer between the zones

3.3.6 Mixing Ratio and Combustion Processes: -

A MATLAB program was written to calculate the induction pressures of mixing for Ammonia, LPG fuel, and air according to the blend of ammonia. LPG is a mixture of many types of hydrocarbons (Ethan, propane, butane, and pentane)

The volume percentage of a component of LPG is shown in table (3.1). Analysis of LPG components provided from Hilla Gas plant shown in Appendix (B).

Table (3.1) LPG composition

Theoretical Analysis

Composition	C_2H_6	C_3H_8	C_4H_{10}	C_5H_{12}
Volumetric fraction %	0.95	66.01	32.42	0.62

The general form of chemical combustion equation

$$aJNH_3 + (1\text{-}J)\sum a_I C_{ni} H_{mi} \left[\frac{x}{\emptyset}\right](O_2 + 3.76\ N_2) \rightarrow e_2 H_2O + e_1CO_2 + e_3CO + x_1\ O_2 + e_4N_2 \quad (3.1)$$

While:

$$\sum a_I C_{ni} H_{mi} = a_1 C_2H_6 + a_2C_3H_8 + a_3C_4H_{10} + a_4C_5H_{12}$$

Where:

n_i: Equivalent NO. of Carbon atoms= 3.327

m_i: Equivalent NO. of Hydrogen atoms =8.6542

Table (3.2) Symbols Definition

Symbols	Meaning
J	Ammonia volume fraction
Ø	Equivalence Ratio
n_i	Equivalent No. of carbon atoms
m_i	Equivalent No. of Hydrogen atoms
e_2	NO. of moles of H_2O in products
e_1	NO. of moles of CO_2 in products
e_3	NO. of moles of CO in products
e_4	NO. of moles of N_2 in Products
x	NO. of moles of O_2 in reactant
x_1	NO. of moles of O_2 in products

$$x = \frac{J}{2} + (1 - J) * (n + \frac{m}{4}) \quad (3.2)$$

Ammonia fraction J is calculated as: -

$$J = \frac{V_{NH3}}{V_{NH3}+V_{LPG}} \quad (3.2a)$$

Where V_{LPG} and V_{NH3} are the volumes of LPG and Ammonia respectively.

overall equivalence ratio for duel fuel calculated using the equation : -

$$\emptyset = \frac{\left(\frac{F}{A}\right)}{\left(\frac{F}{A}\right)_{st}} \quad (3.3)$$

Daltons Law of partial pressures indicates that the ratio of the partial pressure of the fuel and the air is equal to their molar ratio : -

$$P_f=\left(\frac{nf}{nf+nair}\right) p_{mix} \quad (3.4a)$$

For per unit mole of fuel from equation (3.2)

$$P_f=\left(\frac{1}{1+(4.76*x}\right)p_{mix} \quad (3.4b)$$

For a non – stoichiometric mixture, this is modified to:

$$P_f=\frac{1}{1+\left(\frac{4.76*x}{\emptyset}\right)} p_{mix} \quad (3.4.c)$$

While partial pressure for air is calculated from equation (3.4a) the partial pressure of each constituent of the blend can be calculated by the same method

$$P_f = P_{NH3} + P_{LPG} \quad (3.4e)$$

$$P_{NH3} = J * P_f \quad (3.4f)$$

$$P_{LPG} = (1 - J) * P_f \quad (3.4.g)$$

This should be done at a fixed temperature to obtain the best accuracy, although changes in temperature can be compensated in proportion to the temperature

accuracy measured before and after each gas added to the mixture, the mixture of NH_3/LPG is prepared in the ratio indicated in table (3.3) volumetric fuel is adjusted to represent the composition.

Table (3.3) tested Fuel Blends

NH3 %	C_2H_6	C_3H_8	C_4H_{10}	C_5H_{12}	Stiochmetric air / fuel ratio (Vol)
0	0.95	66.01	32.42	0.62	14.240
0.1	0.855	59.409	29.178	0.558	15.226
0.2	0.76	52.808	25.936	0.496	16.358
0.3	0.665	46.207	22.694	0.434	17.672

3.3.7 Stoichiometric Mixture are tested and the calculation for each test are shown below

Ideal combustion, where fuel is ideally burned as equal combustion, full combustion is the burning of the air and fuel mass ratio leading to full fuel combustion **[51].** Stoichiometric Combustion for LPG gives: -

$$e_1 = (1-J) \cdot \sum a \; n_i \qquad (3.5a)$$

$$e_2 = \frac{3J + (1-J) \cdot \sum a \; m}{2} \qquad (3.5b)$$

$$e_3 = 0 \qquad (3.5c)$$

$$e_4 = 3.76 \frac{x}{\emptyset} \qquad (3.5d)$$

$$x_1 = 0 \qquad (3.5e)$$

$$x = e_1 + 0.5\, e_2 \qquad (3.5f)$$

3.3.8 Rich Mixture are tested and the calculation for each test are shown below

The rich mixture occurs when the amount of air available is lower than the stoichiometric quantity , which means that there is not enough air to burn all available fuel It is supposed that the hydrogen combines completely with the oxygen and the rest of oxygen does not have sufficient carbon to be burned completely to produce carbon dioxide This results in partial oxidation of part of the carbon-to-carbon monoxide.

$$e_1 = 3\frac{x}{\emptyset} - J - (1 - J)\sum a\ \left(n + \frac{m}{2}\right) \quad (3.6\ a)$$

$$e_2 = \frac{3J+(1-J).\sum a\ m}{2} \quad (3.6b)$$

$$e_3 = 3\frac{x}{\emptyset} - e_2 - 2\,e_1 \quad (3.6c)$$

$$e_4 = 3.76\frac{x}{\emptyset} \quad (3.6d)$$

$$x_1 = 0 \quad (3.6e)$$

$$x = e_1 + 0.5\,e_2 \quad (3.6f)$$

3.3.9 Lean Mixture are tested and the calculation for each test are shown below

A lean mixture means excesses in the available air , where the reaction kinetics and dissociation are neglected This excess air traverses the process without participating in combustion, However, although it does not react chemically, it has a consequence on the combustion process basically because it reduces the temperature due to its capacity to absorb energy **[52]** The equation for the combustion of a lean mixture is :

$$e_1=(1-J)\,.\,\sum a\ n_I \qquad (3.7a)$$

$$e_2 = e_2 = \frac{3J+(1-J).\sum a\ m}{2} \qquad (3.7b)$$

$$e_3 = 0 \qquad (3.7c)$$

$$e_4 = 3.76\,\frac{x}{\emptyset} \qquad (3.7d)$$

$$x = e_1 + 0.5 \qquad (3.7\ e)$$

$$x_1 = x * (1/\emptyset - 1) \qquad (3.7f)$$

3.4 Density Calculations

The density of the burning mixture to the non-burn mixture density is recognized as the density ratio calculated assuming adiabatic equilibrium of burning gases .

Applying ideal gas law for the initial and final state to get ,

$$P_i = \rho\ R\ T_i \qquad (3.8)$$

$$R = \frac{R_\circ}{M_w} \qquad (3.9)$$

Where R specific gas constant. From equations (3.8 and 3.9) then,

$$(\rho_u)_i = \frac{P*M_{w,i}}{R_\circ T} \qquad (3.10)$$

The unburned gas density (ρ_u) is computed by using the following equation that derived from Dalton's law :

$$\rho_u = X_{air}.\rho_{air} + X_{fuel}.\rho_{fuel} \qquad (3.11)$$

Where X is the mole fraction for each component . This equation can also be used to find the density of burnt mixture at adiabatic flame temperature . The initial and

final temperature, the pressure, the components of fuel affect the density ratio and equivalence ratio and density ratio will be: -

$$Density\ Ratio\ = \frac{\rho_b}{\rho_u} \qquad (3.12)$$

3.5 Flame Propagation Analysis

The density ratios obtained from the GASEQ program to be used with the experimental data obtained from analysis of the Schlieren photos to complete the analysis of the process **[54], [53]**.

3.6 Stretched Flame Speed Analysis

The density gradient appears inside the combustion chamber when the flame radius is measured directly by Schlieren photography , the radius of the flame may be in the shadow image, unlike the actual image because the photographic image does not display the edge of the flame directly.

Flame radius is measured from Schlieren photography , the laminar flame speed (S_n) from the radius – time of flames.

$$Sn=\frac{drsch}{dt} \qquad (3.13)$$

The stretched flame speed is calculated using software (Tracker version 4.87) to collect the Cartesian coordinates , by observing the front of the flame for each subsequent frame, then the film is recorded by the high-speed camera and the output data would be (S_n, r, and t) the table (3. 4) shows the setup of the Tracker Software and how to measure the speed of the flame.

$$S_n = \frac{dr}{dt} = \frac{rj+1-rj}{tj+1-tj} \quad \rightarrow \qquad (3.14)$$

The mean radius is assumed to be the radius that corresponds this speed.

$$R_{(j+1/2)} = \frac{rj+1+rj}{2} \quad \rightarrow \quad (3.15)$$

The data are necessary as a result of this method, the data is dispersed, making it impossible to see a distinct pattern, because of averages of four half–diameters for time per direction to calculate the speed of the flame given by.

$$S_n = \frac{dr}{dt} = \frac{\left((r_{i,j+n+1} - r_{i,j+n+2}) + (r_{i,j-n-1} - r_{i,j-n-2}) + (r_{i+n+1,j} - r_{i+n+2,j}) + (r_{i-n-1,j} - r_{i-n-2,j})\right)/4}{t_{j+1} - t_j} \quad (3.16)$$

The only advantage of the average technique with the tracking software is particularly sensitive to small elevations compared to the endpoints. Large radius effect becomes apparent due to the consequences of the thickness of the electrical code and this increase the error due to a lack of the clarity in the photograph on film and could arise from multi-sources [54].

Table (3.4) Setting of Tracker Software that Measuring Flame Speed.

Clip Setting	
Start frame	**Changeable**
Step size	**5(frame)**
End frame	**Changeable**
Start time	**Changeable**
Frame rate	**4000f/s**
Frame dt	**2.50E-4s**

3.7 Flame Stretched Rate

A general stretch at any point on the surface of the flame is defined as the Lagrangian time derivation of the logarithm of area (A) of any small element on the surface

$$\alpha = \frac{d(lnA)}{dt} = \frac{1}{A}\frac{dA}{dt} \qquad (3.17)$$

For the outwardly propagating spherical flame, the flame stretch rate can be deduced in the following form .

$$\alpha = \frac{1}{A}\frac{dA}{dt} = \frac{2}{ru}\frac{dr}{dt} = \frac{2}{ru}\,Sn \qquad (3.18)$$

The flame stretch rate α points out the expanding rate of the area of flame for spherically expanding flame. Flame stretches rate expressions, regarding the purposes an appropriate unified tensor expression, regarding the strain rate tensor α_s and the stretch rate due to flame curvature, α_c that is:

$$\alpha = \alpha_s + \alpha_c \qquad (3.19)$$

During the pre-pressure period, there exists a linear relationship between the flame propagation speed and the stretch rate that is:

$$S_l - S_n = L_b\,\alpha \qquad (3.20)$$

The Unstretched propagation speed, S_l, can be obtained as the intercept at α=0 value in the plot of S_n against α. The burned gas Markstine length L_b, is the negative slope of the $S_n - \alpha$ fitting curve **[55].** Markstine length can be defined as the decrease in burning velocity per unit stretch**.**

3.8 Turbulent Burning Velocity

In the initial stage of flame propagation, the total volume of the burned gases is around 0.5% of the volume of the combustion chamber , the Unstretched laminar burning velocity, u_l, is related to S_l through the mass conservation across the flame front.

$$A\,\rho_b\,S_l = A\,\rho_u\,u_l \qquad (3.21)$$

$$u_l = S_l\,\frac{\rho b}{\rho u} \qquad (3.22)$$

Where A is the flame front area, $\rho_{u,}$ and ρ_b are the unburned and burned gas densities respectively. The Unstretched laminar burning velocity can be get from equation (3.22), **[56]**.

A universal turbulent burning velocity equation was developed by Bradley et al. **[57]** using a constant-volume spherical combustion chamber. Experiments were conducted under a uniform and isotropic turbulence at ambient pressure and temperature conditions.

Flame imaging and spatial distributions of burnt and unburnt gases were performed and measured by high-speed Schlieren images were also captured. In their investigation, Bradley et al. **[57]** assumed that the volume of the unburnt gas (Vui) inside a spherical flame of radius Rj is equal to the volume of the burnt gas (Vbo) outside this radius, as indicated in Figure (3.28) where Rr is the root radius (the smallest radius), Rt is the tip radius (the largest radius, located at the furthest tip of the flame), Rj is the intermediate radius between Rr and Rt, muo is the mass of the unburned gases outside Rj, mui is the mass of the unburned gases inside Rj, mbi is

the mass of the burned gases inside Rj, and mbo is the mass of the burned gases outside Rj

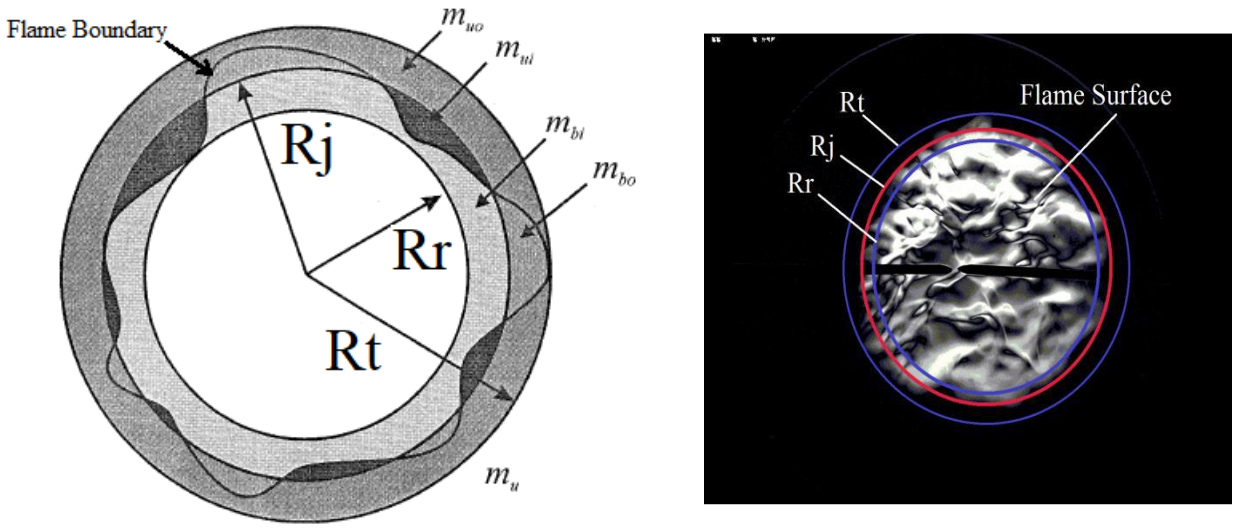

Figure (3.28) Schematic representation of the reference radii and associated masses of burned and unburned gases **[57]** Reference radii of a post-processed turbulent flame

Thus, based on the volume assumption ($Vui = Vbo$), Rj is equal to the average radius, Rv. By equating the two volumes, a mass conservation is deduced as follows:

$$mui/\rho u = mbo/\rho b \qquad (3.23)$$

where ρu and ρb are the burnt and unburnt gas densities, respectively for spherical turbulent flame propagation, the mass rate of burning can be expressed in terms of the spherical surface area $4\pi Rj2$ and the unburned gas density as follows:

$$\frac{d(mbi + mbo)}{dt} = 4\pi \mathrm{Rj}^2 \rho_u u_{trj} \qquad (3.24)$$

where $utrj$ is the mass turbulent burning velocity indicated by the spherical surface area $4\pi Rj2$. The mass burnt within the sphere of radius Rj can be expressed by the product of its volume and density (ρb) as:

$$\mathrm{mbi} = \left(\frac{4}{3}\pi \mathrm{R^3j} - \frac{\mathrm{m_{ui}}}{\rho \mathrm{u}}\right)\rho_b \qquad (3.25)$$

Thus, from equations (3.24) and (3.26), we obtain

$$4\pi Rj^2 \rho_u u_{trj} = 4\pi Rj^2 \rho_u \frac{dR_j}{dt} - \frac{\rho_b}{\rho_u}\frac{dm_{ui}}{dt} + \frac{dm_{bo}}{dt} \qquad (3.26)$$

From the volume assumption, we found:

$$\frac{dm_{ui}}{dt} = \frac{dm_{bo}\left(\rho_u/\rho_b\right)}{dt} \qquad (3.27)$$

the last two terms of Eq. (3.26) become zero, and hence the turbulent burning velocity at radius Rv is determined as:

$$u_{tr}(R_v) = \frac{\rho u}{\rho b}\frac{dR_v}{dt} \qquad (3.28)$$

Bradley et al. [57] plotted the turbulent burning velocity obtained from the above equation based on the average radius, Rv, versus turbulent burning velocity calculated by the Schlieren flame radius, as shown in Figure 3.31 Based on the deduced linear relation, a final turbulent burning velocity equation was obtained (Eq. 3.29). The turbulent burning velocity calculated by this equation, either stated by St or u_{tr} , is widely used in the literature [58–59]. In this thesis, turbulent burning velocity is expressed as St.

$$u_{tr}(R_v) = \left(\frac{1}{1.11}\right)\frac{\rho_b}{\rho_b}\frac{dR_{sch}}{dt} \qquad (3.29)$$

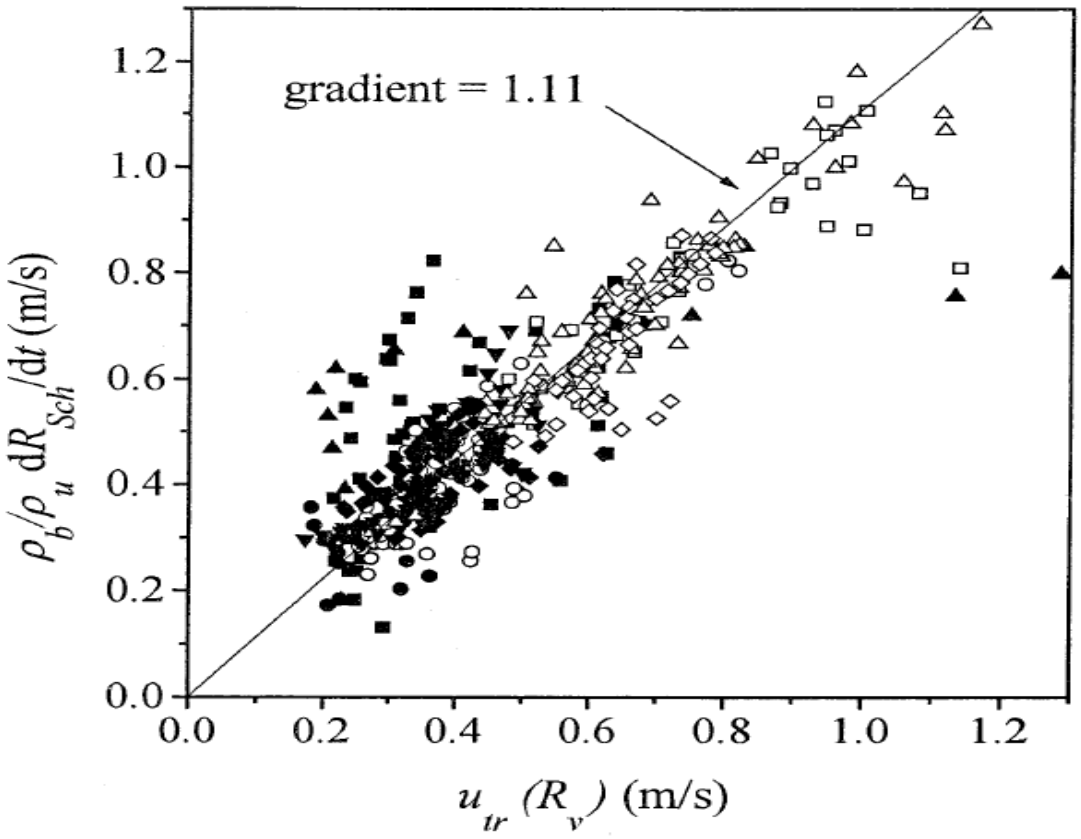

Figure 3.30 Relationship between Schlieren flame radii and turbulent burning velocity $utr(Rv)$ [57]

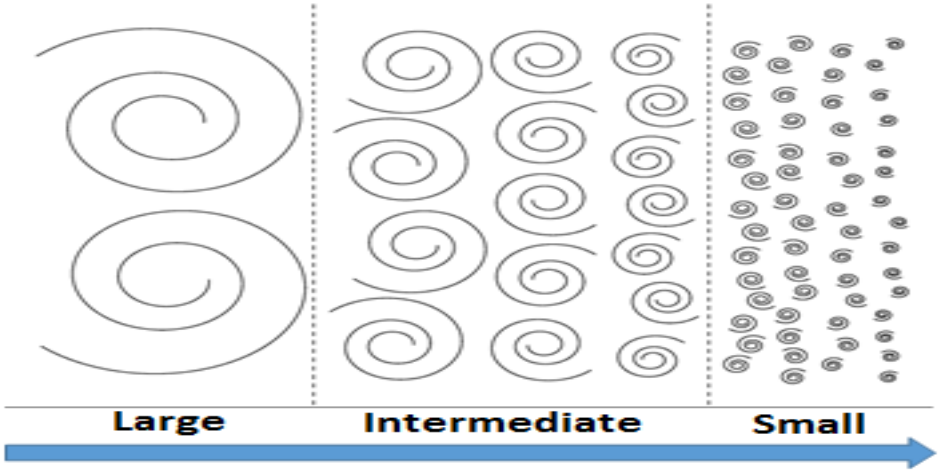

Figure 3.31 Energy Cascade

3.9 Calibration

The term calibration is defined as "a test during which the known measurement values are applied to the energy transformer and corresponding release readings are recorded under specific circumstances". To ensure that all data is read from meters and sensors, calibration has been conducted for all the measuring devices and sensors.

3.9.1 Pressure Gauge Calibration (QYB102 Pressure Transmitter)

The calibrating operation for this device is to be tested by Central Organization for Standardization and Quality Control (COSQC) as shown in appendix (A).

3.9.2 Ammonia Gauge Pressure

The calibrating operation for this device is to be tested by Central Organization for Standardization and Quality Control (COSQC) as shown in appendix (A).

3.9.3 Camera Calibration: -

The calibrating operation for this device is made by the same company that manufactured the device as shown in appendix.

Chapter four

RESULTS AND DISCUSSION

CHAPTER FOUR

4.1 Introduction

The experimental results regarding turbulent flame propagation and turbulent burning velocity will be displayed and analyzed in this chapter. The flame is initiated by spark plug and spread in the (LPG - NH_3 - Air) mixture the combustion process is tested using a photographic approach after being ignited by central electrodes.

At varied initial pressures ranging (100, 200, and 300) kPa, the flame speed and turbulent burning velocity were measured. The initial mixture temperature was 300 K Three NH_3 blending ratios (NH_3 10 %, 20%, and 30%) with LPG and with different equivalence ratio were tested.

4.2 Repeatability Test

Experimental apparatus is specifically manufacturing and built for this study. A repeatability test of one case study is used to confirm the rig validity and measurement accuracy. Previously mentioned, the mixture is prepared inside the CVC. The mixing process is based on the partial pressure blending method. Seven experiments for the CC. the repeatability results are reasonable.

4.3 Validation

Figures (4a) show a comparison between the results obtained from present work with results obtained of other researchers shows relation between Flame radius and Time for pure NH_3 with the initial pressure at 100kPa and temperature 300Kand u=3 m/sec and Ø=1.3 it shows a comparison between the results of present work and the results by [60]

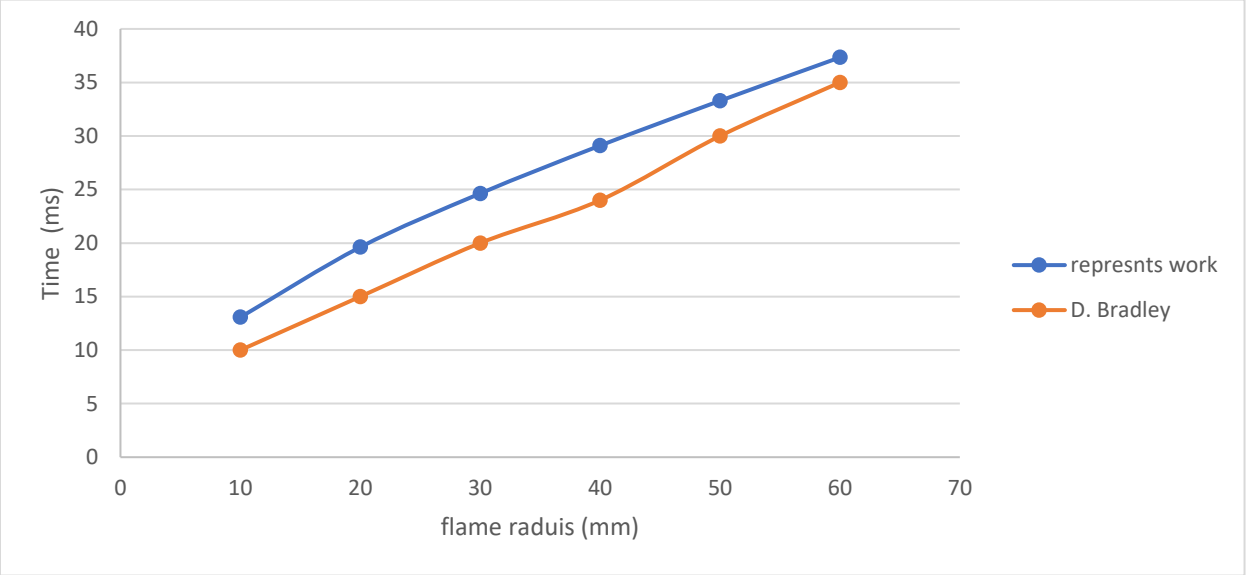

Figure (4a) Flame radius and Time for 100%NH_3 at equivalence ratio Ø=1.3 with initial pressure (100) kPa

4.4 Experimental Results

The combustion chamber was modernized for the purpose of studying the turbulent burning velocity, where four symmetrical impellers were added to obtain turbulence with a homogeneous effect of air swirls inside the combustion chamber, and the flame speed was photographed using the Schliern imaging system for the purpose of measuring the diameter of the flame and measuring the time by calculating the number of frames and from Using Equation No. 3.16, we obtained the values of the flame speed, and the rotational speed of the impellers was taken as 1400 revolutions per minute.

Thus, the value of the turbulence speed was 3 m/sec, and the Reynolds number values were obtained, which were according to the results between (25-99), as changing the pressure value changes from the value of density, which increases the

value of the Reynolds number significantly, taking into account the molar fraction of the components of the mixture and according to the ratio (ammonia - LPG - air).

where the proportion of air changes with the change of the valence ratio (0.8,1,1.3) and this affects the Density as well as viscosity needed by Reynolds No. After calculating the flame speed, we calculate the rate of expansion of the flame brush from equation No. 3.18 and draw the rate of expansion against the speed of the flame.

where the rate of expansion of the flame brush represents the x-axis and the speed of the flame the y-axis. With the largest possible number of points to make a linear equation and with making the value of the flame brush expansion rate zero, we get the values of the y-axis, which represent y and give the value of (s1) show table 4.2.

These results were placed in table No. 4 .1. We note that the difference in the values of laminar and turbulent is only the impellers when not operating the calculations call for a laminar, and when running.

the calculations are turbulent at a speed of 1400 revolutions per minute, and then we apply equation 3.22 in order to obtain the combustion speed, noting that the density value was theoretically extracted using the MATLAB code program.

Table 4.1

	Laminar				Turbulent		
		SL	cm/s			St	cm/s
P / Ø	0.8	1	1.3		0.8	1	1.3
100 kPa	28.64	39.33	33.78	**100 kPa**	49.11	50.58	35.93
100 kPa	22.91	32.46	27.05	**100 kPa**	42.93	44.71	30.15
100 kPa	20.04	27.55	24.17	**100 kPa**	37.78	39.85	26.94
200kPa	27.28	38.32	30.55	**200kPa**	44.03	46.38	32.54
200kPa	21.82	31.645	26.1	**200kPa**	37.78	40.22	27.99
200kPa	19.08	26.88	23.336	**200kPa**	33.87	35.79	25.23
300kPa	24.56	34.95	28.49	**300kPa**	36.9	39.38	28.99
300kPa	19.64	28.94	23.734	**300kPa**	31.74	34.24	24.54
300kPa	17.16	24.64	21.256	**300kPa**	28.36	30.54	21.86

Table 4.2

		Laminar				Turbulent	
		S1				S1	
P / Ø	0.8	1	1.3		0.8	1	1.3
100 kPa	142.405	232.2021	152.5911	y	244.1867	298.6215	162.3031
100 kPa	114.066	191.0426	127.4127	y	213.7431	263.1397	142.0146
100 kPa	99.94571	161.5046	120.3677	y	188.4206	233.6102	134.1625
200kPa	135.6427	226.2391	138.0006	y	218.9277	273.8249	146.9898
200kPa	108.6391	186.2459	122.938	y	188.1019	236.7139	131.8404
200kPa	95.15789	157.5769	116.2144	y	168.9202	209.8095	125.6466
300kPa	122.1182	206.3428	128.6951	y	183.4757	232.4973	130.9537
300kPa	97.78512	170.3257	111.7935	y	158.0295	201.5188	115.59
300kPa	85.58226	144.4455	105.8559	y	141.4401	179.0327	108.8638

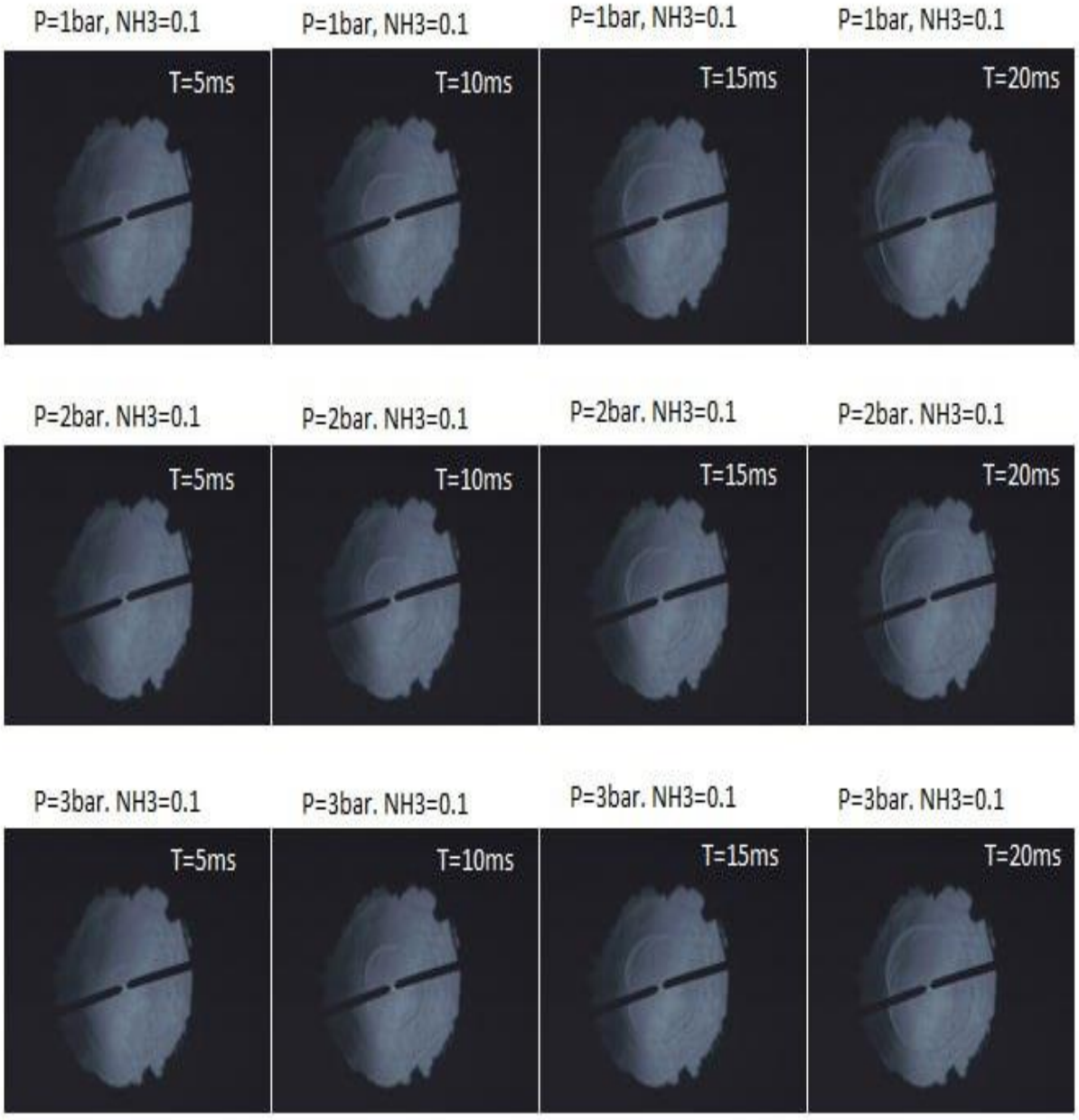

Figure 4.1 Schlieren's photographs illustrate the effect of pressure

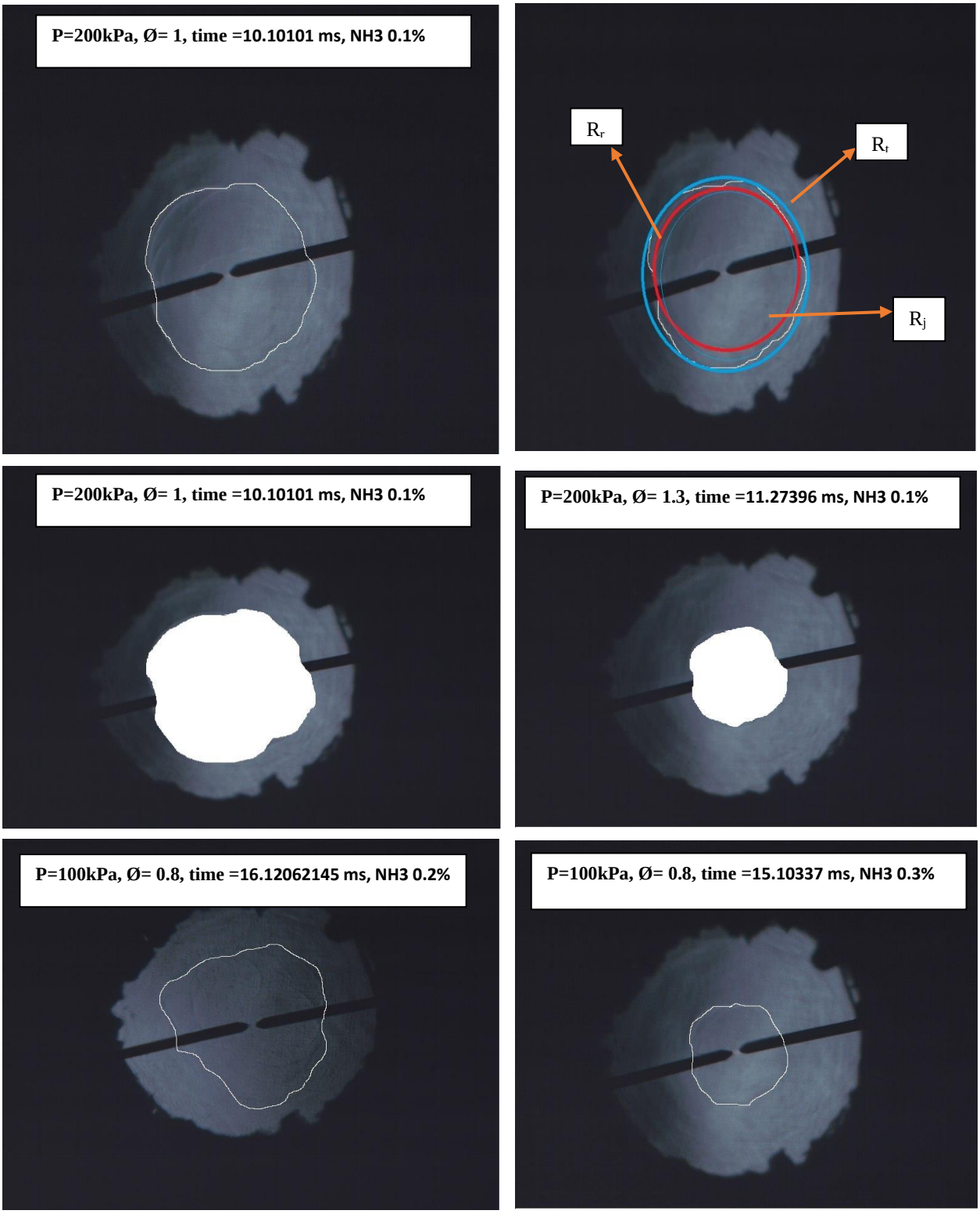

Figure 4.2 Schlieren's photographs

4.5 DISCUSSION

4.5.1 Adiabatic flame temperature

the adiabatic temperature was also calculated theoretically the adiabatic flame temperature is an important parameter that represents the thermodynamic properties of the combustible mixture. Adiabatic flame temperature indicates the heat release capacities of the un-burnt mixture and it is related to various chemical phenomena such as flame propagation speed, flame extinction, flammability limits, etc.

The adiabatic flame temperature has been calculated by MATLAB code program shows Figure (4.3) relationship between adiabatic temperature and equivalence ratio for (10 ,20 ,30) %NH_3 with initial pressure (100) kPa.

4.6 Turbulent flame speed

Turbulent flame speed refers to the rate at which a turbulent flame front propagates through a combustible mixture. It is an important parameter in combustion studies, as it influences various aspects of combustion efficiency, stability, and pollutant emissions in combustion systems.

Figures indicate the effect of increasing the flame radius with increasing time (4.4 to 4.18) shows relationship between Flame radius and Time for concentration (10 ,20 ,30) %NH_3 at equivalence ratio Ø (0.8 ,1 ,1.3) with initial pressure (100, 200 and 300) kPa, the effect of flame radius with time in a turbulent flame can be complex and is influenced by various factors, including turbulence intensity, combustion kinetics, and the initial conditions of the mixture.

We note from the figures that the increase in the radius of the flame is not the passage of time, due to the increase in the burning mixture.

From practical experiments, obtained the speed of the flame as shown figures (4.19 to 4.34) Turbulent flame speed S_n with a flame radius Increasing the speed of the flame as the initial pressure decreases due to the speed of the reaction and the reduction of the chemical reaction.

4.7 stretch rate

note through figures (4.35 ,4.36) shows relationship between turbulent flame speed S_n with a stretch rate The relationship between turbulent flame speed (S_n) and stretch rate is the stretch rate refers to the rate at which a flame front is being stretched or compressed by the turbulent flow of reactants.

Turbulent flames are affected by the complex interaction between turbulence and chemical reactions. The stretch rate plays a crucial role in determining the flame behavior in turbulent flows.

The general relationship between turbulent flame speed and stretch rate can be described Positive Stretch Rate (Compression)When the flame front experiences compression due to the turbulent flow, the reactants are brought closer together, leading to higher reactant concentrations, in regions of positive stretch, the increased concentration of reactants can lead to faster chemical reactions and thus an increase in the turbulent flame speed.

Negative Stretch Rate (Expansion) When the flame front experiences expansion due to the turbulent flow, the reactants are spread apart, resulting in lower reactant concentrations, in regions of negative stretch, the decreased concentration of reactants can slow down chemical reactions and lead to a decrease in the turbulent flame speed.

4.8 Laminar burning velocity

and figures (4.37 to 4.41) shows relationship between Laminar burning velocity S_l with a flame radius Laminar burning velocity for NH3 – LPG – air mixture with the temperature of 298 K, at 0.1, 0.2 and 0.3 MPa. The results show that Laminar burning velocity decreases as the initial pressure increases. This is due to the decrease of thermal diffusivity of the fuel mixture with the increase of initial pressure.

Effect with Equivalence Ratio and effect of Ammonia Gas Percentage show that when the E_{LPG} =0 and E_{NH3} = 100%, the lowest value of the laminar burning velocities is on the lean mixture, and the highest value when it reaches the stoichiometric mixture and begins to decrease on the rich mixture. Figure (4.38) shows that when the E_{LPG} = 100 % and E_{NH3} = 0 %, the lowest value of the laminar burning velocity is on the lean mixture, and the highest value when it reaches the stoichiometric mixture and begins to decrease on the rich mixture.

Whenever the concentration of ammonia exceeds 10% the increase in the laminar burning velocity value begins. that when the concentration of ammonia gas increases, the laminar burning velocity begins to decrease clearly. That is the higher value of S_l. and its highest value at a concentration of 10% of ammonia. The stoichiometric mixture has the highest value for the laminar burning velocity.

4.9 Turbulent burning velocity

and figures (4.42 to 4.46) shows relationship between Turbulent burning velocity S_t with a flame radius and figure (4.47) shows relationship between Turbulent burning velocity S_t with a flame radius and Laminar burning velocity S_l with a flame radius

The results showed that the use of the turbulent system inside the fixed combustion chamber leads to a clear increase in the combustion speed of the mixture of gases (LPG, ammonia, and air) at the ammonia concentration ratios (10-20-30), as well as when changing the pressure (100-200-300), where we obtained The best increase in the combustion speed at pressure (100) and ammonia concentration 10% , because the increase in pressure affects the combustion speed, as well as the concentration of ammonia reduces the combustion speed (LPG) gas.

The higher the concentration of ammonia mixing, as ammonia has a very low combustion speed compared to a high diffusion speed As mixing ammonia with gas (LPG) improves the flame speed, but reduces the combustion speed with increasing the ammonia concentration to a high percentage.

When comparing the combustion speed of turbulent conditions with the combustion speed of laminar conditions, the results showed that the best increase in combustion speed is when it is a turbulent state in ratios Mixing equivalence (0.8) then decreases and approaches lamellar as we tend to increase the mixing ratio and equivalence (1.3, 1).

The reason for this is that the mixture of gases (LPG, ammonia and air) inside the combustion chamber has a relatively high chemical reaction speed, but it needs a good mixing tool and at high proportions Mixing (0.8), the percentage of oxygen inside the combustion chamber is high, and when the air mixing engines are running and relatively large vortices are formed.

The oxygen atoms approach well from the reactants, causing an increase in the combustion speed. In the case of parity (1, 1.3), the percentage of oxygen atoms

inside the combustion chamber Equal or less than the number of moles required, the effect of the turbulent process is less, and the reaction turns from a fast chemical.

4.10 Density ratio

the density ratio the burned materials to the density of the unburned materials decreases clearly when the equivalence ratio is (1) because the adiabatic temperature, which is the highest possible when the valence is equal to (1), and this leads to a significant decrease in the density of the burned materials and it is less when the equivalence is (0.8) and less at equivalence (1.3), because the adiabatic temperature is lower show figure (4.48).

figure (4.48) shows relationship between density ratio with a Ø with initial pressure (100) kPa with ammonia concentration (10 ,20 ,30) % NH_3.

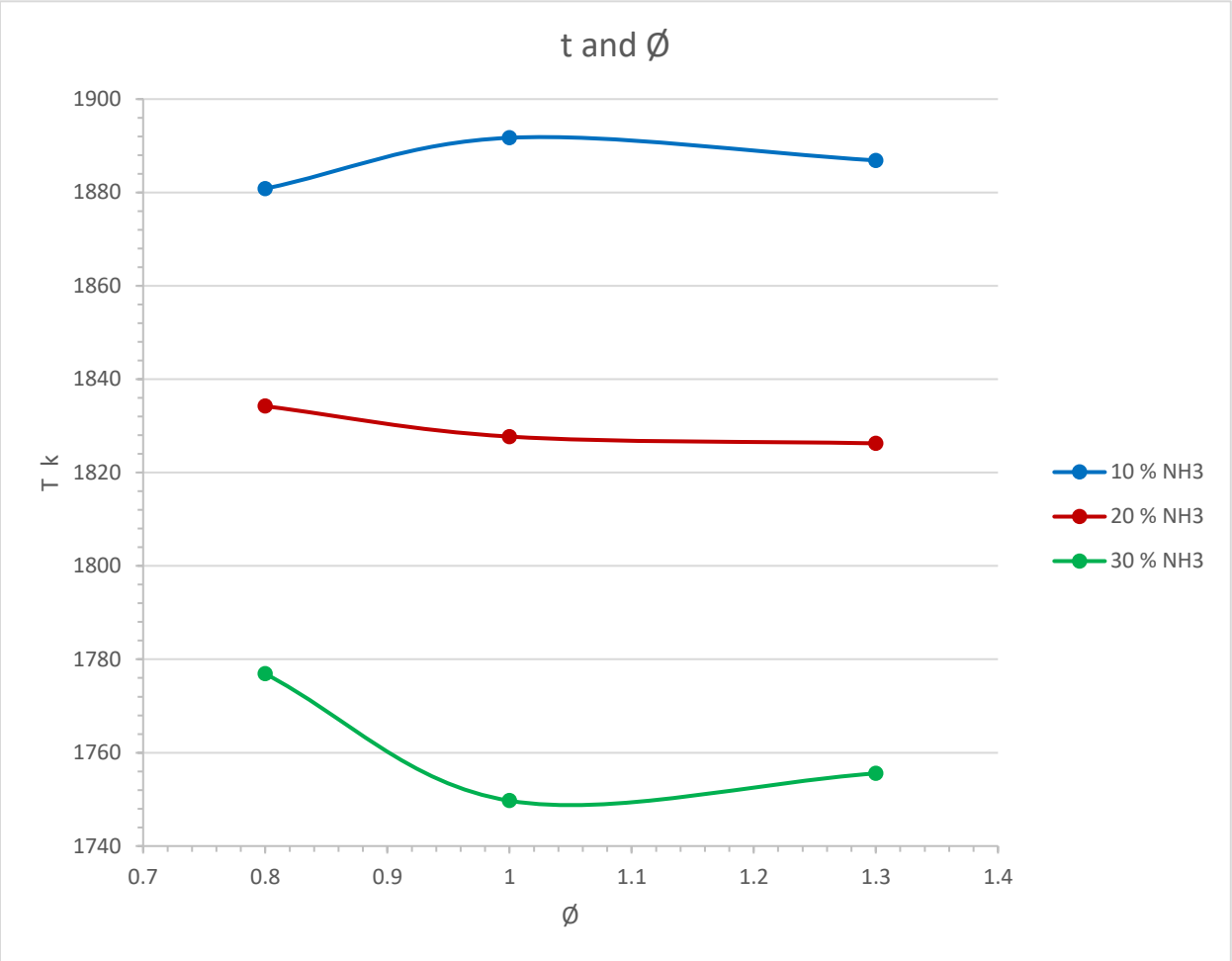

Figure (4.3) adiabatic temperature and equivalence ratio for (10) %NH_3 with initial pressure (100) kPa

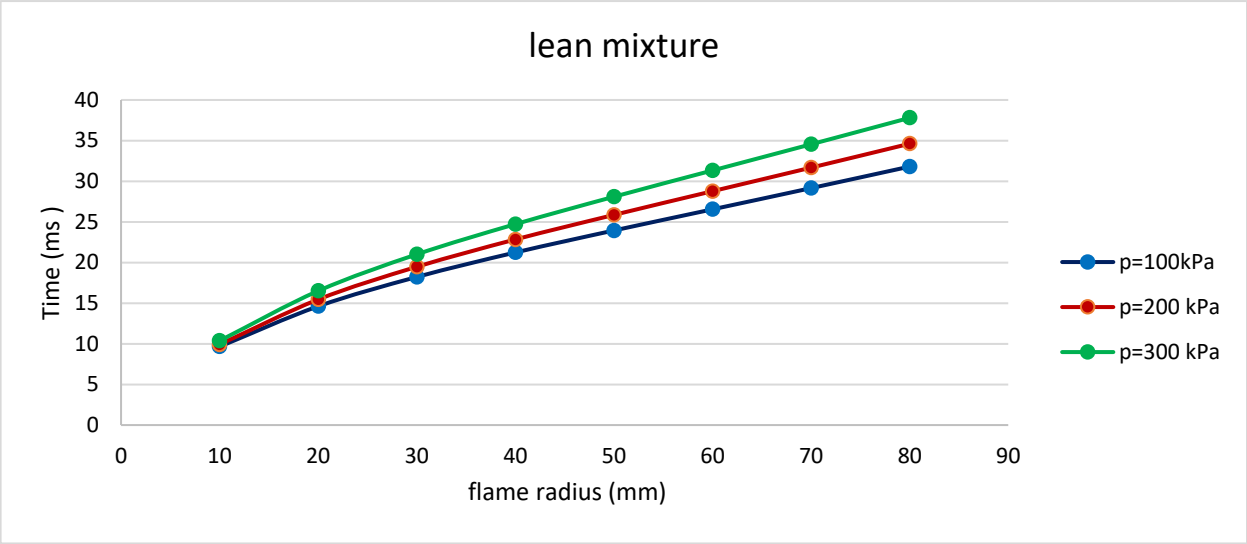

Figure (4.4) Flame radius and Time for 100%NH_3 at equivalence ratio Ø=0.8 with initial pressure (100, 200 and 300) kPa

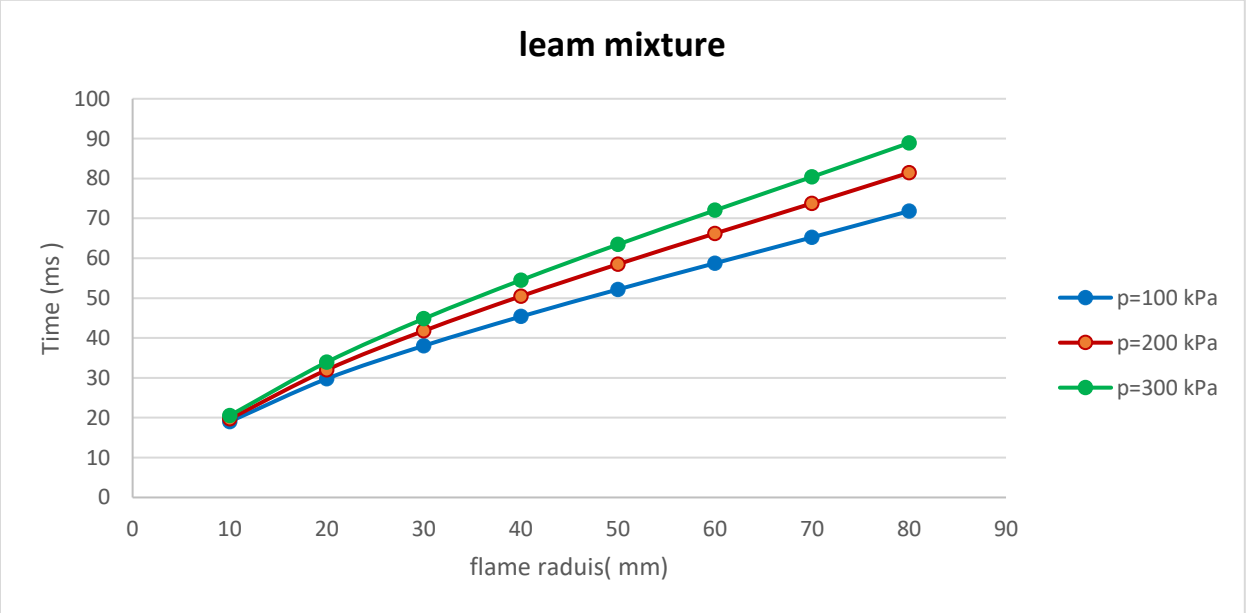

Figure (4.5) Flame radius and Time for 100%LPG at equivalence ratio Ø=0.8 with initial pressure (100, 200 and 300) kPa

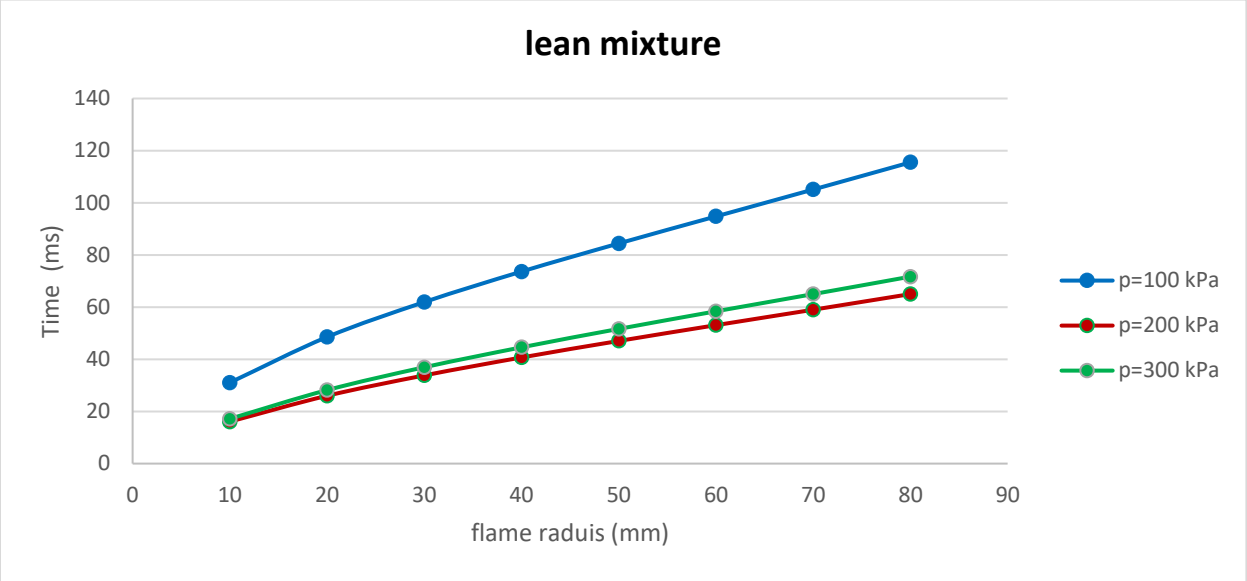

Figure (4.6) Flame radius and Time for 90%LPG + 10%NH_3 at equivalence ratio Ø=0.8 with initial pressure (100, 200 and 300) kPa

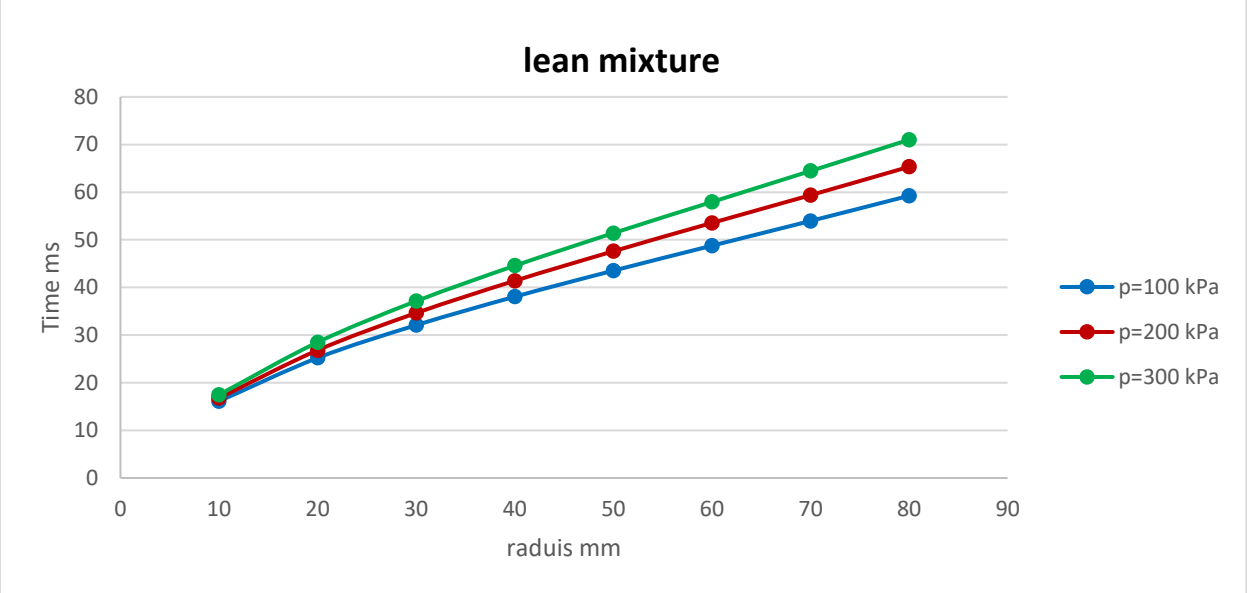

Figure (4.7) Flame radius and Time for 80%LPG + 20%NH_3 at equivalence ratio Ø=0.8 with initial pressure (100, 200 and 300) kPa

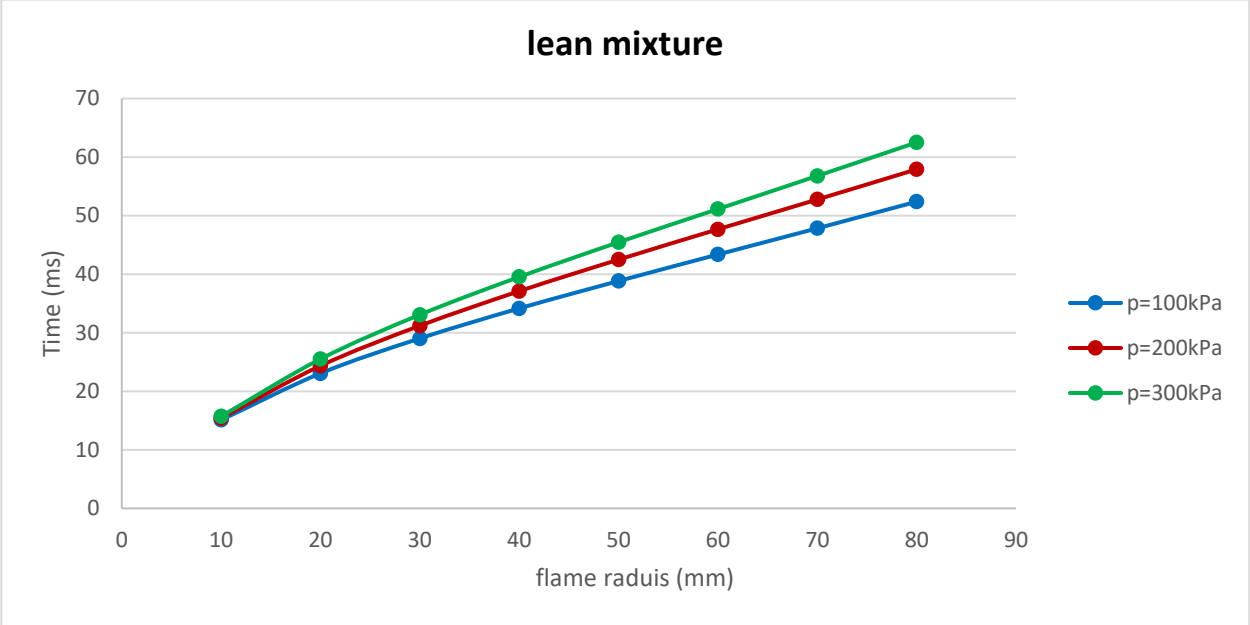

Figure (4.8) Flame radius and Time for 70%LPG + 30%NH_3 at equivalence ratio Ø=0.8 with initial pressure 100, 200 and 300) kPa

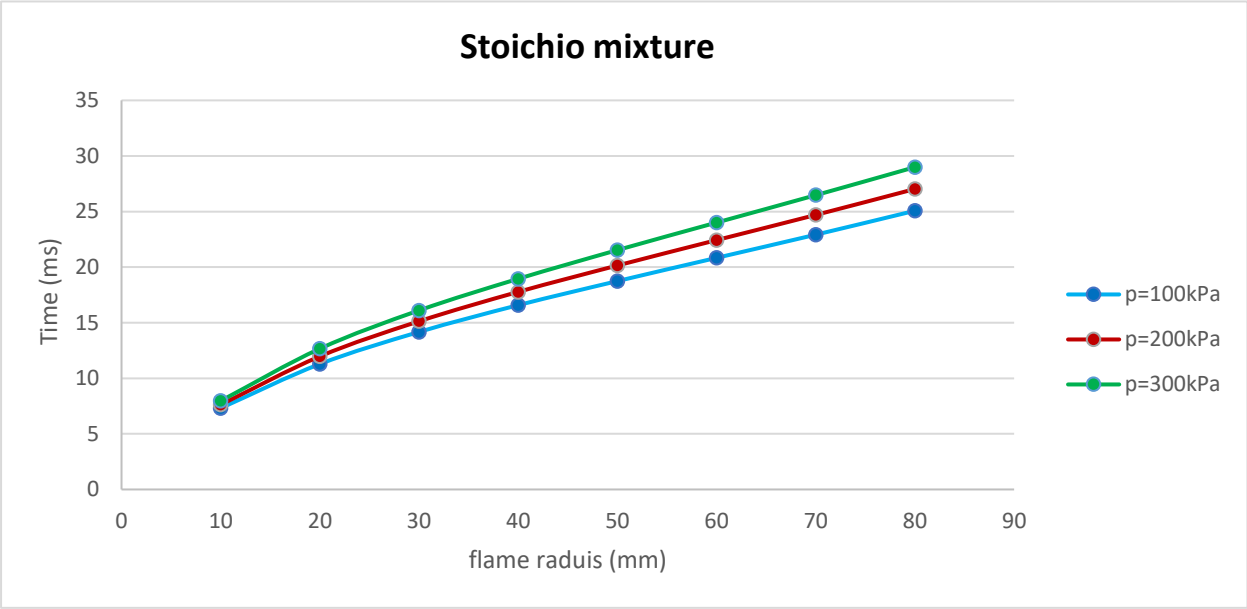

Figure (4.9) Flame radius and Time for 100%NH_3 at equivalence ratio Ø=1 with initial pressure (100, 200 and 300) kPa

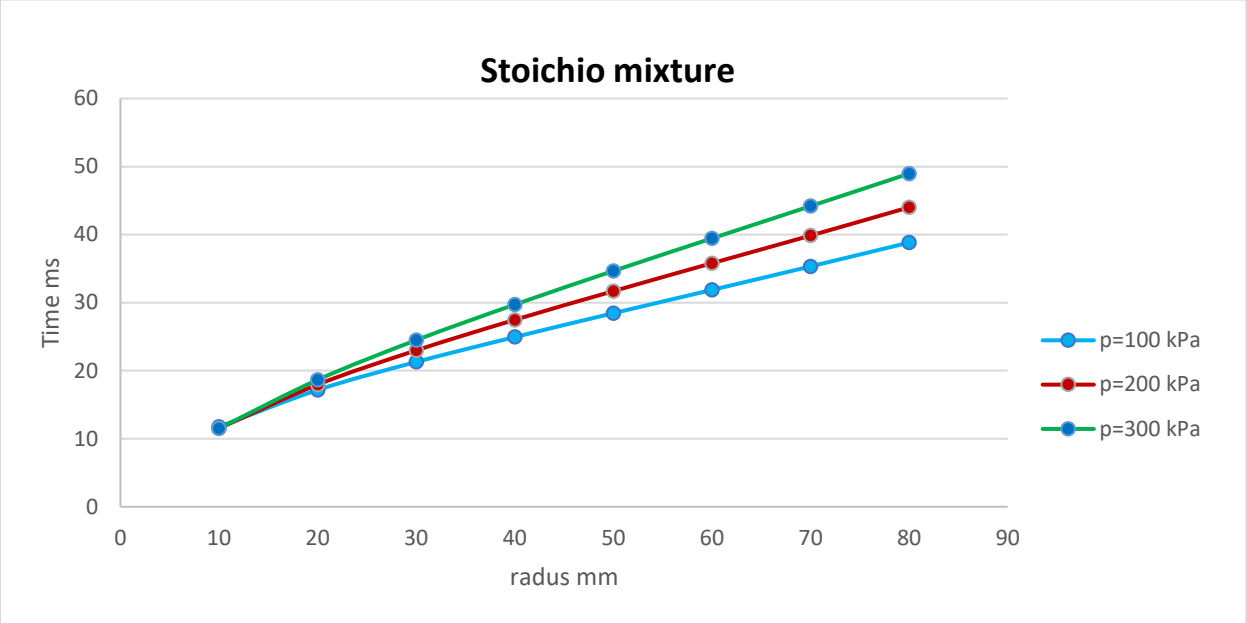

Figure (4.10) Flame radius and Time for 100%LPG at equivalence ratio Ø=1 with initial pressure (100, 200 and 300) kPa

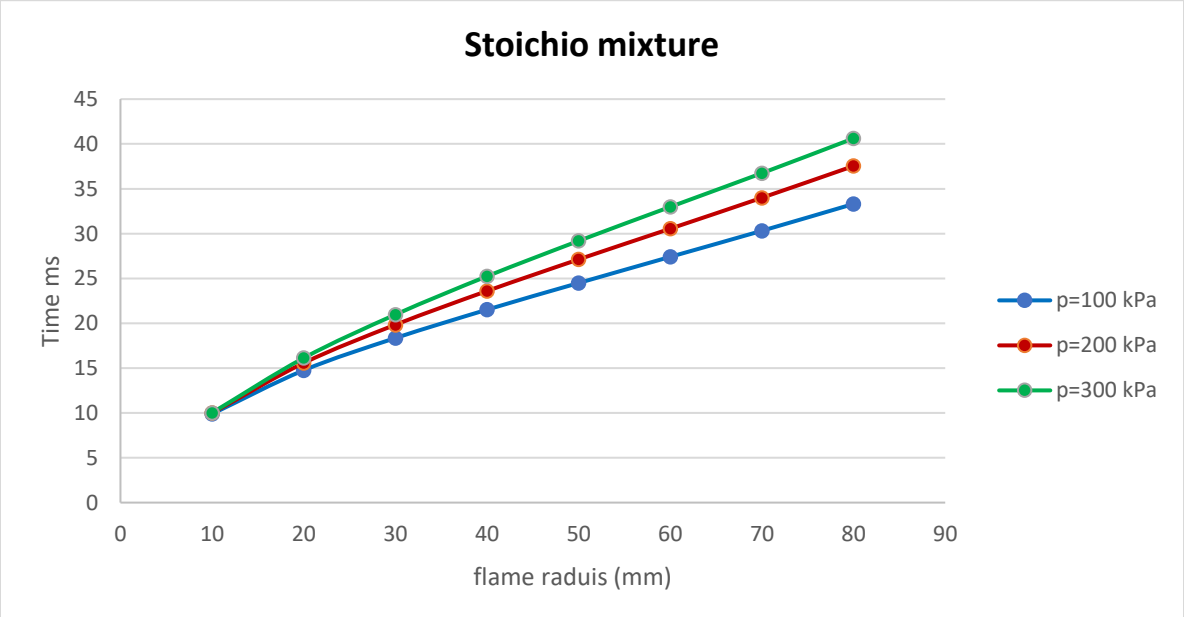

Figure (4.11) Flame radius and Time for 10%LPG at equivalence ratio Ø=1 with initial pressure (100, 200 and 300) kPa

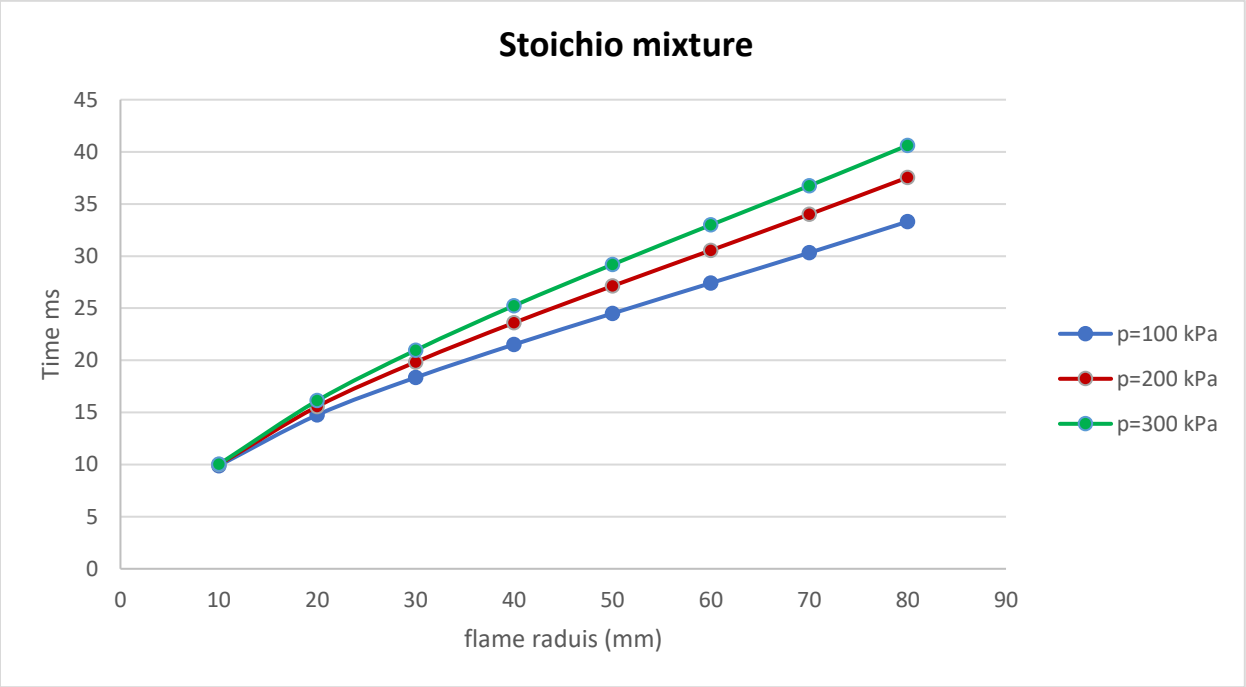

Figure (4.12) Flame radius and Time for 80%LPG + 20%NH_3 at equivalence ratio Ø=1 with initial pressure (100, 200 and 300) kPa

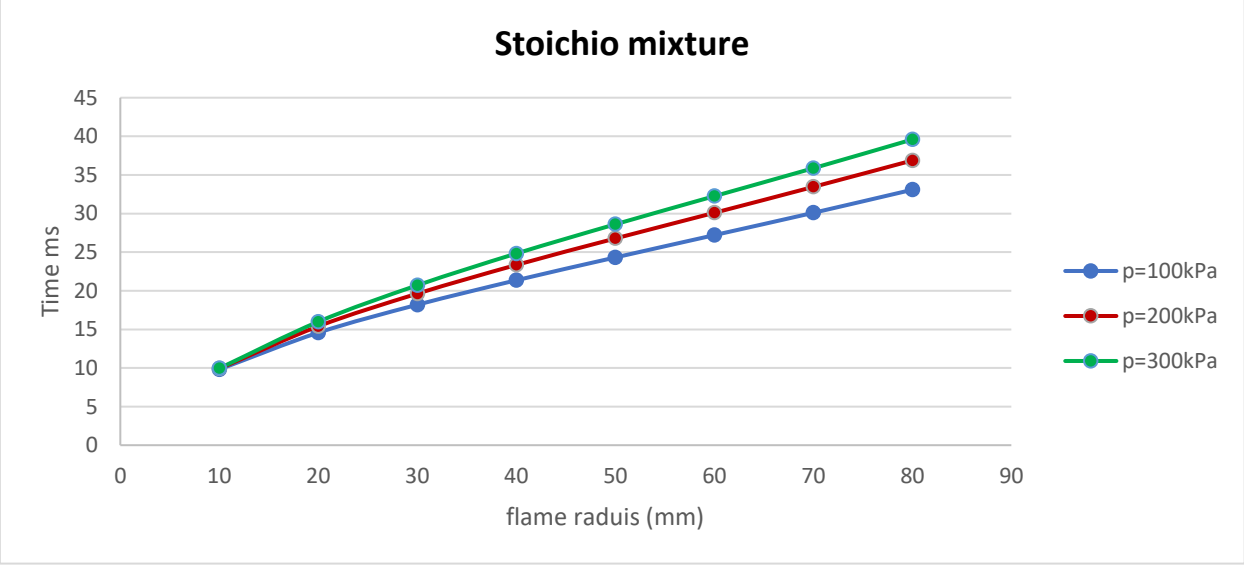

Figure (4.13) Flame radius and Time for 70%LPG + 30%NH_3 at equivalence ratio Ø=1 with initial pressure (100, 200 and 300) kPa

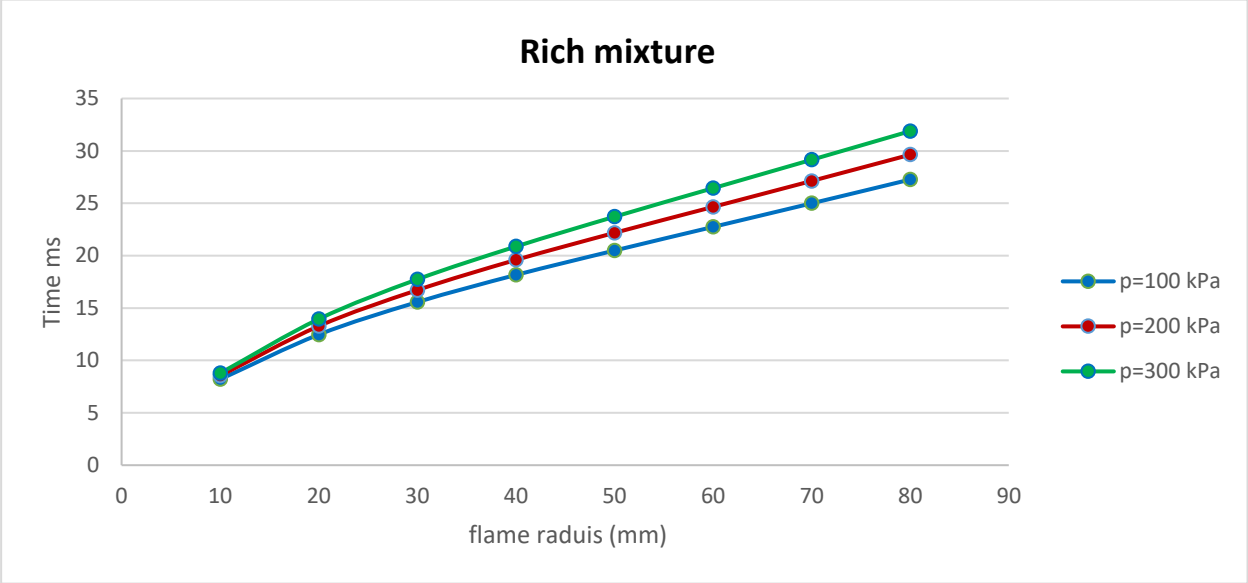

Figure (4.14) Flame radius and Time 100%NH_3 at equivalence ratio Ø=1.3 with initial pressure (100, 200 and 300) kPa

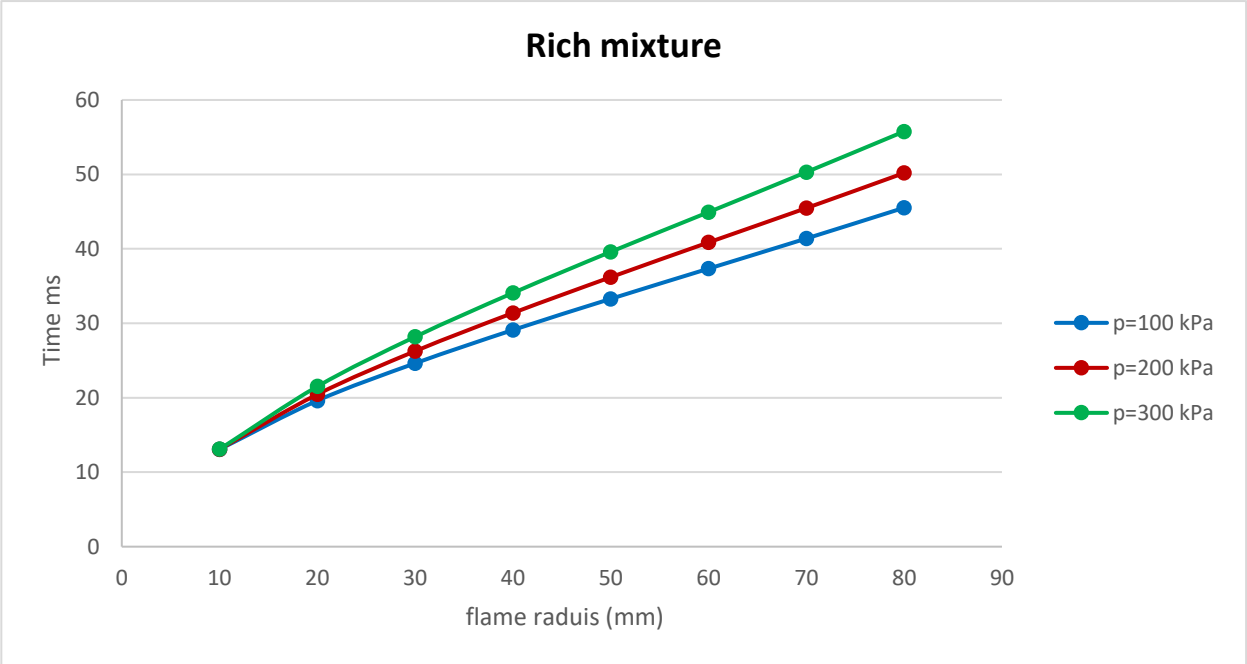

Figure (4.15) Flame radius and Time for 100%LPG at equivalence ratio Ø=1.3 with initial pressure (100, 200 and 300) kPa

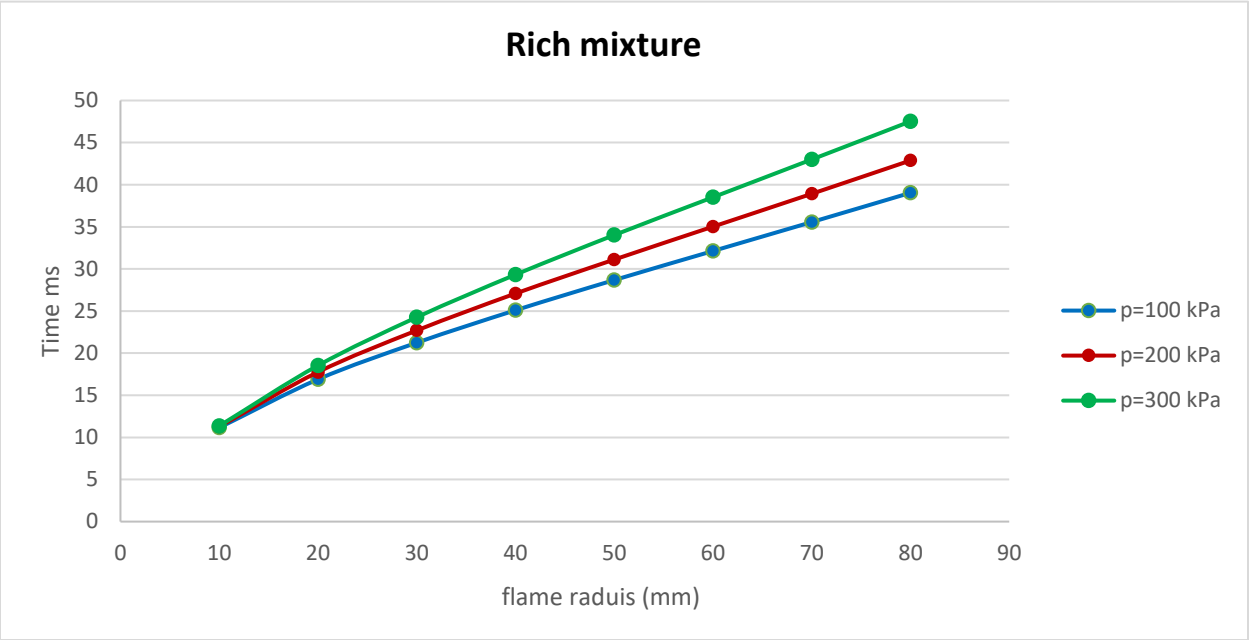

Figure (4.16) Flame radius and Time for 90%LPG + 10%NH_3 at equivalence ratio Ø=1.3 with initial pressure (100, 200 and 300) kPa

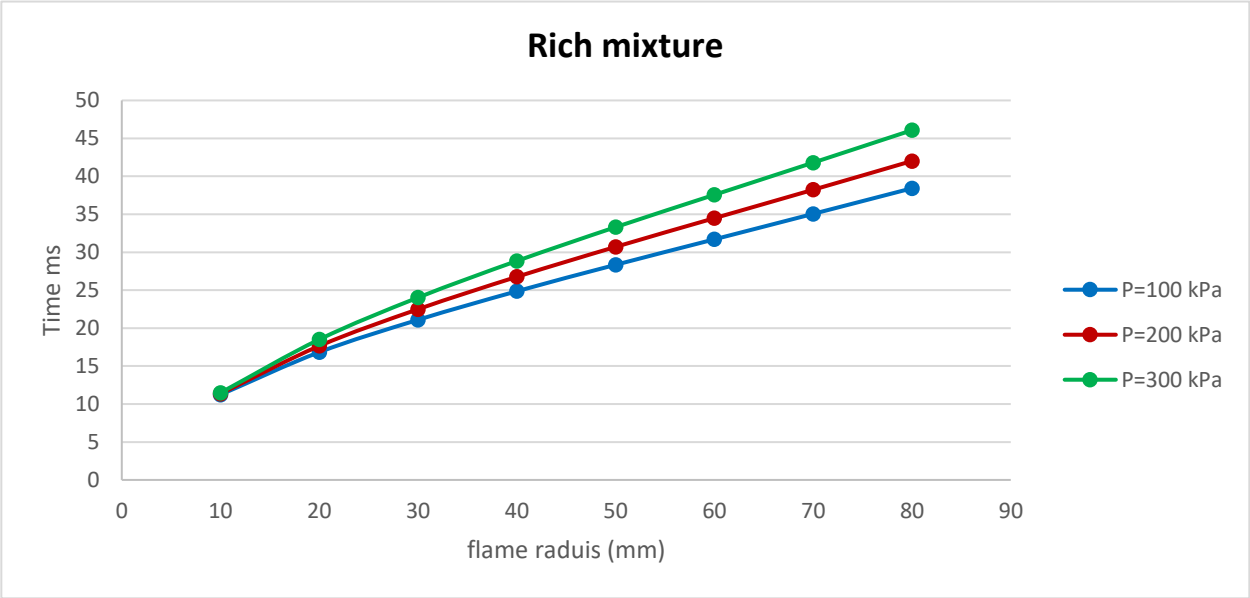

Figure (4.17) Flame radius and Time for 80%LPG + 20%NH_3 at equivalence ratio Ø=1.3 with initial pressure (100, 200 and 300) kPa

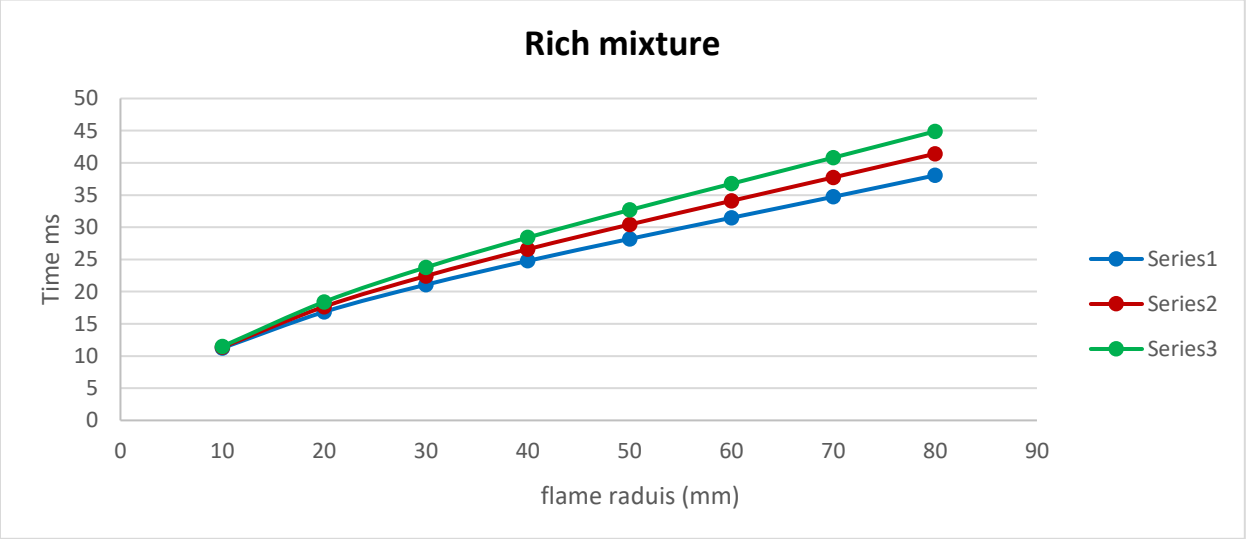

Figure (4.18) Flame radius and Time for 70%LPG + 30%NH_3 at equivalence ratio Ø=1.3 with initial pressure (100, 200 and 300) kPa

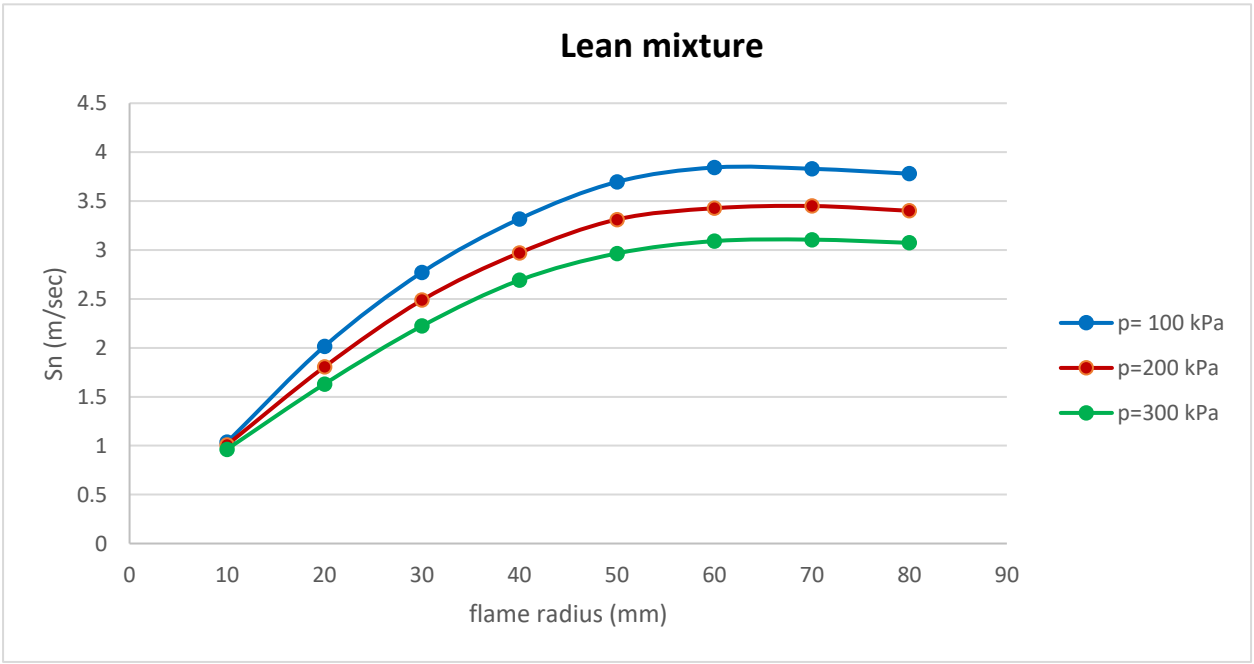

Figure (4.19) Turbulent flame speed S_n with a flame radius for 100% NH_3 at Ø = 0.8 with initial pressure (100, 200 and 300) kPa

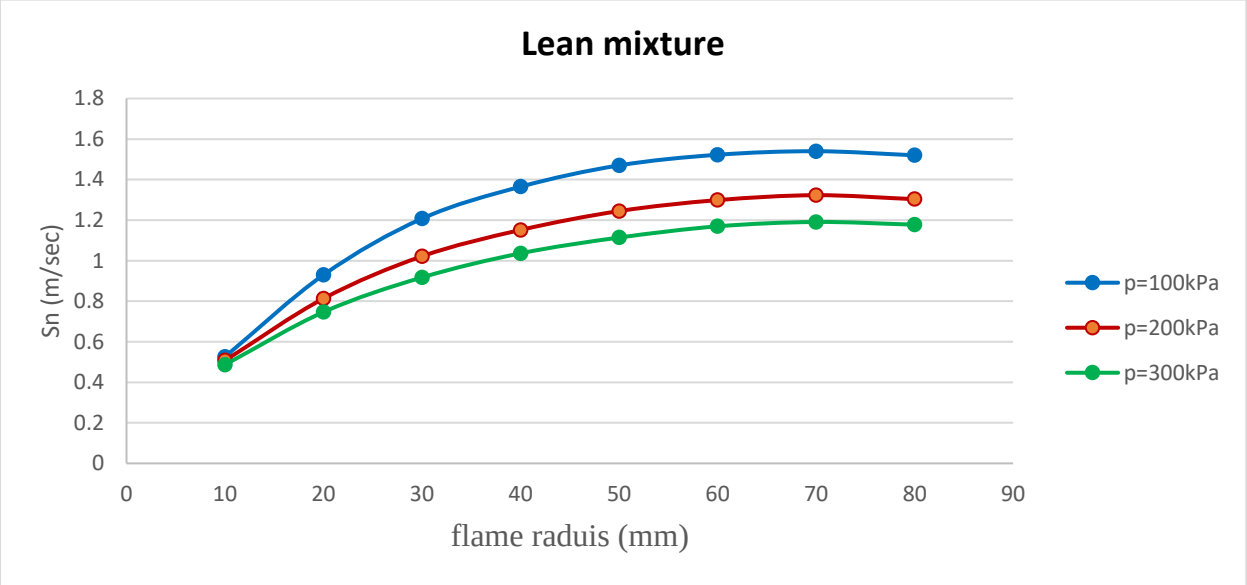

Figure (4.20) Turbulent flame speed S_n with a flame radius for 100% LPG at Ø = 0.8 with initial pressure (100, 200 and 300) kPa

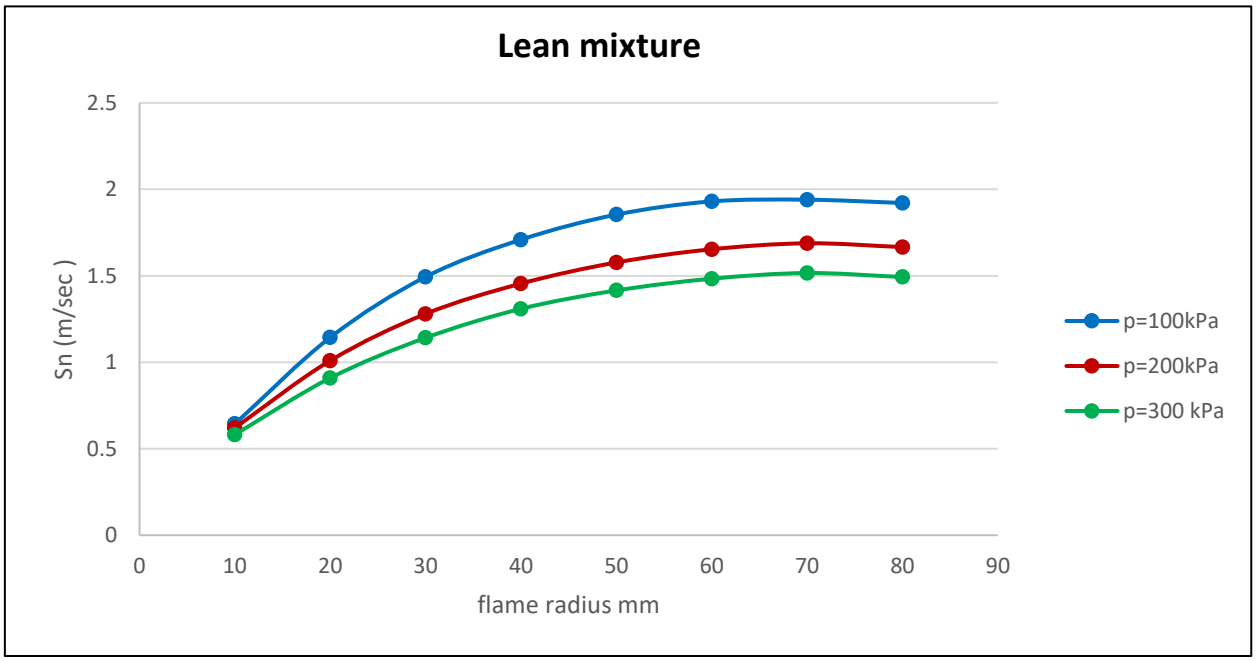

Figure (4.21) Turbulent flame speed S_n with a flame radius for 10% NH_3 and 90% LPG at Ø = 0.8 with initial pressure (100, 200 and 300) kPa

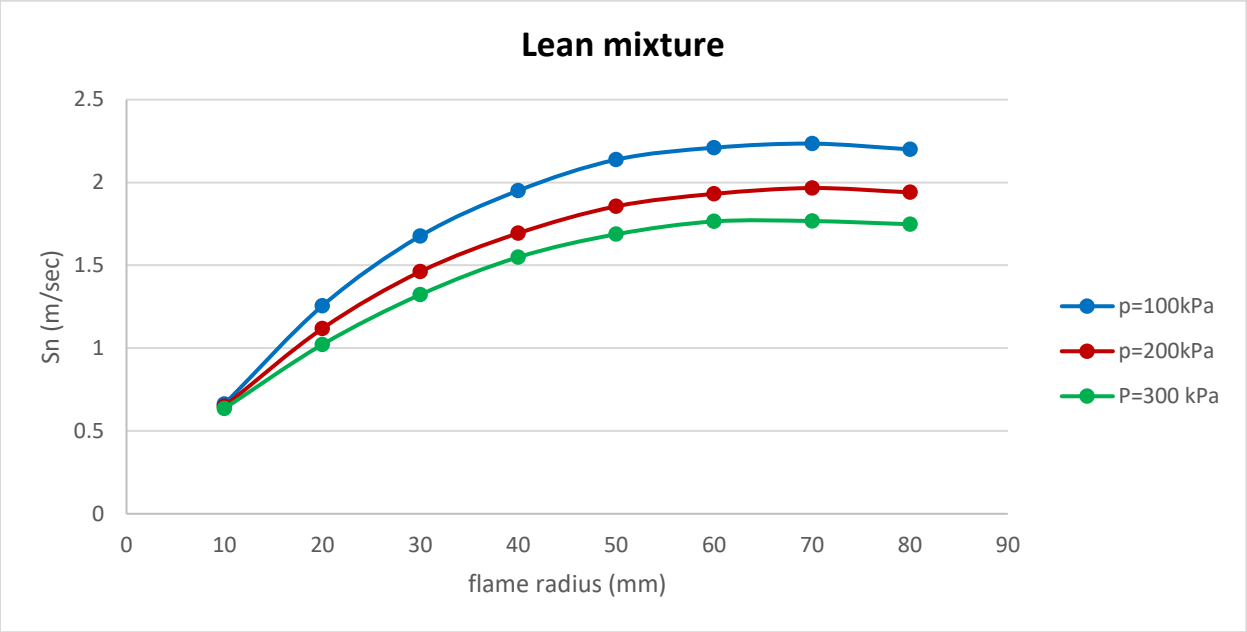

Figure (4.22) Turbulent flame speed S_n with a flame radius for 20% NH_3 and 80% LPG at Ø = 0.8 with initial pressure (100, 200 and 300) kPa

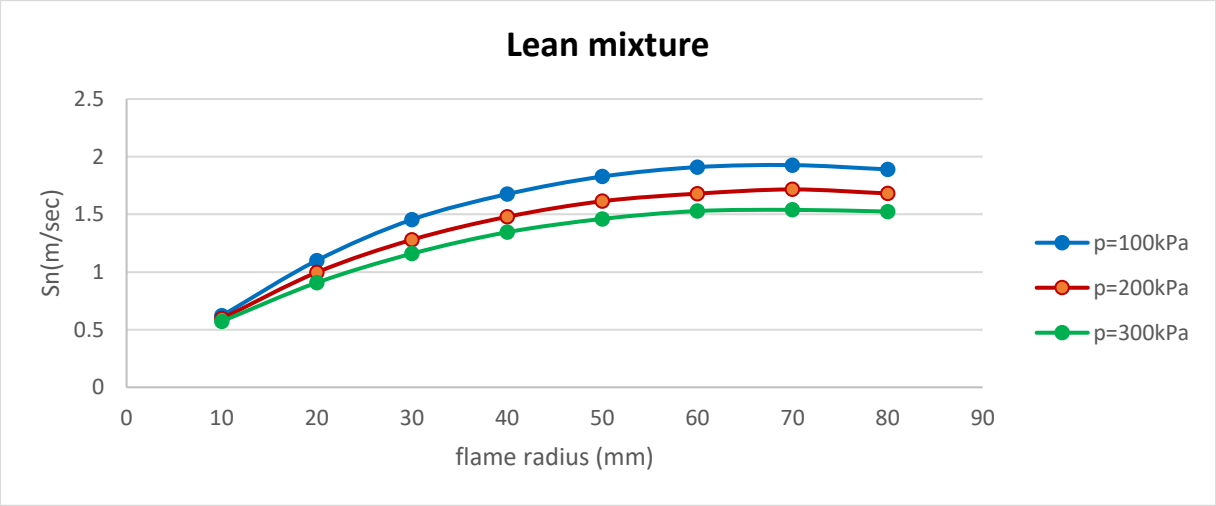

Figure (4.23) Turbulent flame speed S_n with a flame radius for 30% NH_3 and 90% LPG at Ø = 0.8 with initial pressure (100, 200 and 300) kPa

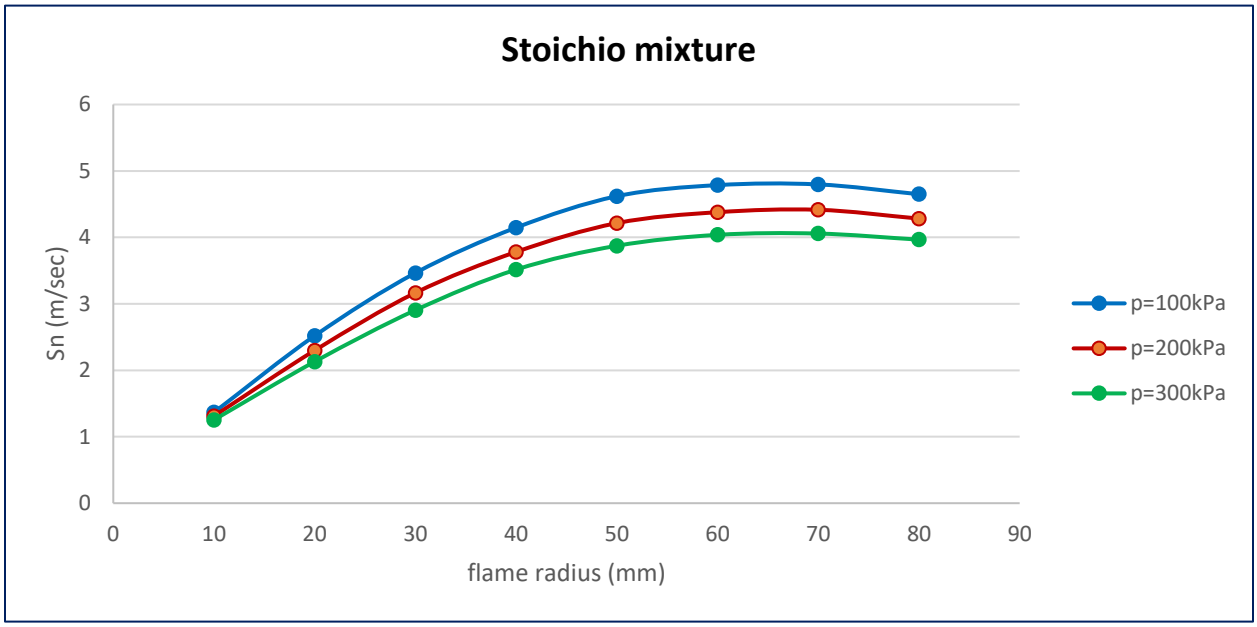

Figure (4.25) Turbulent flame speed S_n with a flame radius for 100% NH_3 at Ø = 1 with initial pressure (100, 200 and 300) kPa

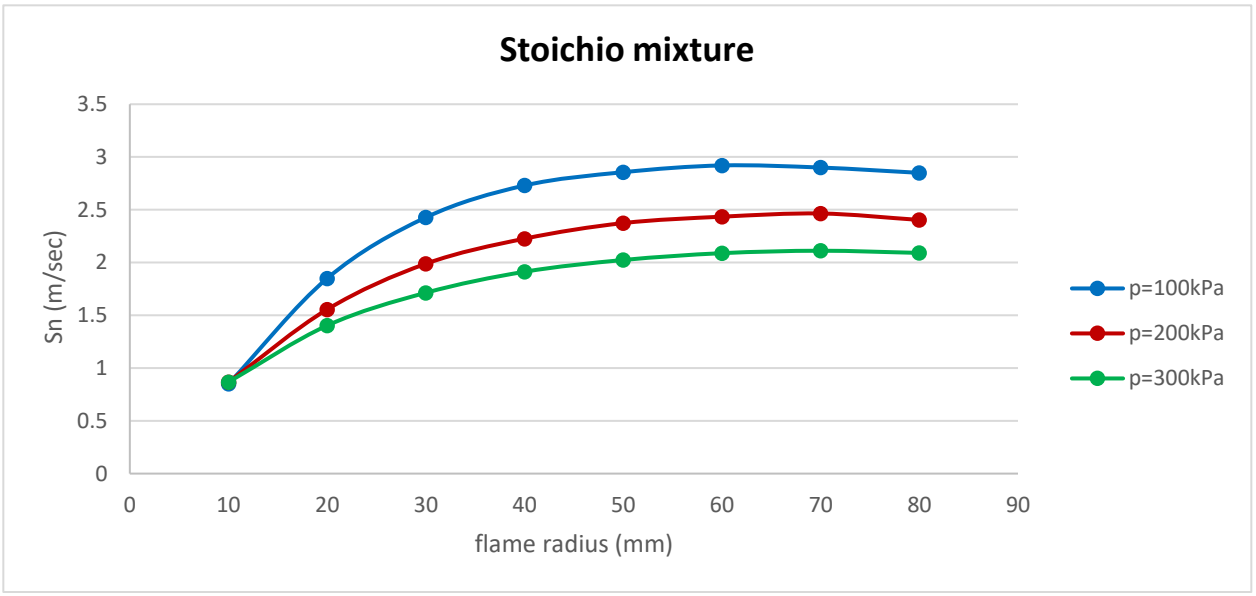

Figure (4.26) Turbulent flame speed S_n with a flame radius for 100% LPG at Ø = 1 with initial pressure (100, 200 and 300) kPa

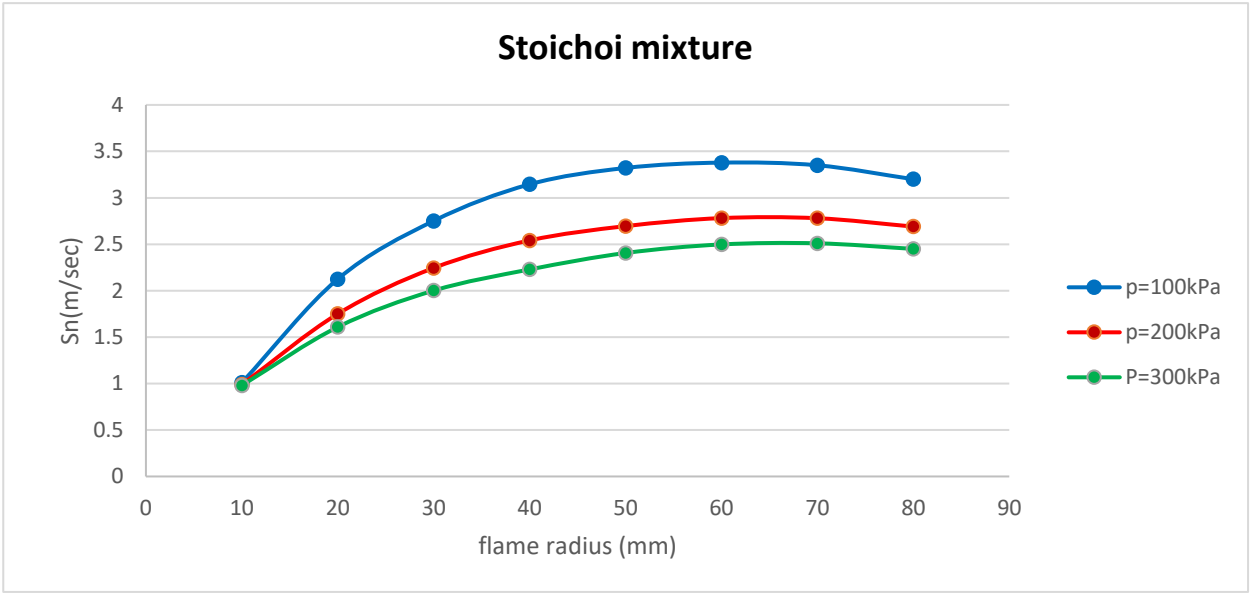

Figure (4.27) Turbulent flame speed S_n with a flame radius for 90%LPG and 10% NH_3 at Ø = 1 with initial pressure (100, 200 and 300) kPa

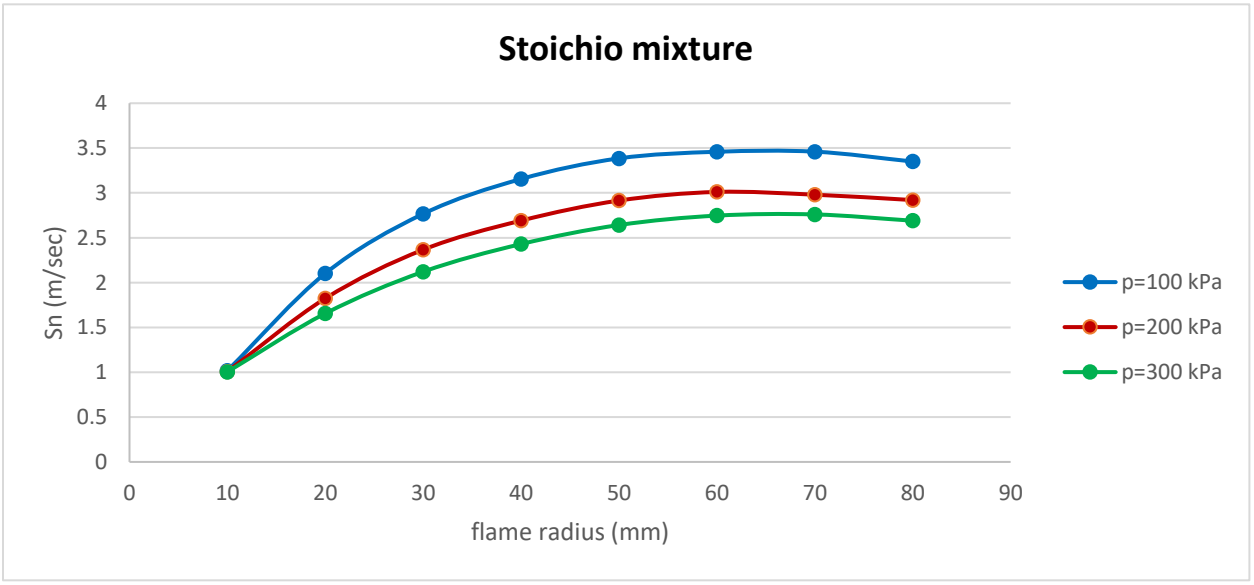

Figure (4.28) Turbulent flame speed S_n with a flame radius for 80%LPG and 20% NH_3 at Ø = 1 with initial pressure (100, 200 and 300) kPa

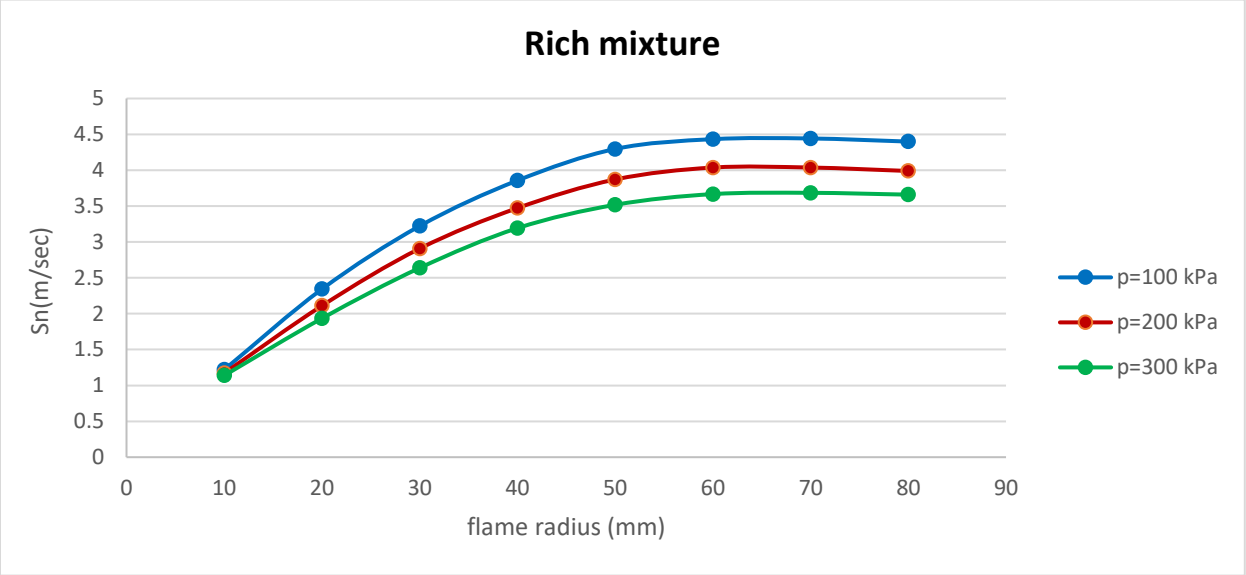

Figure (4.29) Turbulent flame speed S_n with a flame radius for 70%LPG and 30% NH_3 at Ø = 1 with initial pressure (100, 200 and 300) kPa

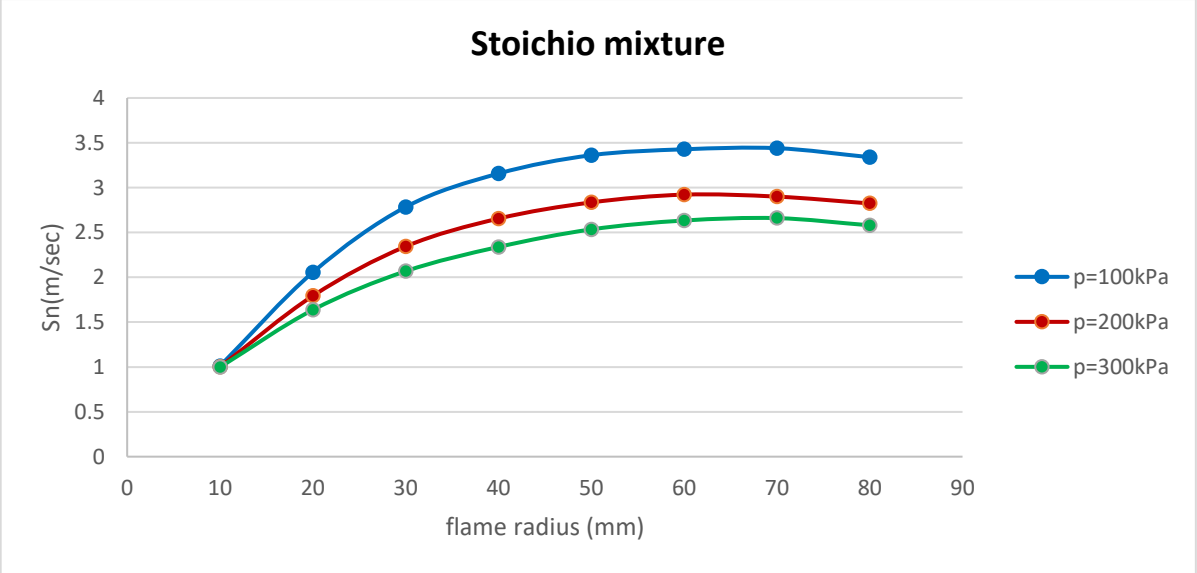

Figure (4.30) Turbulent flame speed S_n with a flame radius for 100% NH_3 at Ø = 1.3with initial pressure (100, 200 and 300) kPa

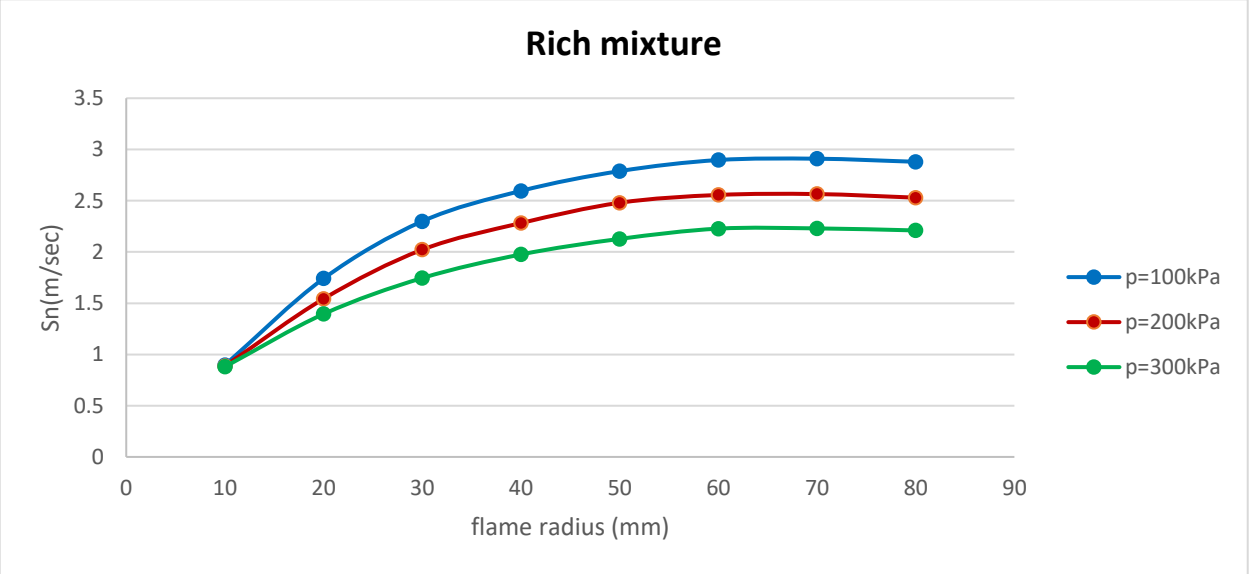

Figure (4.31) Turbulent flame speed S_n with a flame radius for 100%LPG at Ø = 1.3 with initial pressure (100, 200 and 300) kPa

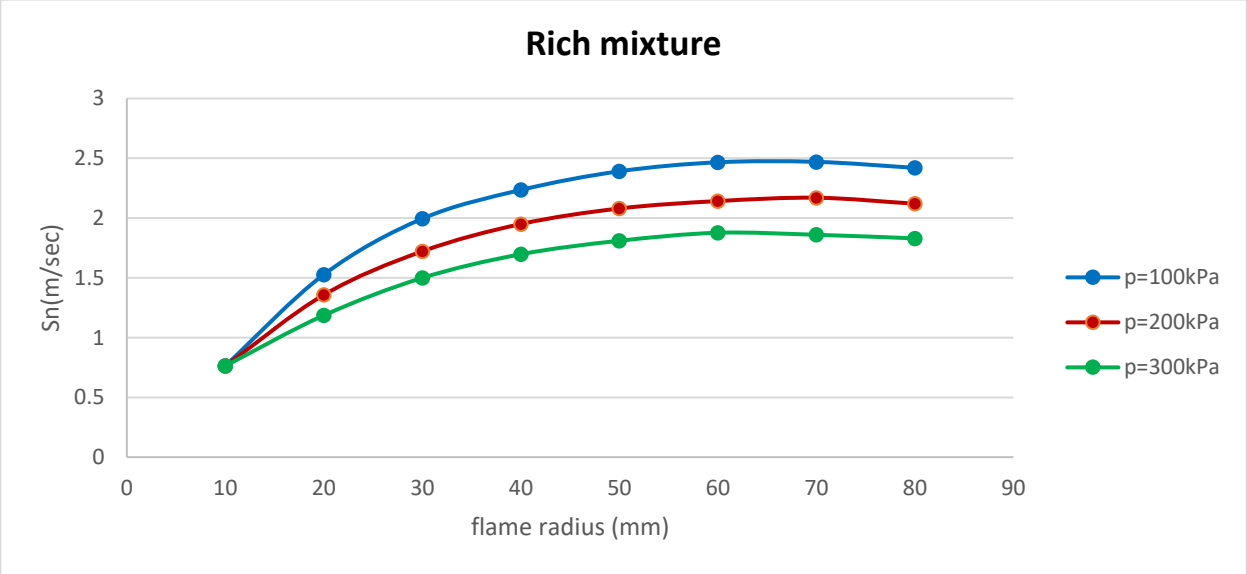

Figure (4.32) Turbulent flame speed S_n with a flame radius for 90%LPG and 10% NH_3 at Ø = 1.3 with initial pressure (100, 200 and 300) kPa

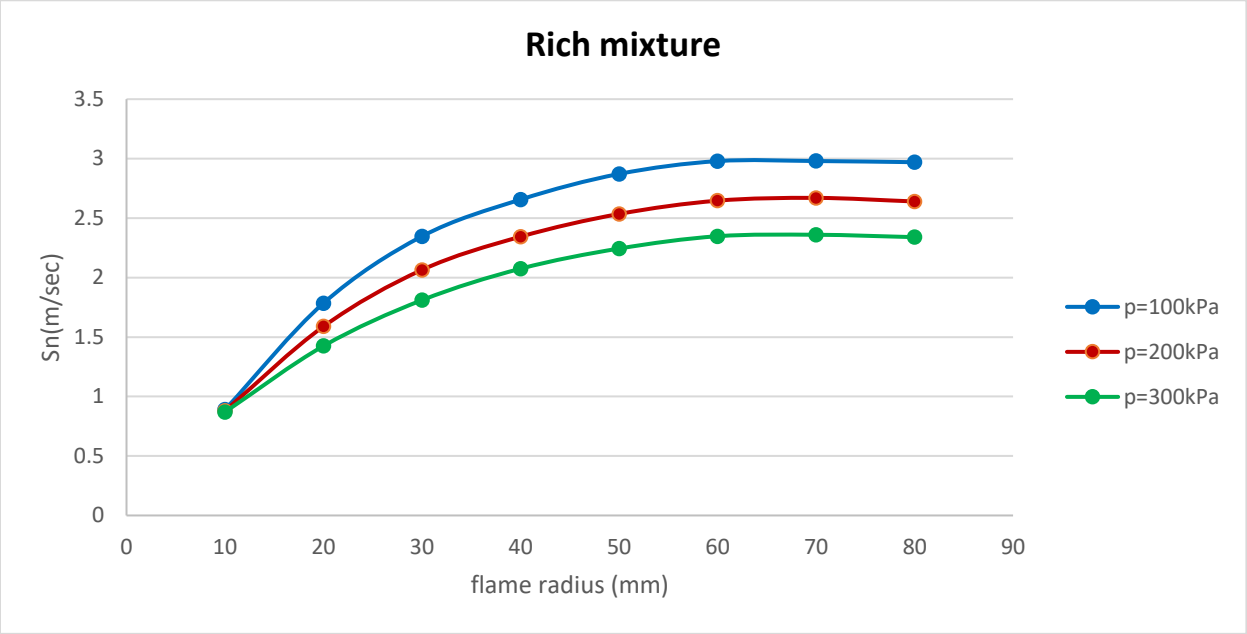

Figure (4.33) Turbulent flame speed S_n with a flame radius for 80%LPG and 20% NH_3 at Ø = 1.3 with initial pressure (100, 200 and 300) kPa

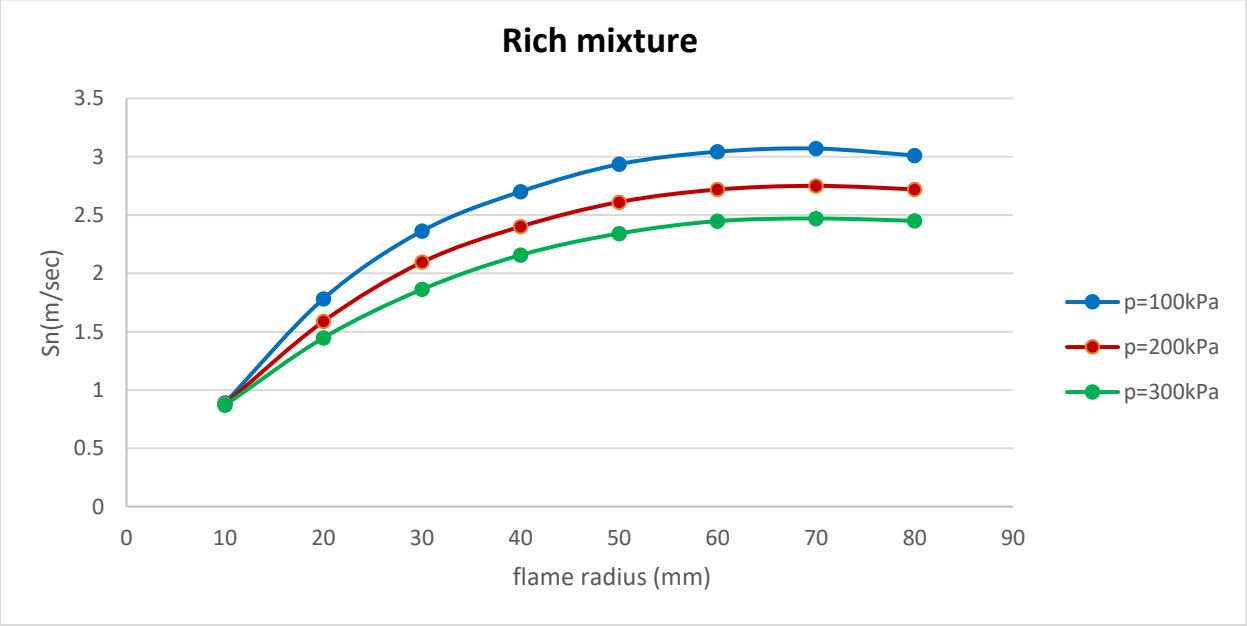

Figure (4.34) Turbulent flame speed S_n with a flame radius for 70%LPG and 30% NH_3 at Ø = 1.3 with initial pressure (100, 200 and 300) kPa

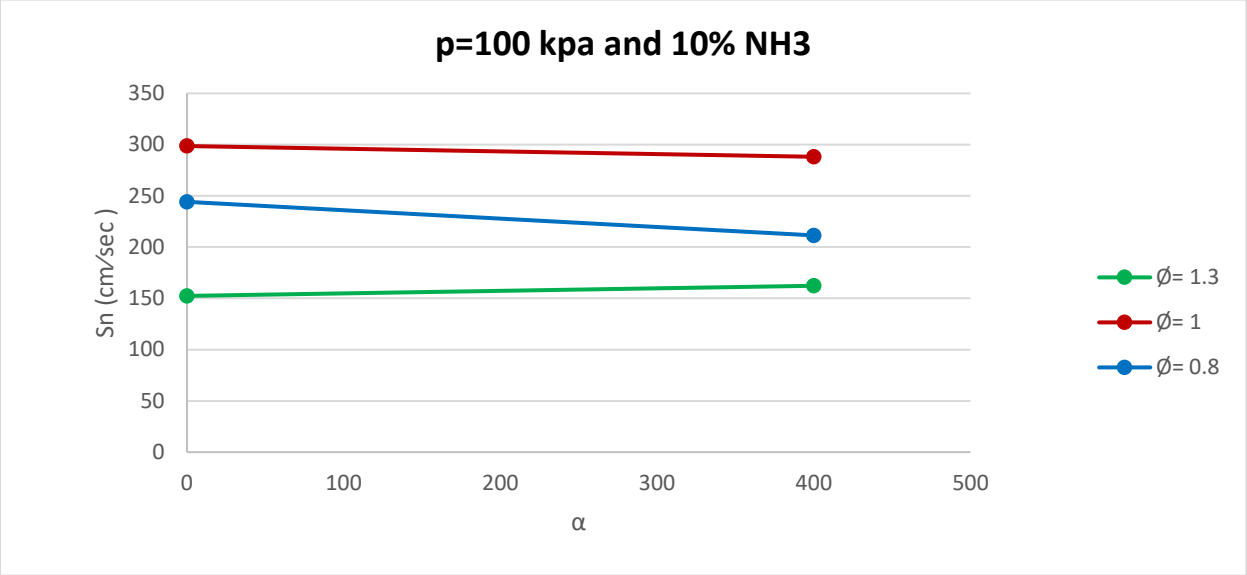

Figure (4.35) Turbulent flame speed S_n with a stretch rate 70%LPG and 30% NH_3 at Ø (0.8,1, 1.3) with initial pressure (200) kPa

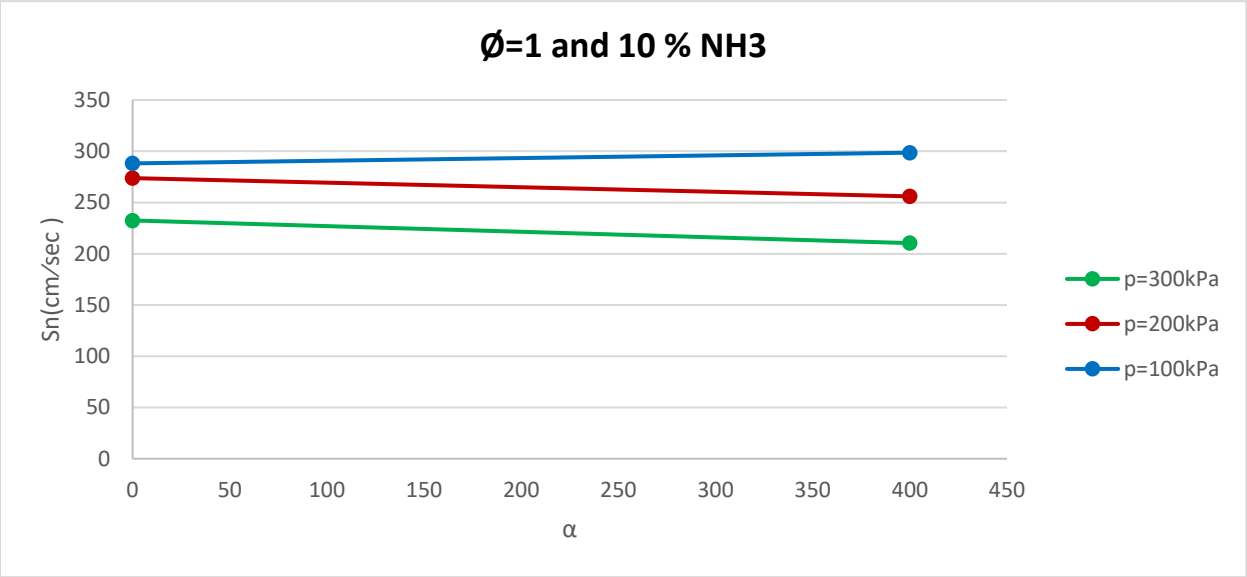

Figure (4.36) Turbulent flame speed S_n with a stretch rate 90%LPG and 10% NH_3 at Ø (0.8,1, 1.3) with initial pressure (100) kPa

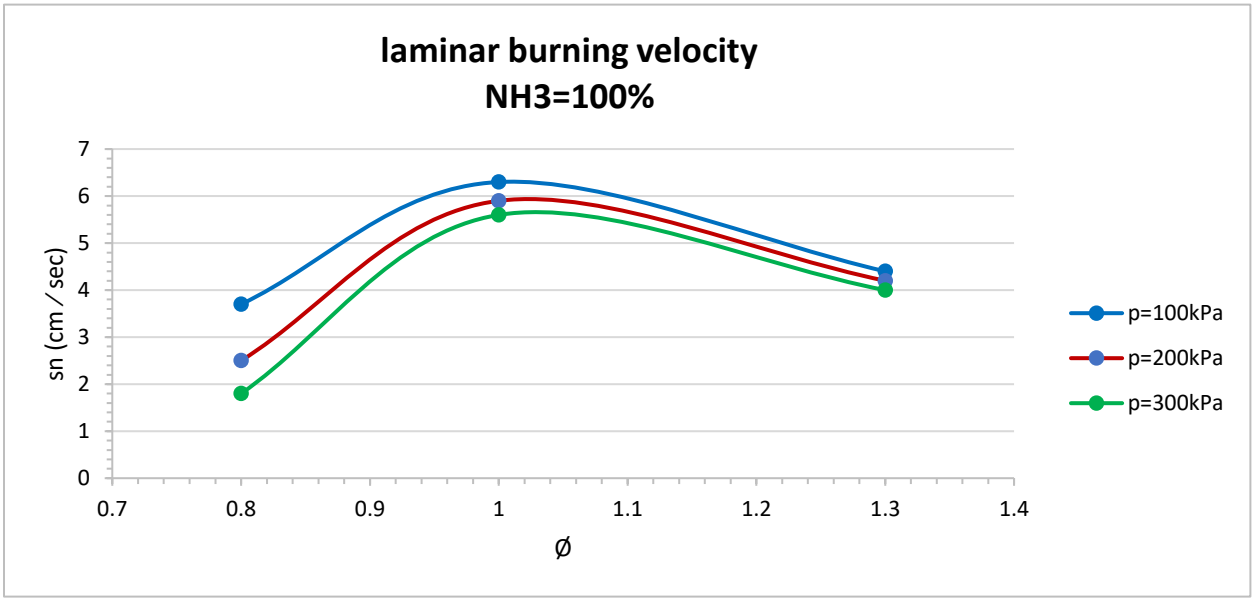

Figure (4.37) Laminar burning veloicty S_l with a flame radius for 100% NH_3 with initial pressure (100, 200 and 300) kPa

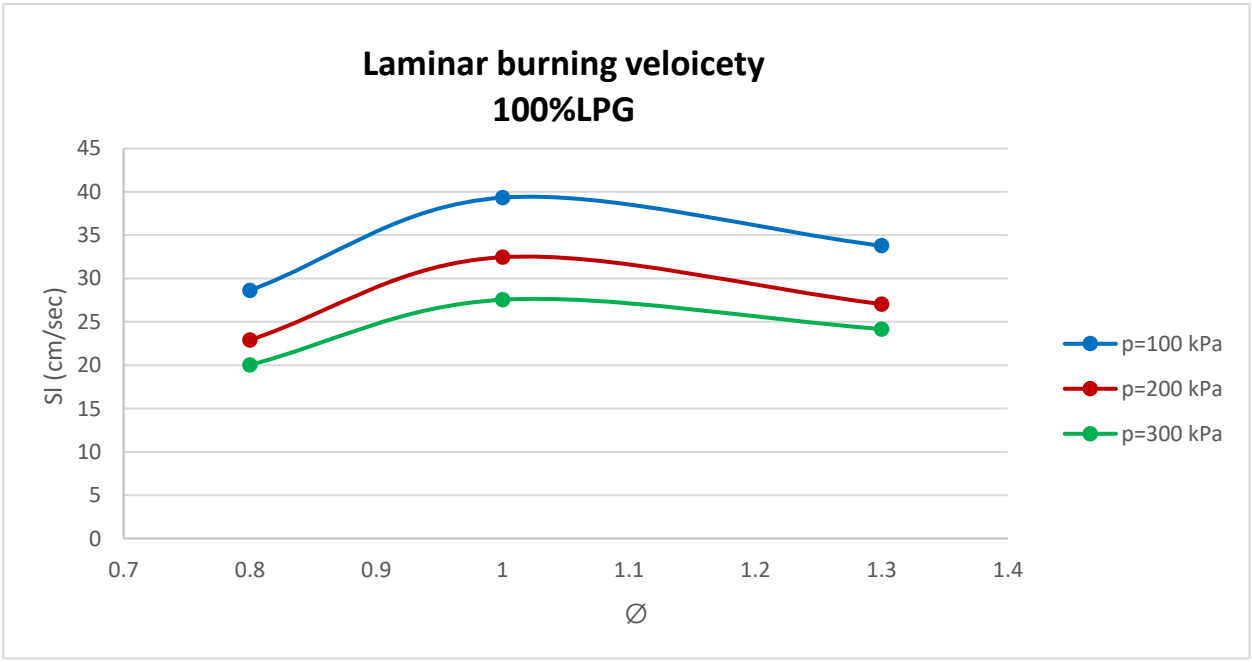

Figure (4.38) Laminar burning velocity S_l with a flame radius for 100% LPG with initial pressure (100, 200 and 300) kPa

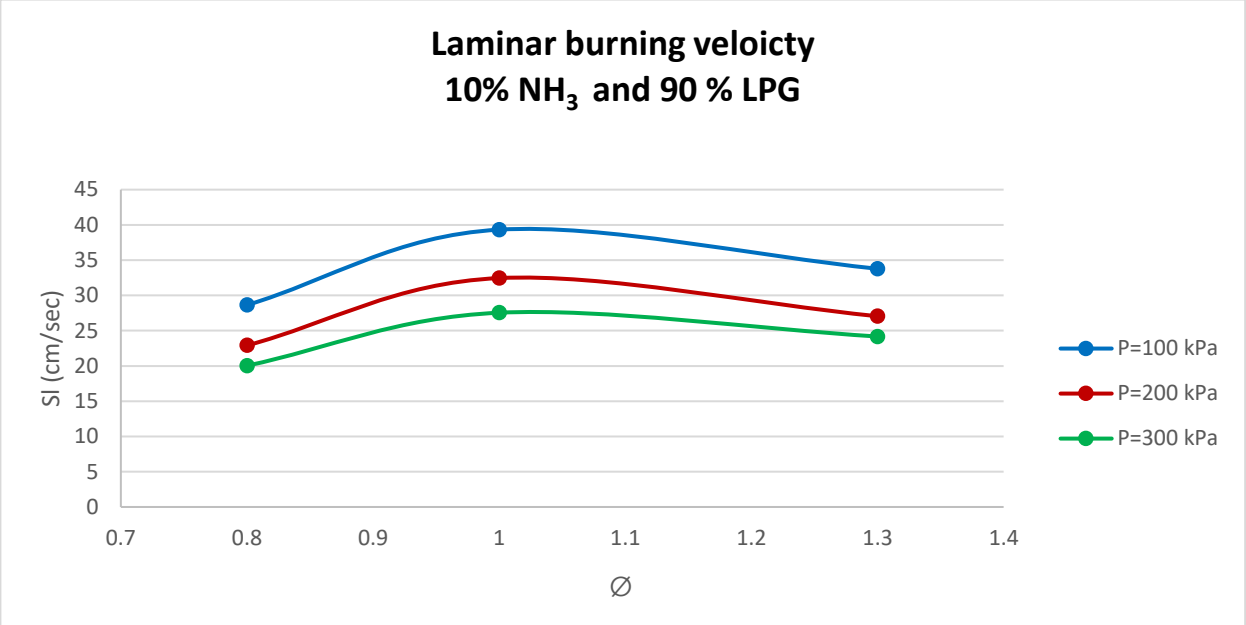

Figure (4.39) Laminar burning veloicty S_l with a flame radius for 90% LPG and 10% NH_3 with initial pressure (100, 200 and 300) kPa

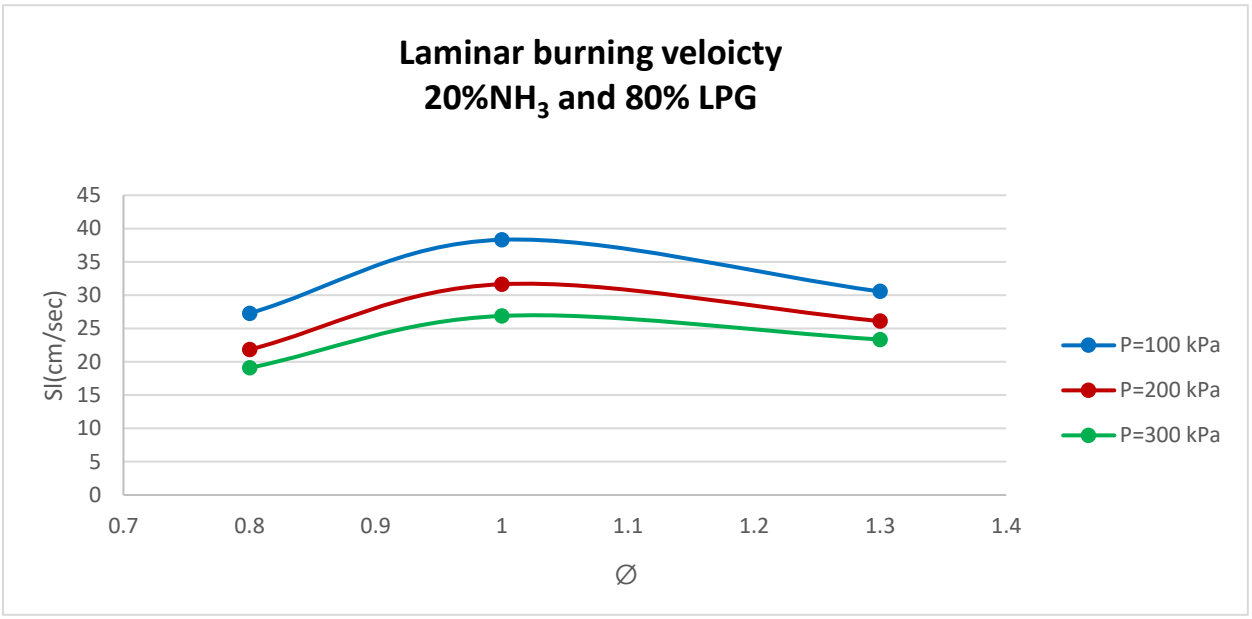

Figure (4.40) Laminar burning veloicty S_l with a flame radius for 80% LPG and 20% NH_3 with initial pressure (100, 200 and 300) kPa

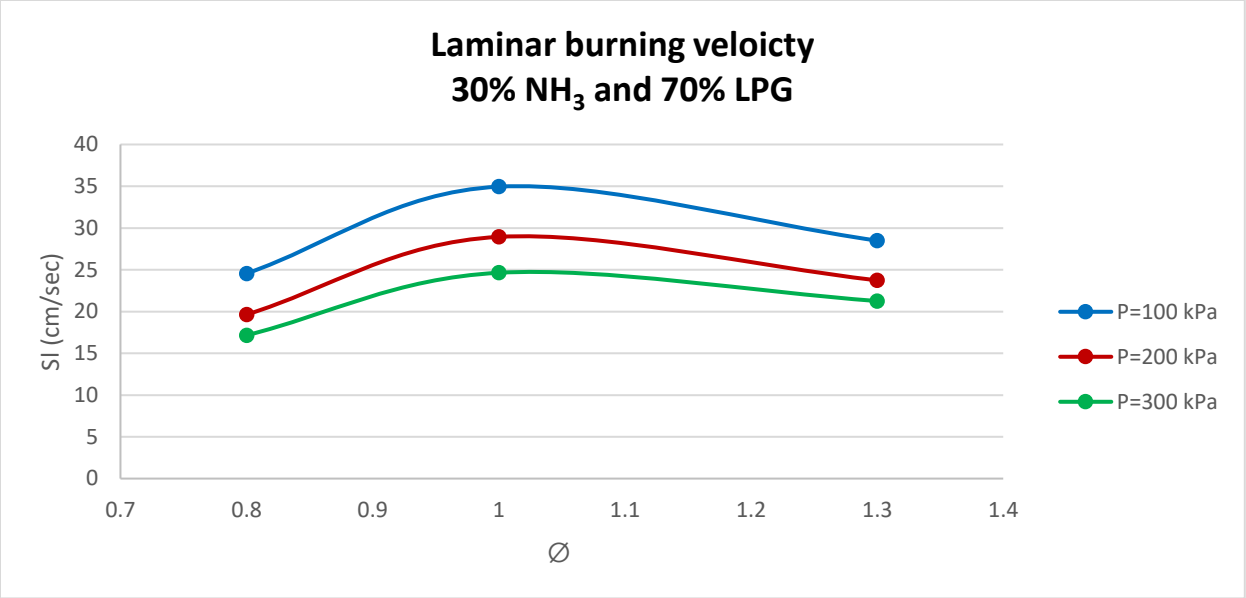

Figure (4.41) Laminar burning veloicty S_l with a flame radius for 70% LPG and 30% NH_3 with initial pressure (100, 200 and 300) kPa

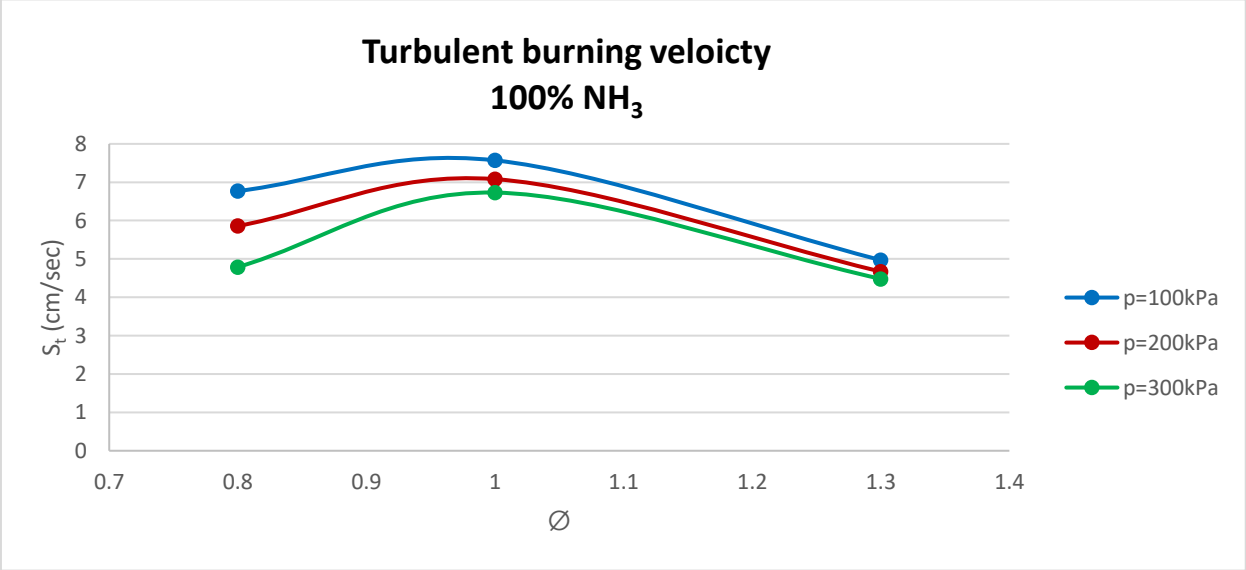

Figure (4.42) Turbulent burning veloicty S_t with a flame radius for 100% NH_3 with initial pressure (100, 200 and 300) kPa

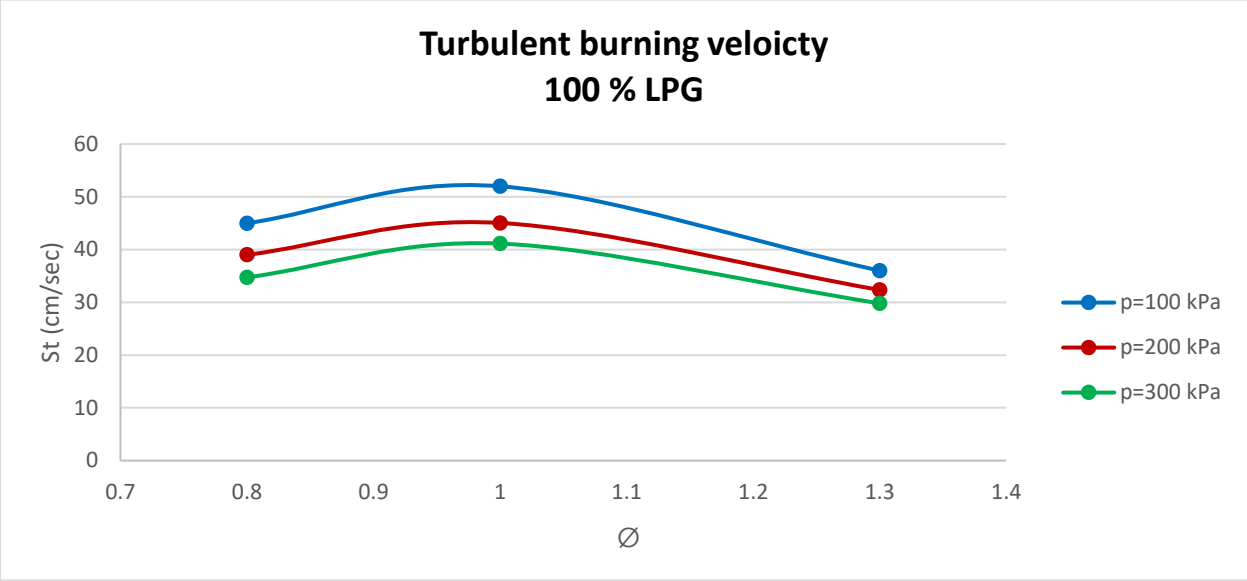

Figure (4.43) Turbulent burning velocity S_t with a flame radius for 100% LPG with initial pressure (100, 200 and 300) kPa

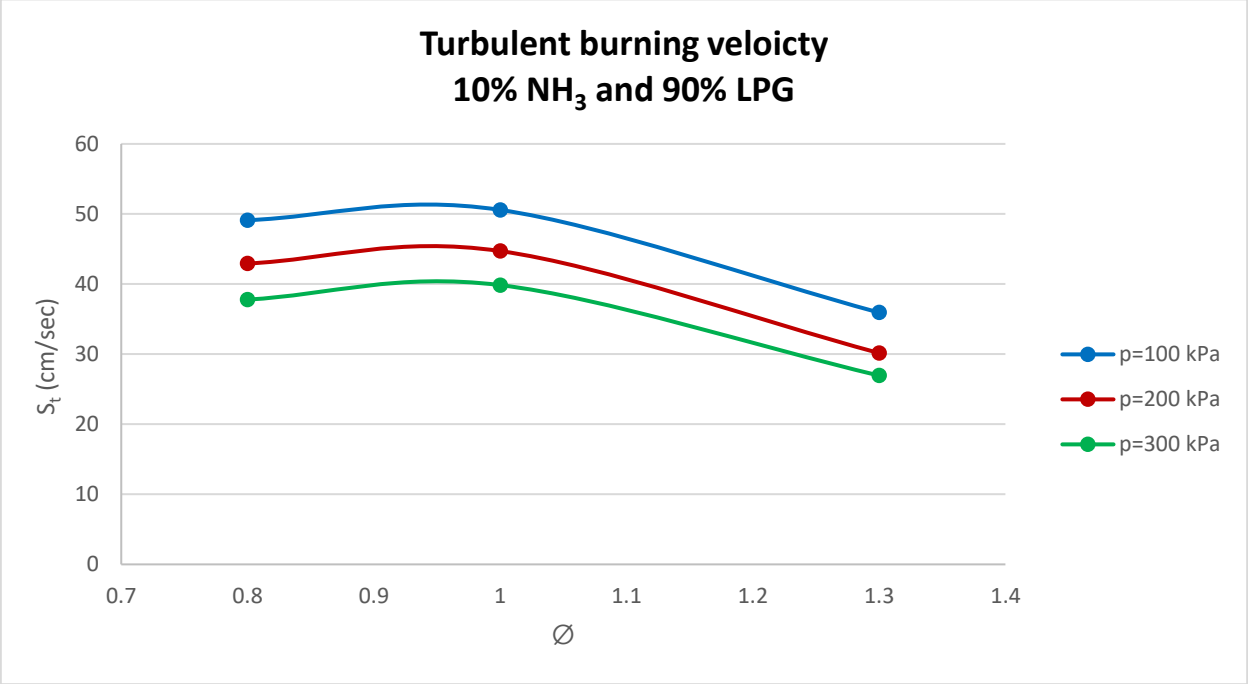

Figure (4.44) Turbulent burning velocity S_t with a flame radius for 90% LPG and 10% NH_3 with initial pressure (100, 200 and 300) kPa

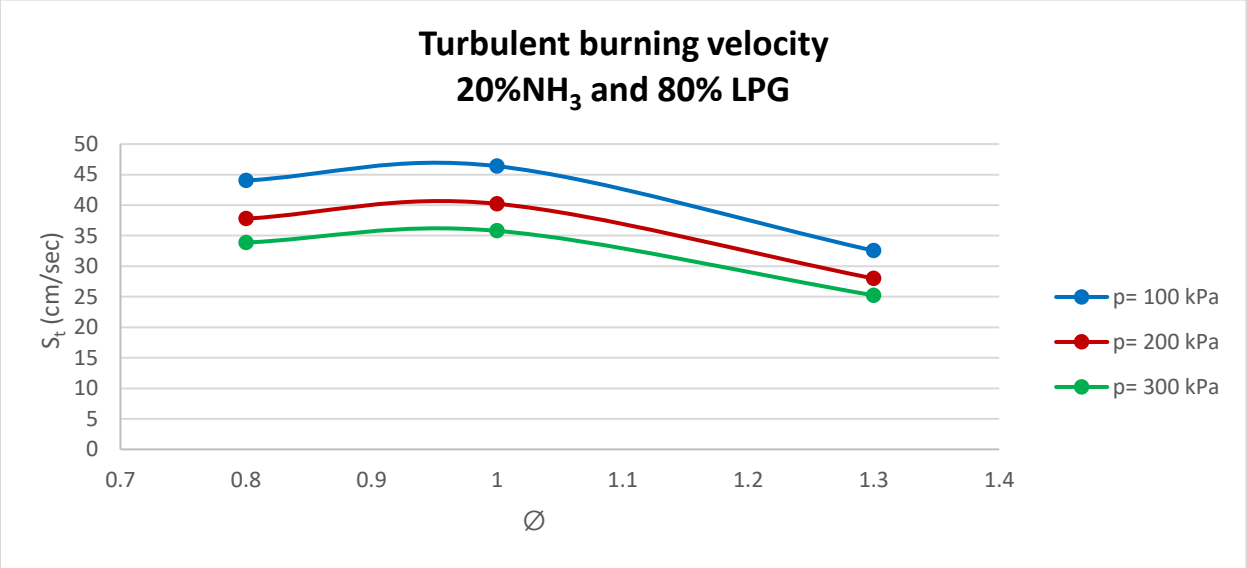

Figure (4.45) Turbulent burning veloicty S_t with a flame radius for 80% LPG and 20% NH_3 with initial pressure (100, 200 and 300) kPa

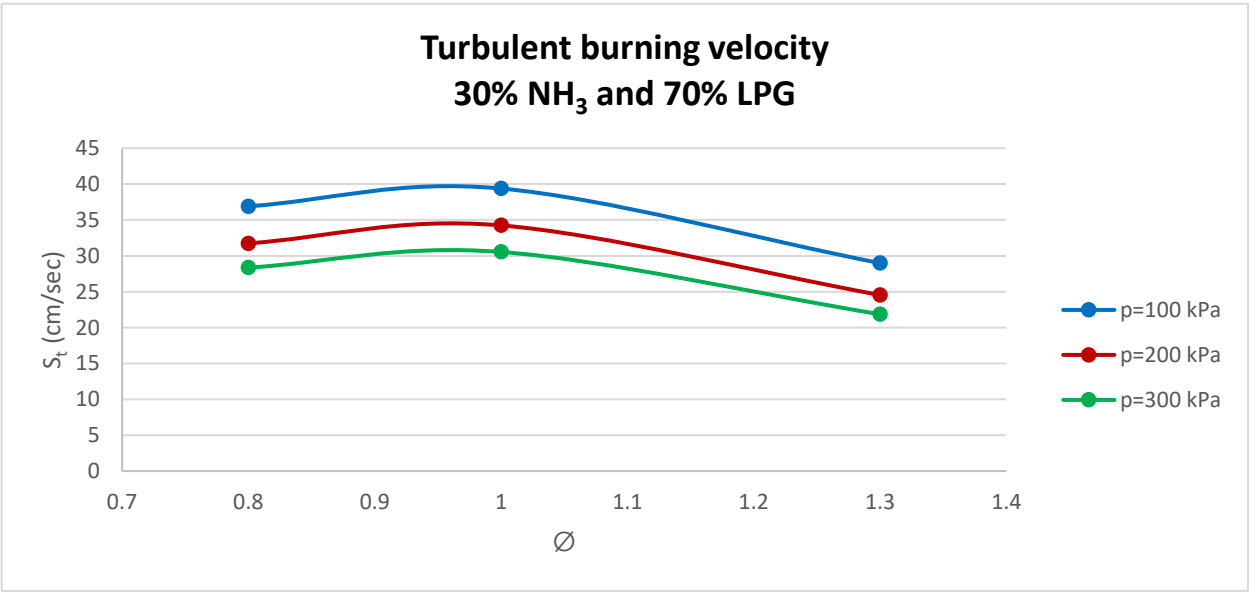

Figure (4.46) Turbulent burning veloicty S_t with a flame radius for 70% LPG and 30% NH_3 with initial pressure (100, 200 and 300) kPa

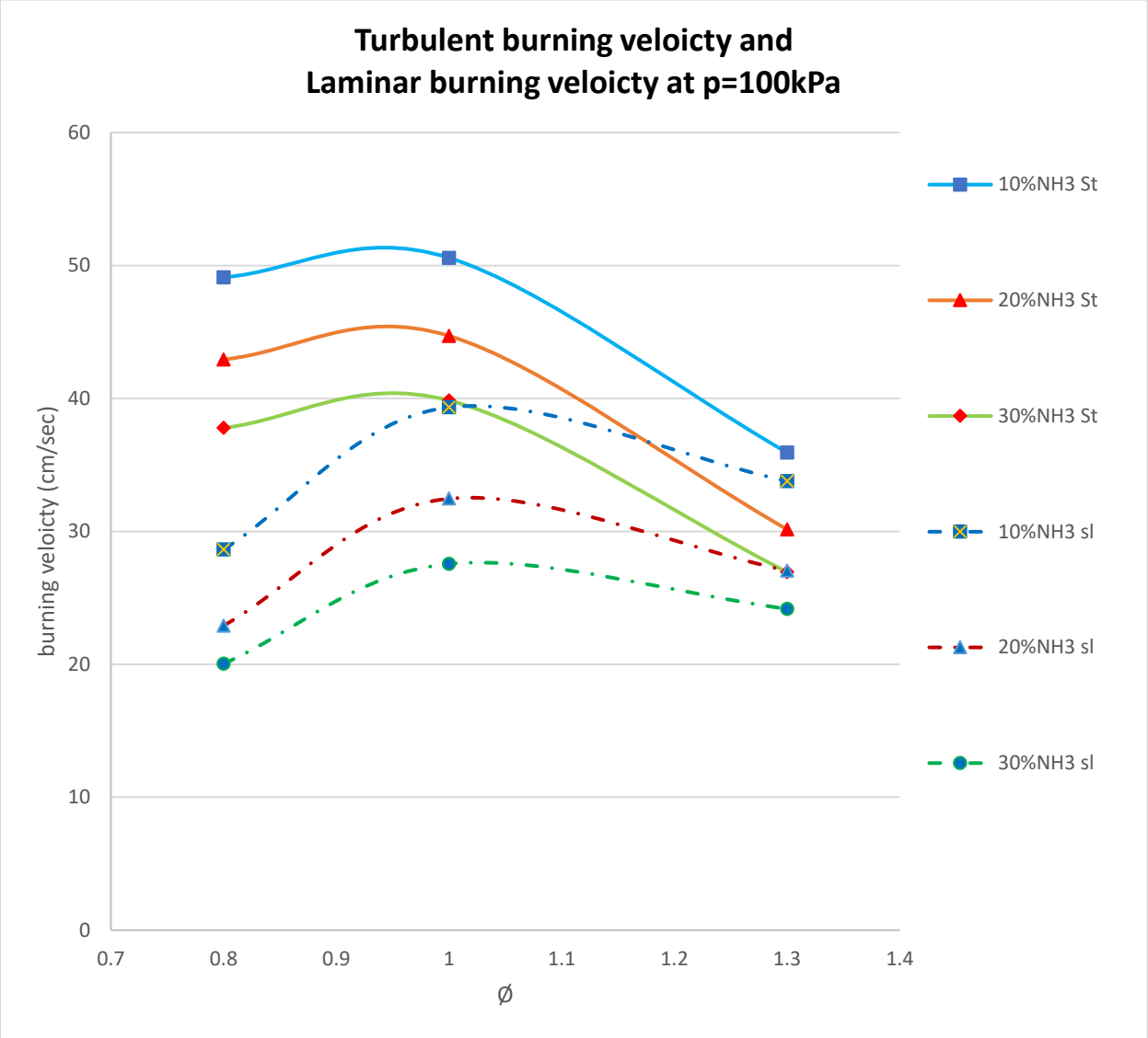

Figure (4.47) Turbulent burning velocity S_t with a flame radius for 70% LPG and 30% NH_3 with initial pressure (100, 200 and 300) kPa

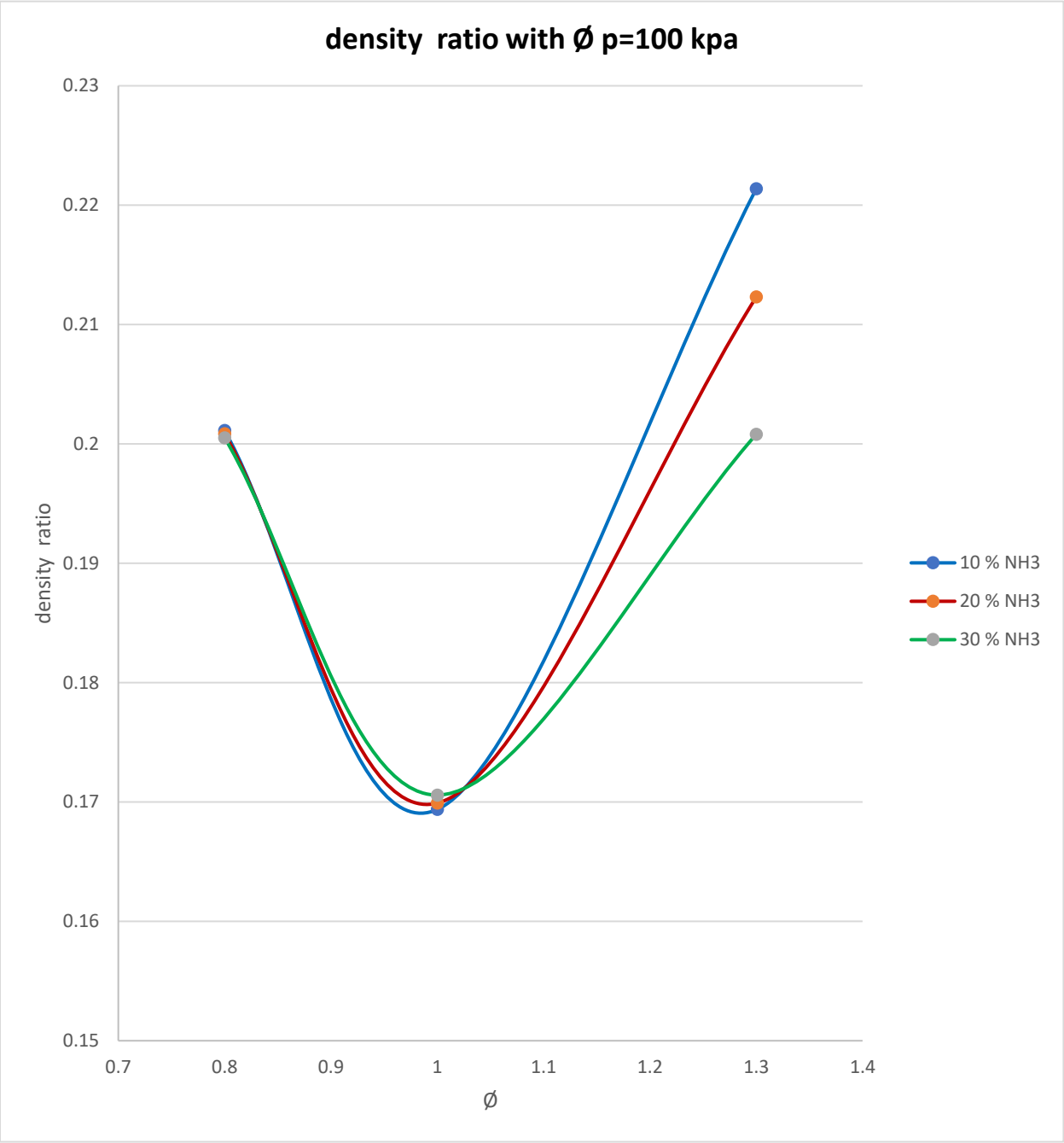

Figure (4.48) density ratio with a Ø with initial pressure (100) kPa with ammonia concentration (10 ,20 ,30) % NH_3

Chapter five

CONCLUSION AND RECOMMENDATION

5.1 CONCLUSION

The study involving the combustion behavior of a mixture of gases (LPG, ammonia, and air) within a combustion chamber. The study seems to have investigated the effects of turbulent conditions, pressure, ammonia concentration ratios, and mixing equivalence on combustion speed. Here's a summary of the key findings and observations from your provided text:

1. Turbulent Conditions and Combustion Speed

The use of a turbulent system within the fixed combustion chamber leads to an increase in the combustion speed of the gas mixture.

The presence of turbulence enhances the mixing of the reactants, which in turn improves the combustion speed of the mixture.

2. Pressure and Combustion Speed

Higher pressure (100) leads to increased combustion speed.

An increase in pressure generally has a positive effect on combustion speed due to its impact on reactant concentrations and reaction rates.

3. Ammonia Concentration and Combustion Speed

Lower concentrations of ammonia (10%) result in the best increase in combustion speed, Ammonia has a low combustion speed compared to other components, and higher concentrations can reduce the overall combustion speed of the mixture.

4. Mixing Equivalence and Combustion Speed

The best increase in combustion speed is observed in turbulent conditions with a mixing equivalence ratio of 0.8.

As the mixing ratio and equivalence increase (1.3, 1), the combustion speed decreases and approaches laminar conditions.

5. Reasons for Combustion Speed Variations

Efficient mixing is crucial for achieving high combustion speeds. Turbulent conditions promote good mixing, leading to faster chemical reactions.

In cases of higher equivalence ratios (1, 1.3), the effect of turbulence is reduced, and slower chemical reactions occur due to insufficient oxygen availability.

6. Combustion Chamber Conditions and Density Ratio

Combustion chamber conditions such as adiabatic temperature and density ratios play a role in combustion behavior.

An adiabatic temperature that corresponds to an equivalence ratio of 1 result in a significant decrease in the density of burned materials, impacting combustion speed.

5.2 RECOMMENDATION

We recommend several important points:

1- Repeat the practical experiments with the use of variable turbulent speed and compare them to get the best results.
2- using propellers with multiple blade inclination angles and repeating practical experiments and comparing the obtained results.
3- changing the type of fuel used, using multiple types, and comparing the results obtained.
4- repeating the practical experiments, using an equivalence coefficient of less than 0.8, and comparing the obtained results with the results of the practical experiment of the current study.

Refences

1. Bozza, F., De Bellis, V., Tufano, D., Malfi, E., Müller, C., & Habermann, K. (2019). *A quasi-dimensional model of pre-chamber spark-ignition engines* (No. 2019-01-0470). SAE Technical Paper.
2. Zirwes, T., Häber, T., Zhang, F., Kosaka, H., Dreizler, A., Steinhausen, M., ... & Bockhorn, H. (2021). Numerical study of quenching distances for side-wall quenching using detailed diffusion and chemistry. *Flow, Turbulence and Combustion*, *106*, 649-679.
3. Fries, D., Ochs, B. A., Saha, A., Ranjan, D., & Menon, S. (2019). Flame speed characteristics of turbulent expanding flames in a rectangular channel. *Combustion and Flame*, *199*, 1-13.
4. Boerner, L. K. (2019). Industrial ammonia production emits more CO2 than any other chemical-making reaction. Chemists want to change that. *Chem. Eng. News*, *97*(24), 1-9.
5. Lanzafame, P., Abate, S., Ampelli, C., Genovese, C., Passalacqua, R., Centi, G., & Perathoner, S. (2017). Beyond solar fuels: renewable energy-driven chemistry. *ChemSusChem*, *10*(22), 4409-4419.
6. Reitze Jr, A. W., & Heaven, J. B. (2005). The Hydrogen Economy and Its Potential Impacts. *Envtl. L. Rep. News & Analysis*, *35*, 10003.
7. Bouwman, A. F., Boumans, L. J. M., & Batjes, N. H. (2002). Estimation of global NH3 volatilization loss from synthetic fertilizers and animal manure applied to arable lands and grasslands. *Global biogeochemical cycles*, *16*(2), 8-1.
8. Ghavam, S., Vahdati, M., Wilson, I. A., & Styring, P. (2021). Sustainable ammonia production processes. *Frontiers in Energy Research*, *9*, 34.
9. Kelley, A. P., & Law, C. K. (2009). Nonlinear effects in the extraction of laminar flame speeds from expanding spherical flames. *Combustion and Flame*, *156*(9), 1844-1851.
10. Sadiq, A. M., Sleiti, A. K., & Ahmed, S. F. (2020). Turbulent flames in enclosed combustion chambers: characteristics and visualization—a review. *Journal of Energy Resources Technology*, *142*(8), 080801.
11. Masri, A. R. (2021). Challenges for turbulent combustion. *Proceedings of the Combustion Institute*, *38*(1), 121-155.
12. Zirwes, T., Häber, T., Zhang, F., Kosaka, H., Dreizler, A., Steinhausen, M., ... & Bockhorn, H. (2021). Numerical study of quenching distances for side-wall quenching using detailed diffusion and chemistry. *Flow, Turbulence and Combustion*, *106*, 649-679.
13. Arnaud, E., Mémin, E., Sosa, R., & Artana, G. (2006). A fluid motion estimator for schlieren image velocimetry. In *Computer Vision–ECCV 2006: 9th European*

Conference on Computer Vision, Graz, Austria, May 7-13, 2006. Proceedings, Part I 9 (pp. 198-210). Springer Berlin Heidelberg.
14. CHAKRABORTY, N. I. L. A. N. J. A. N., Mastorakos, E., & Cant, R. S. (2007). Effects of turbulence on spark ignition in inhomogeneous mixtures: a direct numerical simulation (DNS) study. *Combustion science and technology*, *179*(1-2), 293-317.
15. Zhang, L., Zhang, S., Zhou, H., Ren, Z., Wang, H., & Wang, X. (2022). Efficient Combustion of Low Calorific Industrial Gases: Opportunities and Challenges. *Energies*, *15*(23), 9224.
16. A.K.C.L. Au, D. Bradley and M. Lawes, *I Flame stretch rate as a determinant of turbulent burning velocity*, Phil. Trans. R. Soc. Lond. A 338 (1992), pp. 359–387.
17. J.B. Heywood, *Internal Combustion Engine Fundamentals*, Mcgraw-hill, New York, 1988.
18. N. Peters, Turbulent Combustion, Cambridge University Press, Cambridge, 2000
19. G.R.A. Groot, Modelling of Propagating Spherical and Cylindrical Premixed Flames, Technische Universiteit Eindhoven, 2003.
20. Fries, D., Ochs, B. A., Saha, A., Ranjan, D., & Menon, S. (2019). Flame speed characteristics of turbulent expanding flames in a rectangular channel. *Combustion and Flame*, *199*, 1-13.
21. Lipatnikov, A. (2012). *Fundamentals of premixed turbulent combustion*. CRC Press.
22. Lipatnikov, A., & Chomiak, J. (2007). Global stretch effects in premixed turbulent combustion. *Proceedings of the Combustion Institute*, *31*(1), 1361-1368.
23. Lipatnikov, A. N., & Chomiak, J. (2002). Turbulent flame speed and thickness: phenomenology, evaluation, and application in multi-dimensional simulations. *Progress in energy and combustion science*, *28*(1), 1-74.
24. Kobayashi, H., Tamura, T., Maruta, K., Niioka, T., & Williams, F. A. (1996, January). Burning velocity of turbulent premixed flames in a high-pressure environment. In *Symposium (international) on combustion* (Vol. 26, No. 1, pp. 389-396). Elsevier.
25. Domingo, P., & Vervisch, L. (2023). Recent developments in DNS of turbulent combustion. *Proceedings of the Combustion Institute*, *39*(2), 2055-2076.
26. De Vries, J. (2009). *A study on spherical expanding flame speeds of methane, ethane, and methane/ethane mixtures at elevated pressures*. Texas A&M University.
27. Bradley, D., Gaskell, P. H., & Gu, X. J. (1996). Burning velocities, Markstein lengths, and flame quenching for spherical methane-air flames: a computational study. *Combustion and flame*, *104*(1-2), 176-198.
28. Tamadonfar, P., & Gülder, Ö. L. (2015). Effects of mixture composition and turbulence intensity on flame front structure and burning velocities of premixed turbulent hydrocarbon/air Bunsen flames. *Combustion and Flame*, *162*(12), 4417-4441.

29. Benim, A. C., & Syed, K. J. (2015). Flashback Due to Turbulent Flame Propagation in the Core Flow. *Flashback Mechanisms in Lean Premixed Gas Turbine Combustion*, 45-57.
30. Halouane, Y., & Dehbi, A. (2017). CFD simulations of premixed hydrogen combustion using the Eddy Dissipation and the Turbulent Flame Closure models. *international journal of hydrogen energy*, *42*(34), 21990-22004.
31. Renou, B., Mura, A., Samson, E., & Boukhalfa, A. (2002). Characterization of the local flame structure and the flame surface density for freely propagating premixed flames at various Lewis numbers. *Combustion science and technology*, *174*(4), 143-179.
32. Wabel, T. M., Skiba, A. W., Temme, J. E., & Driscoll, J. F. (2017). Measurements to determine the regimes of premixed flames in extreme turbulence. *Proceedings of the Combustion Institute*, *36*(2), 1809-1816.
33. Hamlington, P. E., Poludnenko, A. Y., & Oran, E. S. (2011). Interactions between turbulence and flames in premixed reacting flows. *Physics of Fluids*, *23*(12).
34. Peters, N. (1999). The turbulent burning velocity for large-scale and small-scale turbulence. *Journal of Fluid mechanics*, *384*, 107-132.
35. Pocheau, A. (1992). Front propagation in a turbulent medium. *Europhysics Letters*, *20*(5), 401.
36. Yakovenko, I., Kiverin, A., & Melnikova, K. (2022). Computational Fluid Dynamics Model for Analysis of the Turbulent Limits of Hydrogen Combustion. *Fluids*, *7*(11), 343.
37. Zhen, G., & Leuckel, W. (1997). Effects of ignitors and turbulence on dust explosions. *Journal of Loss Prevention in the Process Industries*, *10*(5-6), 317-324.
38. Weiß, M., Zarzalis, N., & Suntz, R. (2008). Experimental study of Markstein number effects on laminar flamelet velocity in turbulent premixed flames. *Combustion and Flame*, *154*(4), 671-691.
39. Martínez-Sanchis, D., Sternin, A., Tagscherer, K., Sternin, D., Haidn, O., & Tajmar, M. (2022). Interactions between flame topology and turbulent transport in high-pressure premixed combustion. *Flow, Turbulence and Combustion*, *109*(3), 813-838.
40. Borghi, A. (1985). *Mezzo secolo di anarchia*. Anarchismo.
41. Alsultani, R. K. E. Experimental study of the Laminar burning velocity and Markstine length of NH3–LPG-air premixed flames.
42. Bradley, D., Lau, A. K. C., Lawes, M., & Smith, F. T. (1992). Flame stretch rate as a determinant of turbulent burning velocity. *Philosophical Transactions of the Royal Society of London. Series A: Physical and Engineering Sciences*, *338*(1650), 359-387.

43. Gotoh, T., Fukayama, D., & Nakano, T. (2002). Velocity field statistics in homogeneous steady turbulence obtained using a high-resolution direct numerical simulation. *Physics of Fluids*, *14*(3), 1065-1081.
44. Chowdhury, S., Gurpinar, E., Su, G. J., Raminosoa, T., Burress, T. A., & Ozpineci, B. (2019, June). Enabling technologies for compact integrated electric drives for automotive traction applications. In *2019 IEEE transportation electrification conference and expo (ITEC)* (pp. 1-8). IEEE. ad.
45. Fallon, T., & Rogers, C. B. (2002). Turbulence-induced preferential concentration of solid particles in microgravity conditions. *Experiments in fluids*, *33*(2), 233-241.
46. Skewis, W. H. (2011). Mechanical Seal Failure Modes. *Handbook of Reliability Prediction Procedures for Mechanical Equipment*.
47. Ruan, B. (2002). A semi-analytical solution to the dynamic tracking of non-contacting gas face seals. *J. Trib.*, *124*(1), 196-202.
48. Sabban, L., & van Hout, R. (2011). Measurements of pollen grain dispersal in still air and stationary, near homogeneous, isotropic turbulence. *Journal of Aerosol Science*, *42*(12), 867-882.
49. Morsy, M. E., & Yang, J. (2021). Numerical and experimental study on turbulence statistics in a large fan-stirred combustion vessel. *Experiments in Fluids*, *62*(5), 116.
50. Bunjong, D., Pussadee, N., & Wattanakasiwich, P. (2018, December). Optimized conditions of Schlieren photography. In *Journal of Physics: Conference Series* (Vol. 1144, No. 1, p. 012097). IOP Publishing.
51. Parsinejad, F., Matlo, M., & Metghalchi, M. (2004). A mathematical model for Schlieren and Shadowgraph images of transient expanding spherical thin flames. *J. Eng. Gas Turbines Power*, *126*(2), 241-247.
52. Xie, Y., Li, J., Yang, J., & Cracknell, R. (2023). Laminar burning velocity blending laws using particle imaging velocimetry. *Applications in Energy and Combustion Science*, *13*, 100114.
53. Yasiry, A. S., & Shahad, H. A. K. (2016). An experimental study of the effect of hydrogen blending on burning velocity of LPG at elevated pressure. *International Journal of Hydrogen Energy*, *41*(42), 19269–19277
54. Winterbone , Desmond E., Advanced Thermodynamics for Engineers, Wiley 1997.
55. Hu, K., Wang, T., Shen, C., Weng, C., Zhou, F., Xia, M., & Weng, L. (2023). Overview of Underwater 3D Reconstruction Technology Based on Optical Images. *Journal of Marine Science and Engineering*, *11*(5), 949.
56. Hayakawa, A., Goto, T., Mimoto, R., Arakawa, Y., Kudo, T., & Kobayashi, H. (2015). Laminar burning velocity and Markstein length of ammonia/air premixed flames at various pressures. *Fuel*, *159*, 98-106.
57. D. Bradley, M.Z. Haq, R. a. Hicks, T. Kitagawa, M. Lawes, C.G.W. Sheppard et al., *Turbulent burning velocity, burned gas distribution, and associated flame surface definition*, Combust. Flame 133 (2003), pp. 415–430

58. S. Zheng, X. Zhang, T. Wang and J. Liu, *An experimental study on premixed laminar and turbulent combustion of synthesized coalbed methane*, Energy 92 (2015), pp. 355–364
59. S. Ravi, A. Morones, E.L. Petersen and F. Güthe, *Effects of hydrogen addition on the flame speeds of natural gas blends under uniform turbulent conditions*, Vol. 4A Combust. Fuels Emiss. (2015), pp. V04AT04A066
60. Bradley, D., Haq, M. Z., Hicks, R. A., Kitagawa, T., Lawes, M., Sheppard, C. G. W., & Woolley, R. (2003). Turbulent burning velocity, burned gas distribution, and associated flame surface definition. *Combustion and Flame*, *133*(4), 415-430.

APPENDIX (A)

Calibration of Pressure Transmitters

C.O.S.Q.C
IRAQ

Accredited CABs
IQAS
Accreditation no. CL 869

Calibration Certificate

FOR-TC-012

Central Organization for Standardization and Quality Control (COSQC)
Metrology Department/Mass & Pressure Section/Pressure Lab.
P.O. Box13032 Algeria street, Baghdad ,Tel:7765180 E-Mail : cosqc@cosqc.gov.iq

Certificate No: PRE/ 506 /2021
Date of issue : 4/ 11 /2021

Annex 1/ Results

APP.Pressure	Reading		Mean Reading	Deviation (M-A)	Error
	Upward	Downward	KPa	KPa	% of F.S
KPa	KPa	KPa			
-50	-49.8	-49.6	-49.70	0.30	0.30
0	0.0	0.0	0.00	0.00	0.00
100	99.7	100.1	99.90	-0.10	0.01
200	199.8	200.1	199.95	-0.05	0.01
500	499.7	499.7	499.70	-0.30	0.03
700	699.7	699.7	699.70	-0.30	0.03

Max. Expanded Uncertainty =	± 0.27	KPa

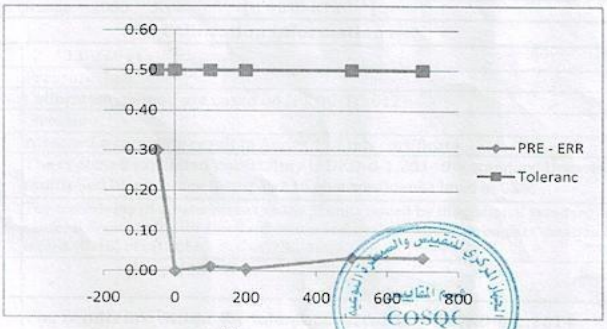

COSQC

Calibrated by:
Nabeel Lateef

Revisid by :
Saif Ali

Approved by:
Saif Ali
Head of Maas & Pressure Section

APPENDEX (A)

Calibration of Pressure Gauge Ammonia

Calibration Certificate

Central Organization for Standardization and Quality Control (COSQC)
Metrology Department/Mass & Pressure Section /Pressure Lab.

P.O. Box13032 Al jadria street, Baghdad ,Tel:7765180
E-Mail : cosqc@cosqc.gov.iq

Certificate No: PRE/ 505 /2021
Date of issue : 4/ 11 /2021

Annex 1/ Results

APP.Pressure	Reading		Mean Reading	Deviation (M-A)	Error
	Upward	Downward			
kg/cm²	kg/cm²	kg/cm²	kg/cm²	kg/cm²	% of F.S
0	0.0	0.0	0.00	0.00	0.00
2	2.0	2.1	2.05	0.05	0.42
4	4.1	4.2	4.15	0.15	1.25
6	6.1	6.2	6.15	0.15	1.25
8	8.2	8.2	8.20	0.20	1.67
10	10.2	10.2	10.20	0.20	1.67

Max. Expanded Uncertainty =	± 0.13 kg/cm²

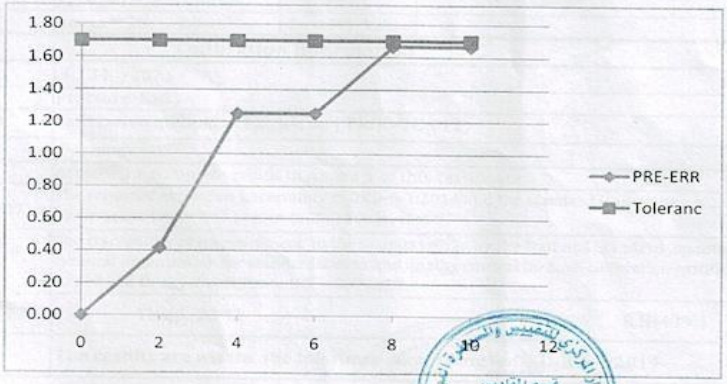

Calibrated by:
Nabeel Lateef

Revisid by :
Saif Ali

Approved by:
Saif Ali
Head of Maas & Pressure Section

APPENDEX (A)

Calibration of Camera High - Speed

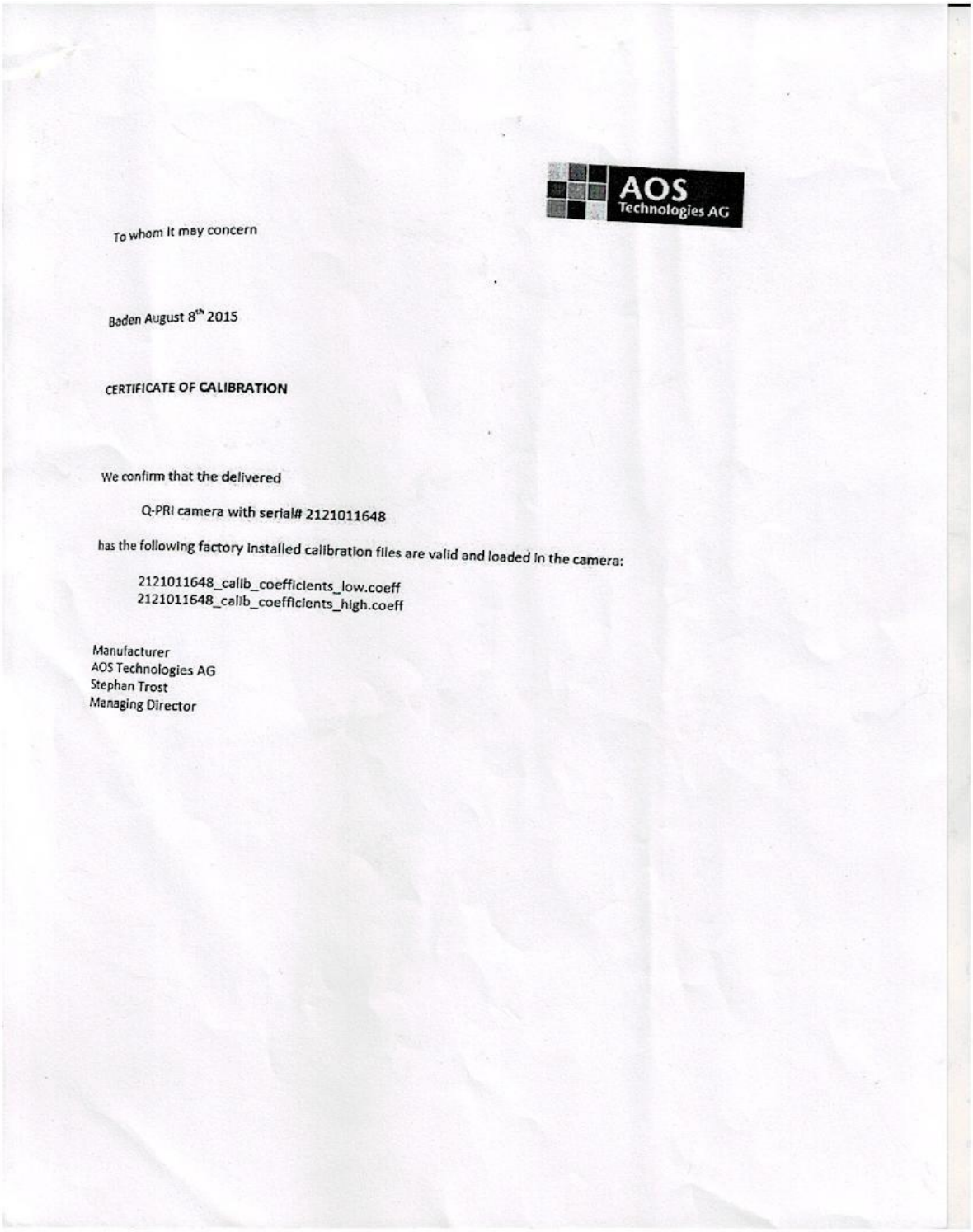

AOS Technologies AG

To whom it may concern

Baden August 8th 2015

CERTIFICATE OF CALIBRATION

We confirm that the delivered

Q-PRI camera with serial# 2121011648

has the following factory installed calibration files are valid and loaded in the camera:

2121011648_calib_coefficients_low.coeff
2121011648_calib_coefficients_high.coeff

Manufacturer
AOS Technologies AG
Stephan Trost
Managing Director

APPENDIX (A)

Camera Calibration High-Speed

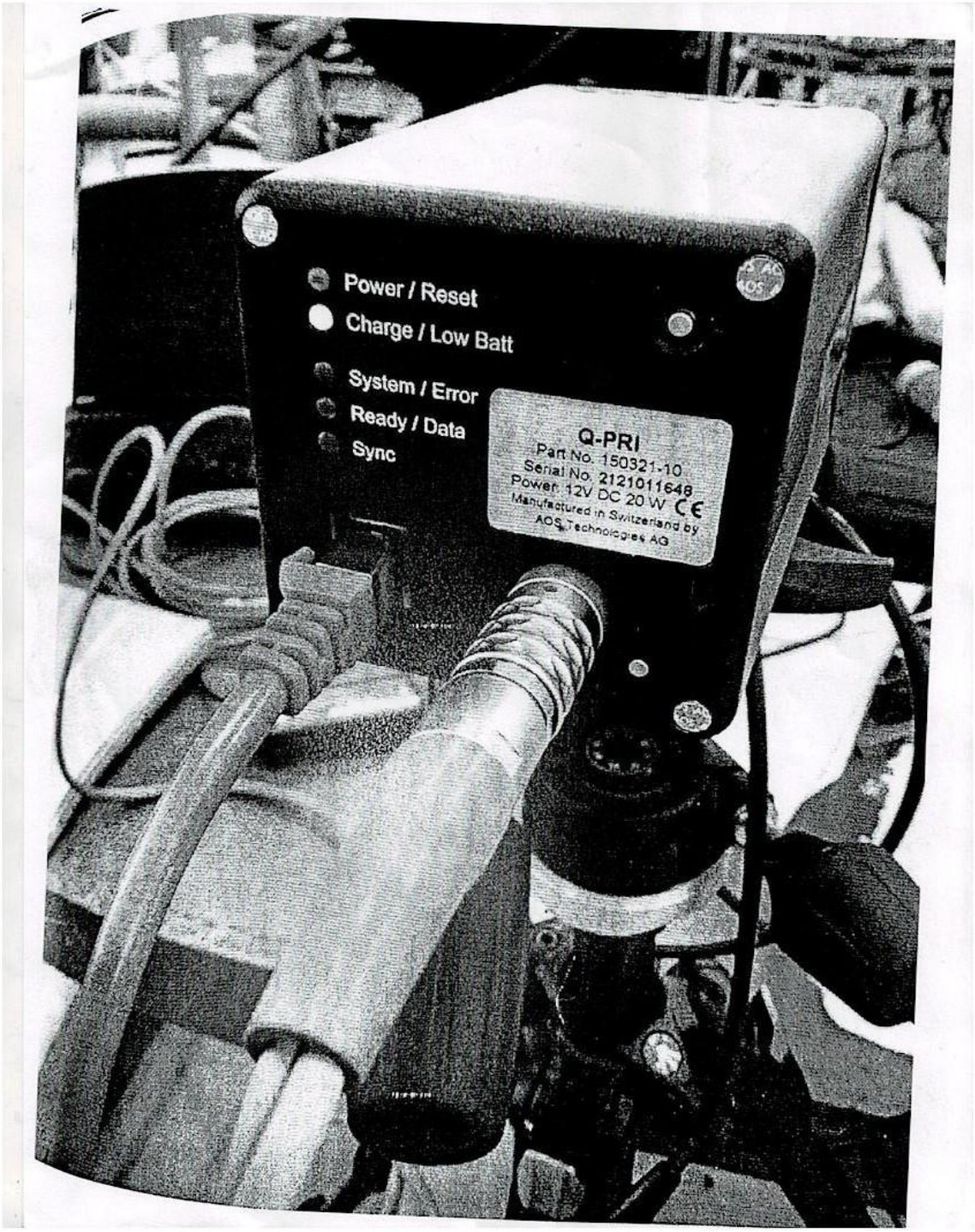

APPENDIX (B)
Analysis of LPG components provided from Hilla Plant

الشركة العامة لتعبئة وخدمات الغاز

State Company for Gas Filling and Services

GAS Analysis Dept

الفرع /بابل

وحدة المختبر

مواصفات الغاز السائل المستلم من شركة غاز الجنوب إلى مستودع غاز الحلة للفترة من ٢٠٢١/٢/١١ إلى ٢٠٢١/٢/٢٠

composition	11/2	12/2	13/2	14/2	15/2	16/2	17/2	18/2	19/2	20/2	الملاحظات
C4MOL %	0.89	0.61	0.72	0.79	0.95	0.73	0.72	0.86	0.65	0.66	
C3MOL %	64.34	58.27	60.02	60.24	66.01	56.60	59.18	59.49	57.47	58.34	
C4MOL %	32.50	39.76	37.41	37.77	32.42	42.38	39.83	39.18	40.70	39.64	
C5MOL %	2.27	1.36	1.85	1.2	0.62	0.29	0.27	0.47	1.18	1.36	
Density at 15.6C°	0.538	0.540	0.544	0.535	0.534	0.539	0.540	0.539	0.539	0.544	
Vapor Pressure(Kg\cm²)at(37.8C°)	8.5	8.7	8.5	8.4	8.6	8.5	8.1	8.3	8.1	8.4	
Corrosion copper strip	1b	1b	1b	1b	1b	1b	1b	1b	1b	1b	
Evaporated Temp at(95%)	+2	+3	+2	+3	+2	+2	+2	+2	+2	+2	

ملاحظات

- النسب القياسية لل (C_4) هي (0.6) و(C_5) (2.0) .

رائد سعدي كاظم

م . وحدة المختبر

APPENDIX (C)
List of Publications

Mathematics for applications
Print ISSN: 1805-3610
Online ISSN: 1805-3629

Ref: MFA- KG-189001
Date: 1st Oct, 2023

Samer Mohammed Abdulhaleem, Jaafar Sami Shaban
Mechanical Engineering Department, Research University of Babylon

E-mail: eng.samer.mohammed@uobabylon.edu.iq,
jafar.shaban.engh412@student.uobabylon.edu.iq

Congratulations upon the acceptance of your research paper into our Scopus Indexed Journal.

It's my pleasure to inform you that, after the peer review, your paper, "**The impact of turbulence on the burning speed of a combination of air, ammonia, and LPG gas at certain concentrations**" has been ACCEPTED to publish with *Mathematics for Applications*. It will be published in the upcoming issue of 2023. I believe that our collaboration will help to accelerate the global knowledge creation and sharing one-step further. Please do not hesitate to contact me if you have any further questions.

Sincerely,

Managing Editor

Mathematics for Applications

editor@mathsapplication.com

ICRIE 2023 4TH INTERNATIONAL CONFERENCE ON RECENT INNOVATIONS IN ENGINEERING

University of KURDISTAN Hewlêr

CERTIFICATE OF ORAL PRESENTATION

This is to certify that

Jaffar sami Shaban Shaban

Has successfully presented a scientific paper titled

A Study of the Effect of Ammonia Blending on Burning Velocity of LPG at Initial Pressure with High-Speed Camera's

in the 4th International Conference on Recent Innovations in Engineering ICRIE 2023,
University of Duhok, College of Engineering,
13th – 14th September 2023.

James H. Haido

Professor Dr. James H. Haido
Chairman of the Conference & Dean of Engineering College

University of KURDISTAN Hewlêr

4th International Conference on Recent Innovations in Engineering (ICRIE2023)

OFFICIAL ACCEPTANCE LETTER

September 7, 2023
Manuscript ID: # 1570926298

Dear Jaafar Sami Shaban

Congratulations! It is my pleasure to inform you that after the blind peer review, your paper entitled "A Study of the Effect of Ammonia Blending on Burning Velocity of LPG at Initial Pressure with High-Speed Camera" has been accepted for presentation at the 4th International Conference on Recent Innovations in Engineering (ICRIE 2023) conference which will be taking place from September 13th to 14th 2023 in Duhok city, Kurdistan Region-Iraq. Accordingly, your manuscript is accepted for publication in a Special Issue in the Journal of the University of Duhok (JUD), Volume 26, Issue 2, 2023.

You are cordially invited to present your paper at the ICRIE2023 at the Conference Hall of the University of Duhok.

Thank you for considering submitting your Research with ICRIE2023. Please do not hesitate to contact us if you have any further questions.

James H. Haido

Respectfully Yours,
Prof. Dr. James H. Haido, ICRIE2023 Chairman

https://icrie.uod.ac/ 13-14 Sept 2023 info.icrie@uod.ac

European Quarter
Schuman Roundabout, 1040 Brussels
Belgium

EMAIL: ADMIN@GENIUS-JOURNALS.ORG
WEBSITE: WWW.GENIUSJOURNALS.ORG

GENIUS JOURNALS PUBLISHING

Date: 14th August, 2023

To,
Jaafar Sami Shaban B.Sc. (Mech.Eng. 2008)
jafar.shaban.engh412@student.uobabylon.edu.iq

Assist Prof. Dr. Samer Mohammed Abdulhaleem
eng.samer.mohammed@uobabylon.edu.iq

GREETINGS!

Dear Author/s,

We are pleased to inform you that, the manuscript you have submitted entitled "**Experimental study of turbulent burning velocity at an initial pressure (100,200,300) kPa**" has been accepted for publication in **Volume 21, of Eurasian Journal of Engineering and Technology (EJET) (ISSN: 2795-7640)**. The manuscript has been passed through the rigorous peer review process, grammatical check and plagiarism check and will be published in said volume of our journal.

Thanks and Regards,

DR. R. SCHLAUDERER
Editor In Chief

1040, BRUSSELS GENIUS JOURNALS BELGIUM

International Scientific Research Publishing Group
H No.20 Balaganj, District: Sylhet, Pin Code: 3128 Bangladesh
Sub Branch: R.K Choudhury Road, Bharalumukh, Guwahati-781009, Assam, India
Website: https://isrpgroup.org/ **E-mail:** isrpublisher@gmail.com

ACCEPTANCE LETTER

Dear
Jaafar Sami Shaban and Dr. Samer Mohammed Abdul Haleem

Manuscript Number: OMRN2074ID-KG-1075

Manuscript Title: Using high-speed cameras, a study was conducted to determine how ammonia blending affected the speed at which LPG burned at initial pressure

Dear
Sir/Madam

On behalf of ISRP, I Nasim Ahmed (**Managing Director of ISRP group**) take pride and pleasure to inform you that our Reviewer has reviewed your article and recommended your Article for publication in our Upcoming issue (SRJMD: Volume-3: Issue-4; Jul-Aug, 2023).

Journal:

Scientific Research Journal of Multidisciplinary
ISSN Print : 2788-9459 | ISSN Online : 2788-9467
Frequency : Bi-Monthly
Language : English
Origin : Kenya
Website : https://isrpgroup.org/srjmd/

Indexing:
Google Scholar, Index Copernicus, Research Bible, World Cat, Eurasian Scientific Journal Index (ESJI) Citefactor, SHERPA/RoMEO, Scientific Indexing Services (SIS), Road- Directory of Open Access Scholarly Resources, Directory of Research Journals Indexing (DRJI) and others in Progress

Nasim Ahmed

Nasim Ahmed
Managing Director

REVIEW REPORT

Journal Name: **Scientific Research Journal of Multidisciplinary**

Manuscript No: **OMRN2074ID-KG-1075**

Article Title: Using high-speed cameras, a study was conducted to determine how ammonia blending affected the speed at which LPG burned at initial pressure

SECTION	Review Order	Correct /Wrong	Modification/ Comment
PREPARATION	Sequence (Abstract, Keywords, Introduction, Methodology, Result, Discussion, Conclusion, Acknowledgement, Reference)	Yes	Everything is Correct
	Reference style (APA)	Yes	Good
	Grammar, Sentence Pattern, Punctuation etc.	Yes	Moderate
	Reference arrangement	No	Moderate
MANUSCRIPT CONTENT	Is the Title sounds clearly?	Yes	Clarified
	Is the Topic Important?	Yes	
	Is the Abstract concise and to the point?	No	Moderate
	Is the Objective clear?	Yes	Good
	Is the methodological design that was employed appropriate?	Yes	Good
	Is Mythology was Appropriate?	Yes	Good
	Is Literature drawn objective?	No	Moderate
	Is Analysis of Result/Observation/Findings done Correctly? (Tables and Figure appropriate)?	Yes	Very Good
	Has the author effectively linked their findings to literature that they discussed in their literature review?	Yes	Clarified
	Are the References in the literature review from academically appropriate sources such as peer-reviewed journals?	Yes	Moderate
	Are the References in the literature review relevant?	Yes	
	Are the References were complete and appropriate?	No	
	Is the Conclusion Sound?	Yes	Good
	Is writing clear and concise?	Yes	Clarified

Is Paper original	Plagiarism percentage
Yes/~~No~~	29 %

Reviewer Commentif any

Review Report Recommended/ disposition of the manuscript

Category	Criteria
A	Strongly Recommended
B	**Acceptable (as written with no need for any revisions)**
C	Acceptable (with minor revisions/Editorial correction)
D	Ask for revisions and continue with a second review
E	Rejection (Do not accept for publication)

Final Decision Category:
(Select ~~A/B/C/D/E~~)

Nasim Ahmed

Nasim Ahmed
(Director, ISRP GROUP.)

الخلاصة

دراسة تجريبية على خليط غازي مختلط ومضطرب في غرفة احتراق تحتوي على مراوح كان الاضطراب منتظمًا ومتناحي الخواص، في حين تم تحقيق التغيرات في السرعة المضطربة جذر متوسط التربيع من خلال التغيرات في سرعة المراوح. أدى اشتعال الشرارة المركزية إلى انتشار متوسط للهب الكروي.

تم قياس التوزيعات المكانية للغازات المحروقة وغير المحترقة أثناء الانتشار، كما تم التقاط صور شليرين عالية السرعة في وقت واحد، وأجريت التجربة بضغوط أولية مختلفة (100، 200، و300 كيلو باسكال) ونسب التكافؤ (0.8، 1، و1.3).

لمعالجة وتحليل الصور التي تم الحصول عليها بواسطة نظام شليرين تم استخدام كود برنامج. MATLAB

تم العثور على توزيعات نسب الغازات المحروقة وغير المحترقة حول المحيطات لجميع أنصاف الأقطار في جميع مراحل الانفجار، وتم اشتقاق القيم المتوسطة لهذه النسب كدالة لمتوسط نصف قطر اللهب يزداد سمك فرشاة اللهب مع نصف قطر اللهب.

تعتمد طريقة تحديد سرعة الاحتراق المضطرب على نصف قطر اللهب المرتبط المختار. يتم فحص التعاريف المختلفة وعرض أنصاف أقطار اللهب المختلفة، بالإضافة إلى سرعات الاحتراق المضطربة المرتبطة بها. تتم مقارنة سرعات الاحتراق المضطرب والصفيحي.

ويوضح كيف يمكن الحصول على هذا الأخير بسهولة من صور سينمائية شليرين. في انفجار معين، تزداد سرعة الاحتراق بمرور الوقت ونصف القطر، نتيجة للتوسع المستمر في الطيف الفعال للاضطراب الذي تعرض له اللهب.

وكان التركيز الأساسي على حساب سرعة الاحتراق المضطرب على أساس متوسط قطر لهب الاحتراق، والذي يتأثر بالقطر غير المنتظم الناتج عن الاضطراب. وفي ظل ظروف معينة، تم التوصل إلى أن سرعة الاحتراق الصفيحي هي 28.64 سم/ثانية.

بالإضافة إلى ذلك، عندما تم تغيير الظروف لتصبح نفس نسبة التكافؤ وضغوط أولية مختلفة أو نفس الضغط الأولي ونسب تكافؤ مختلفة، كانت سرعة الاحتراق المضطرب المحسوبة أعلى عند 49.11 سم/ثانية. يمكن أن تعزى هذه الزيادة في سرعة الاحتراق في ظل الظروف المضطربة إلى التأثير المفيد للاضطراب على كفاءة الاحتراق.

وتشير النتائج إلى أن الاضطراب يحسن سرعة الاحتراق ويعزز كفاءة احتراق خليط الوقود

تعطي نتائج هذه الدراسة مزيدًا من الفهم لعمليات الاحتراق من خلال تحسين كفاءة الاحتراق لمختلف التطبيقات، مثل المحركات والأفران.

جمهورية العراق
وزارة التعليم العالي والبحث العلمي
جامعة بابل /كلية الهندسة
قسم الهندسة الميكانيكية

دراسة تجريبية لخصائص اللهب المضطرب لغاز البترول المسال المخلوط بالأمونيا

رسالة

مقدمة الى جامعة بابل /كلية الهندسة وهي جزء من متطلبات نيل شهادة الماجستير في الهندسة /قسم الهندسة الميكانيكية / قدرة

اعدت من قبل

جعفر سامي شعبان

بأشراف

أ . د سامر محمد عبد الحليم

1445 هـ

2023 م